THE ROLE OF LOADING AND THE MICROENVIRONMENT ON THE REGULATION OF LYMPHATIC FUNCTION AND HEALTH

A Dissertation
Presented to
The Academic Faculty

by

Joshua Hooks

In Partial Fulfillment
of the Requirements for the Degree
Doctor of Philosophy in
Bioengineering

Georgia Institute of Technology
August 2019

THE ROLE OF LOADING AND THE MICROENVIRONMENT ON THE REGULATION OF LYMPHATIC FUNCTION AND HEALTH

Approved by:

Dr. J. Brandon Dixon, Advisor
School of Mechanical Engineering
Georgia Institute of Technology

Dr. Michael Davis
School of Biomedical Engineering
Georgia Institute of Technology

Dr. Andrés J. García
School of Mechanical Engineering
Georgia Institute of Technology

Dr. Mariappan Muthuchamy
College of Medicine
Texas A&M University

Dr. C. Ross Ethier
School of Biomedical Engineering
Georgia Institute of Technology

Date Approved: April 19, 2019

ACKNOWLEDGEMENTS

I would like to thank my parents and sister for their support and guidance over the course of my life, but especially over the last 5-6 years of graduate school. Your emotional (and financial) support has been critical for me to reach the completion of this degree. A special thank you to my girlfriend for keeping me fed and sane through the last month of writing and final experiments. I have the most supportive friends and fellow lab mates that I could have ever hoped for. I would like to thank them for the hours of tossing around research ideas, discussing politics or philosophy, and making the best of graduate school. This could go on for pages, so in brief, thank you to my entire support network. There are not words to express how grateful I am.

On the research side of things, I would like to acknowledge my advisor, Dr. Dixon for all of his support. His guidance and mentorship have pushed me to become a more independent, creative, researcher. I feel prepared and excited to continue being a researcher; learning more about and contributing to the fields of medicine and bioengineering. Thank you to all the funding sources, research collaborators and core managers who were able to contribute their resources and expertise to the successful execution of this work.

TABLE OF CONTENTS

LIST OF FIGURES

LIST OF SYMBOLS AND ABBREVIATIONS

ALDT	Axillary Lymph Draining Tissue
ALN	Axillary Lymph Node
ALND	Axillary Lymph Node Dissection
BCRL	Breast Cancer Related Lymphedema
BLN	Brachial Lymph Node
CL	Control, contralateral, LEG
ECM	Extracellular Matrix
eNOS	Endothelial Nitric Oxide Synthase
GFP	Green Fluorescent Protein
LEC	Lymphatic Endothelial Cell
LMC	Lymphatic Muscle Cell
NIR	Near-infrared
PEG	Poly(ethylene glycol)
SMA	α-Smooth muscle actin
VEGF	Vascular Endothelial Growth Factor
VSMC	Vascular Smooth Muscle Cell
WL	Wounded Leg

SUMMARY

The lymphatic system is composed of vessels and nodes and exists in almost all of the soft tissue of your body. It plays a large role in maintaining fluid homeostasis, immune cell trafficking, and lipid transport. Interstitial fluid that enters the lymphatic system through initial lymphatics is deemed “lymph” and is transported from the anatomical region where it is collected to the blood circulation. Unlike the venous system, lymphatic vessels must actively pump to drive lymph flow. Lymphatic dysfunction often leads to the development of swelling known as lymphedema. This buildup of fluid alters loading conditions of the local lymphatic network and lymphedema eventually leads to remodeling of the interstitium and lymphatic vessel walls. The extent to which remodeling of these extracellular matrices (ECM) is the cause and/or symptom of lymphatic dysfunction is not clearly understood.

We present multiple studies utilizing engineering tools to better understand how the biomechanical properties and loading of the extracellular matrix regulate lymphatic function. We establish a healthy and remodelled lymphatic muscle cell (LMC) line and explore how LMC phenotype impact their response to 2D culture conditions. We demonstrate regulation of LMC molecular pathway expression via physiologically relevant levels of cyclic stretch. Modular poly(ethylene glycol) (PEG) based hydrogels are used to explore the sensitivity of sprouting lymphangiogenesis to properties of the extracellular matrix. PEG gels can be formulated to produce a robust sprouting network that is sensitive to a variety of molecular regulators. Finally, we present results demonstrating that the PEG hydrogels can be used to successfully transplant lymphatic tissue after damage to local

lymphatic collecting vessel or lymph nodes. Tissue transplanted with this method becomes functionally incorporated into the local lymphatic network.

CHAPTER 1. INTRODUCTION

1.1 General Background

1.1.1 General Anatomy and Structure of the Lymphatic System

Lymphatics are composed of a system of vessels and nodes responsible for returning roughly 8 liters/day of fluid from the interstitial tissue space back into blood circulation, Figure 1. The lymphatics play a critical role in maintaining fluid homeostasis, trafficking immune cells, and transporting lipids[1]. The initial lymphatics, sometimes referred to as lymphatic capillaries, are blind ended vessels composed of lymphatic endothelial cells (LECs). LECs of the initial lymphatics are connected via "button-like" junctions, composed of a unique configuration of VE-Cadherin and CD31, and form flap like structures providing structural integrity along the side of the flap and at the points of entry at the tips[2]. This allows for fluid, large proteins, and cells to enter the initial lymphatics. Once in lymphatic vasculature, this unique mixture of fluid, proteins, and cells is deemed lymph. Entry of fluid and other macromolecules is further assisted by anchoring filament that connect the initial lymphatics to the surrounding interstitial tissue and prevents these vessels from collapsing when the interstitial fluid pressure increases[3,4]. Furthermore, the junctions are aligned in such a way that prevents the escape of lymph from the initial lymphatics even when lymphatic capillary pressure exceeds interstitial fluid pressure. This functionality gives the initial lymphatics a valve-like quality, commonly referred to as "primary lymphatic valves" [1,5–8]. These unique features of initial lymphatics are outlined in Figure 1.

As initial lymphatics begin to connect downstream they form larger lymphatic vessels known as pre-collecting vessels. These pre-collecting vessels are characterized by the formation of a basement membrane surrounding the endothelial cells and sporadic coverage by specialized smooth muscle cells referred to as lymphatic muscle cells (LMCs). Despite the basement membrane, pre-collectors continue to have anchoring filaments, presumably to assist in lymph transport and structural support[9].

Pre-collecting vessels transition in mature lymphatic collecting vessels with continuous LMC coverage and the presence of unidirectional valves. The mature basement membrane between the LECs and LMCs is primarily composed of collagen and elastin fibers and provides full structural support to the vessel. Collagen and elastin also provide support to the bileaflet, unidirectional, valves that are spaced every 1-3 millimeters in humans [10,1112]. In addition to limiting the backflow of lymph within the lymphatic system, these valves allow us to separate the collecting vessel into discrete functional units known as lymphangions, the region of vessel between two valves, Figure 2. The valves are slightly biased to remain open, explaining why there is a small amount of retrograde flow observed in the upstream lymphangion before valve closure[13 14].

There is no central pump to drive lymph flow within the lymphatic system and there is no passive pressure gradient that would allow for continuous flow downstream. Therefore, lymph transport is dependent on the intrinsic contractility of the highly specialized lymphatic muscle cells. LMCs are capable of coordinated, phasic, contractions to propel lymph from one lymphangion to a downstream lymphangion[15]. The unique physiology of the lymphatic muscle cells will be explored in more detail in the following sub-section. In addition to LMC contractility, extrinsic factors, such as skeletal muscle

contractions, arterial pulsations, passive movements, and respiration contribute to lymph flow by expanding or constricting nearby lymphangions[7,16]. Failure of lymphatics to successfully transport lymph forms the basis of most lymphatic diseases, such as lymphedema, resulting in chronic swelling of the soft tissues.

Afferent collecting vessels eventually lead to lymph nodes where some lymph is "processed" by resident immune cells and some lymph enters the blood circulation via high endothelial venules (HEV) within the node[17]. The majority of lymph continues out of the lymph node through efferent collecting vessels and eventually into large lymphatic ducts. The two major lymphatic ducts are directly connected to the subclavian veins, separated by a unidirectional lymphovenous valve, that allows lymph to be deposited into the venous circulation but prevents blood flow back into the lymphatics. This network of fluid drainage across the body, the unique primary lymphatic valves that allow for entry of cells and macromolecules, and the relatively slow flow rate of lymph compared to blood flow assist the lymphatics in their additional roles of transporting cells, proteins, lipids, and other macromolecules from the soft tissue into the blood stream.

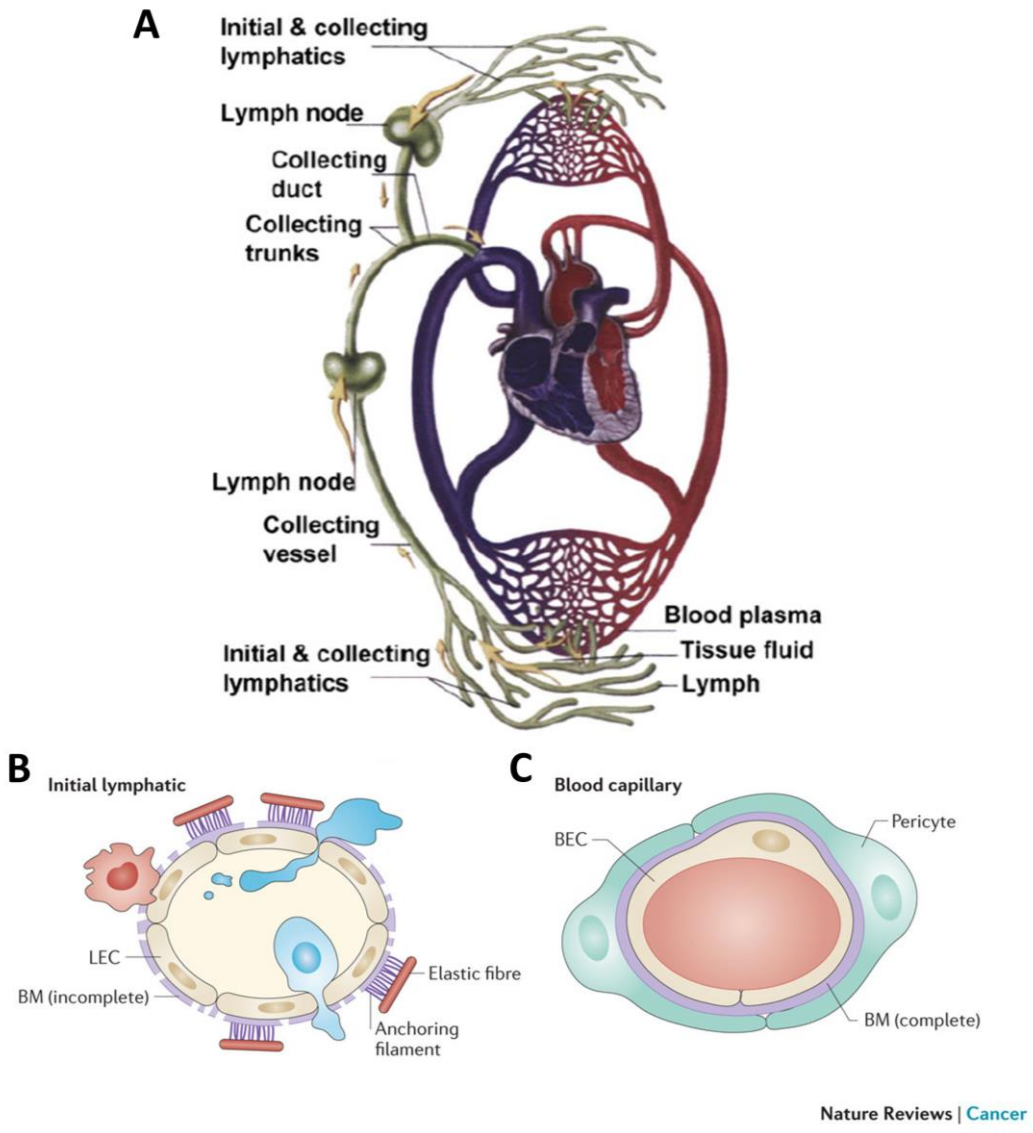

Figure 1: Overview of lymphatic structure and anatomy. (A) Structure of the lymphatic network and how initial lymphatics collect tissue fluid and connect downstream to the collecting lymphatic vessel. (B) The initial lymphatic vessels exhibit a discontinuous basement membrane and loose endothelial cell junctions, in contrast to blood capillaries that have a continuous basement membrane. This specialized structure of the initial lymphatics allows the paracellular transport of cells and proteins into the initial lymphatic lumen, but transport also happens through transcellular pathways. Anchoring filaments, which are responsible for pulling the initial lymphatic vessel open during the filling up stage are also shown. Modified from the publications of Yu et al, 2009[18] (top) and Stacker et al, 2014[19] (bottom).

1.1.2 Lymphatic Muscle Physiology and Remodelling

As stated earlier, lymphatic muscle cells (LMCs) play a primary role in generating lymph flow. They are arranged circumferentially around the lymphatic collecting vessels with brief interruptions around the valve regions[20]. These valves also break the collecting vessel into discrete contractile units referred to as lymphangions (Figure 2). Contractions are coordinated with depolarization waves traveling across adjacent cells to coordinate contractile waves. Influx of calcium through T-type and L-type calcium channels helps to regulate the frequency and amplitude of these contractions[21–23]. LMCs contain the majority of contraction proteins found in vascular smooth muscle cells (VSMCs), including vascular α-smooth muscle actin, smooth muscle myosin heavy chains, myosin light chains, and tropomyosin[15,24–26]. In addition, LMCs contain contractile proteins typically reserved to striated muscle cell. Freshly isolated collecting vessels have stained positive for, skeletal actin, and cardiac actin. Furthermore, it has been demonstrated that some collecting vessels, from regions such as the mesentery, express cardiac troponin and cardiac/skeletal slow-twitch β-myosin heavy chains, but expression levels of these highly specialized proteins seem to vary depending on the anatomical region of the collecting vessel. While the exact functional implications of these proteins within LMCs are still being explored, the presence of these proteins help to explain their unique contractile capacity. [27]. For example, the peak maximum shortening velocity (V_{max}) of mesenteric lymphatic vessels has been measured to be 0.48 ±0.04 lengths/s, which is 2.3 times higher than mesenteric arteries and 11.4 times faster than mesenteric veins[28]. A chain of lymphatic vessels is able to overcome a relatively large pressure gradient, with measurement in vivo reporting pumping pressures in excess of 30 mmHg in human legs [29], 40 mm Hg in human arms [30], and 35 mmHg in rats [31].

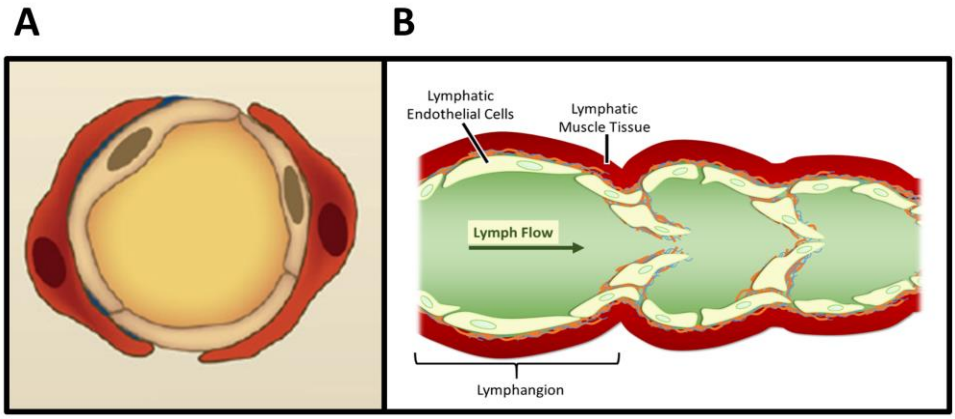

Figure 2: The mature lymphatic collecting vessel. (A) Cross-sectional view of the collecting vessel showing luminal lymphatic endothelial cells (off-white) surrounded by a single layer of lymphatic muscle cells (red). (B) The lymphatic endothelial cells (LECS) are supported by a layer of basement membrane composed primarily of extracellular fibrils of collagen and elastin (seen in orange and blue). These fibers also provide structural support to the bileaflet valves. The entire collecting vessel is surrounded by a layer of lymphatic muscle cells which contracts to propel lymph flow downstream. Panel A adapted from Tammela et al, 2010.

A major challenge to researching LMCs is the loss of many of their unique proteins when cultured *in-vitro* (Figure 3)[15]. After seeding onto plastic, LMCs lose expression for much of the skeletal/cardiac proteins. LMCs also alter their expression of many markers of mature smooth muscle cells, such as an overexpression of vascular smooth muscle actin and a reduction in smooth muscle myosin heavy chain II (SM2), Figure 3. In VSMCs a similar change in protein expression has been shown to be indicative of a phenotypic change[32–34]. VSMC phenotype is considered plastic, with cells changing from a fully differentiated, "contractile" phenotype when in a healthy vessel, to a "synthetic" phenotype" under pathological or unnatural conditions, such as in response to vessel damage, hypertension, or during *in-vitro* culture. This synthetic state is associated with elevated proliferation, migration, and increased synthesis of extracellular matrix. To what extent LMCs exhibit a similar synthetic phenotype and the exact implications of the protein expression changes observed so far are areas of active research.

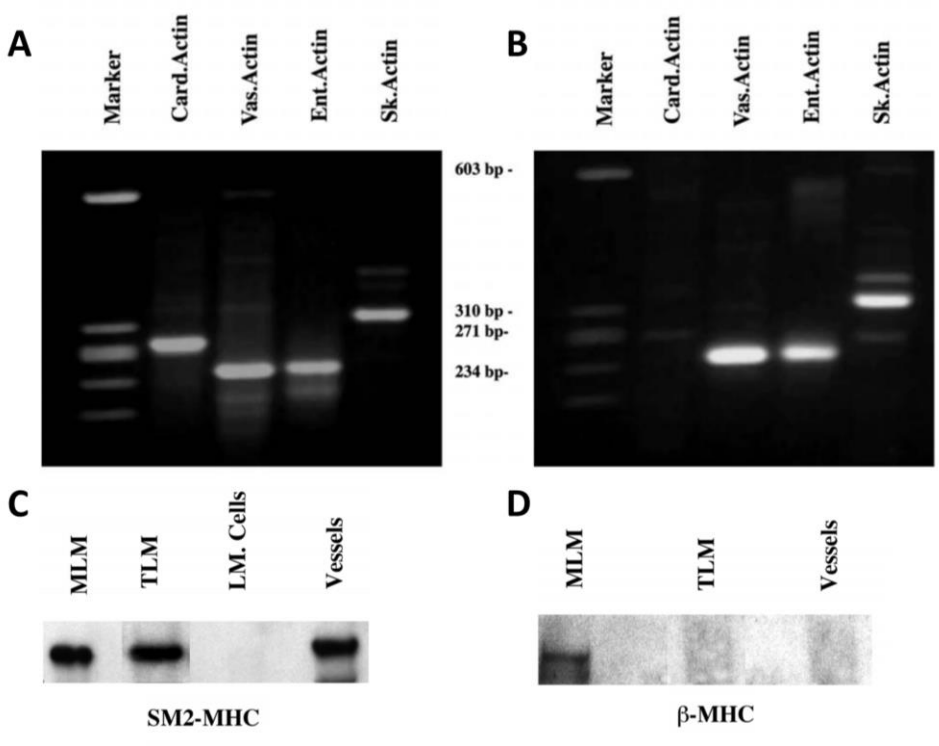

Figure 3: Altering LMC protein expression between mesenteric lymphatic muscle (MLM), thoracic duct lymphatic muscle (TLM), *in-vitro* cultured lymphatic muscle (LM. Cells), and arterioles (vessels). (A) PCR analysis of common actin isoforms of freshly isolated mesenteric lymphatic muscle. (B) PCR analysis of actin expression in LMCs isolated from mesenteric lymphatic vessels after 7-10 days of culture *in-vitro*. Gene expression for cardiac actin has been significantly reduced. (C) Western Blot showing that smooth muscle myosin heavy chain 2 (SM2) expression is absent in the *in-vitro* LMC cultures. (D) Western Blot reveals that only mesenteric lymphatic muscle (MLM) expresses the β isoform of myosin heavy chain. All panels modified from Muthuchamy et al, 2003[35].

1.1.3 Lymphatic Dysfunction and Lymphedema

Lymphedema is defined as swelling, generally occurring in the extremities, due to lymphatic impairment or blockage. Swelling typically manifests as "pitting edema" and can be accompanied with restricted range of mobility and fibrosis of the skin[36–38]. Primary lymphedema due to inherited, genetic, factors is rare. Typically, primary lymphedema will manifest at infancy, but there are cases of mid or late onset primary lymphedema that are

linked to genetic causes. Secondary lymphedema is much more common and occurs when lymphatic function is impaired due to another known disease or injury. Globally, the biggest cause of lymphedema is due to lymphatic filariasis which is caused by a parasitic worm that resides in lymphatics and is transmitted via mosquito bites. Filariasis deposited under the skin during a bite will migrate to the lymphatic system and disrupts healthy lymphatic function. In most developed countries, lymphedema is primarily the result of cancer related surgery and treatments and is particularly documented to occur after breast cancer. Due to a mixture of the surgery to remove the primary tumour, lymph node removal to limit cancer metastasis, radiation, and/or chemotherapy, an estimated of 10-20% of breast cancer patient survivors will develop lymphedema at some point in their life[39]. While the swelling and other symptoms of lymphedema are manageable if diagnosed early, there is no cure and most patients must maintain some level of therapy to avoid reoccurrence. Patients who are diagnosed late are burdened with a lifetime of disease management which can often result in pain, severe disfigurement, compromised immune function, and an increased rate of infection.

While the exact cause and pathogenesis of breast cancer related lymphedema (BCRL) is unknown, our understanding of risk factors and symptoms is growing. Historically, there have been several perceived risk factors including the severity of surgeries and number of lymph nodes removed, total dose of radiation , patient age, BMI, and others but there is limited clinical data to quantify the relative importance of each[40]. Recent work has shown that patients with elevated lymphatic pumping prior to breast cancer related treatments are much more likely to develop lymphedema later on[41,42]. These studies indicate that patients that go on to develop lymphedema have a predisposition to its

development regardless of surgery or treatments. Lymphatic workload and output increases further following lymph node dissection and cancer treatments and eventually tip into chronic failure. Furthermore. once lymphedema has been acquired it has been shown that pressures are elevated in lymphatic capillaries compared to healthy individuals[43]. Taken together, these studies would imply a pathology analogous to high preload and high afterload cardiac failure in systemic hypertension, but definitive studies to support this failure model have yet to be thoroughly conducted.

These results indicate that the workload on the collecting vessel is critical to the development and progression of lymphedema and therefore recent studies have begun to look more closely at the function and structure of lymphatic collecting vessels during lymphedema progression. It has been found that vessels undergo hyperplasia and a narrowing of the lumen during late stages of lymphedema[44]. Collecting vessels see an increase in SMA positive cells, collagen in and around the vessel walls, and a reduction in SM2 positive cells[45] (Figure 4). The lymphatic specific mechanisms of how these changes occur in LMCs is unclear, but the morphological changes noted so far are reminiscent of the synthetic phenotype in vascular smooth muscle cells. It has been well documented that VSMCs in hypertensive or atherosclerotic vessels become more proliferative, mobile, and excrete additional ECM to thicken vessel walls[46], but much more research remains to be done to explore the extent of these similarities in lymphatic vasculature. **While we have begun to understand that lymphatic collecting vessels near an injury never return to pre-injury levels of pumping and lymph transport[47], long term remodeling of collecting vessels, and the exact functional impact of this remodeling, is severely understudied.**

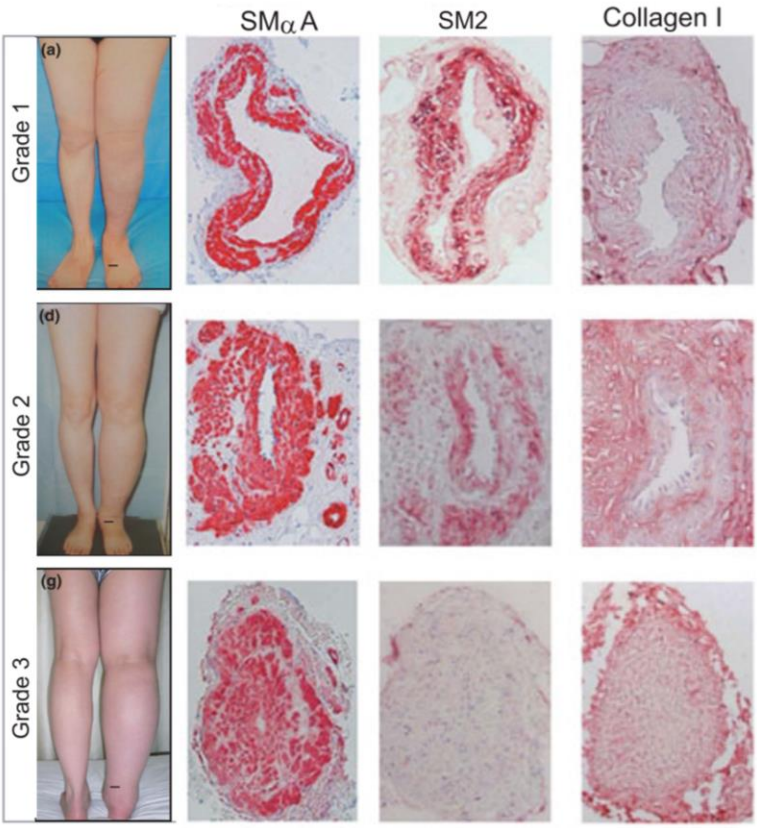

Figure 4: Progression of Lymphatic Collecting Vessel Phenotype During Leg Lymphedema Progression. As lymphedema worsens, shown as a progression from grade 1 to grade 3, the collecting vessel walls become thicker and the lumen becomes more stenotic. αSmooth muscle actin (SMαA) positive cells proliferate and expand, lymphatic muscle cells eventually lose their expression of smooth muscle myosin heavy chain 2 (SM2), and the collagen composition of the vessel wall increases. Modified from Ogata 2015 [45]

In animal models, it has been found that lymphedema is dependent on macrophage and $CD4^+$ T-cell presence. These immune cell populations are associated with worsening lymphedema through a variety of mechanisms including fibrosis, increased ECM synthesis and tissue remodeling and inflammation driven lymphangiogenesis[48,49]. Inhibition of fibrosis through manipulation of immune cell recruitment has been shown to reduce swelling and improve lymphatic function following surgical insult[50]. Inflammation driven lymphangiogenesis appears to have a mixed role in lymphedema pathology. In some

studies, VEGF-C driven lymphangiogenesis has been shown to reduce swelling in animal models of lymphedema, while other studies have shown that it may worsen outcomes[51–54]. As the context and extent of lymphangiogenesis can sometimes propagate or alleviate dysfunctional states it is unclear how to best regulate lymphangiogenesis as a therapy[55]. These discrepancies may in part be due to variation in how VEGF-C levels are elevated (exogenous application vs cellular overexpression) and variation in animal models of lymphedema. Recent work has shown that the benefits of lymphangiogenesis during lymphedema progression are also dependent on when the intervention begins following surgical insult[56]. **Due to their critical role in regulating lymphedema outcomes, we need a better understanding of lymphangiogenesis following surgical insult and the regulatory role of the ECM on lymphatic function.**

1.1.4 Lymphangiogenesis

Lymphangiogenesis is the process of proliferation and migration of lymphatic endothelial cells to form new functional initial lymphatic vessels and has been the focus of lymphatics research for decades[57,55,58,59]. Lymphatic endothelial cells express vascular endothelial growth factor receptors (VEGFR), which trigger growth and proliferation of the cell once bound to their ligand. Unlike vascular endothelial cells, LECs primarily express the VEGFR-3 subtype which binds with the highest affinity to vascular endothelial growth factor C (VEGF-C). Since this discovery, VEGFC has been used successfully in numerous studies to drive lymphatic growth in-vitro and in-vivo[60]. More recently it has been shown the VEGF-C driven lymphangiogenesis can produce leaky initial lymphatics that can possibly propagate disease states, adding a layer of complexity to its application as a therapy to lymphatic dysfunction[51,61,62]. Recent research has shown that there is a

heterogeneity to VEGFR-3 expression in developing or immature initial lymphatics. Lymphatic endothelial cells along the leading edge of sprouts, commonly referred to as the tip cells, have higher levels or VEGFR-3 and their behavior is reliant on molecular regulators such as neuropilin-2[63–65].

1.1.5 The Extracellular Matrix (ECM) of the Basement Membrane and Interstitial Tissue

The collecting vessel wall is supported through a basement membrane that is composed of a variety of extracellular matrix proteins. As initial lymphatics transition into precollectors a patchy basement membrane of both laminin and type IV collagen has been observed[66]. The collecting vessel wall has a basement membrane that is composed of an inner layer of elastin and an outer layer of collagen fibers[67,68]. Cells of the vessel wall interact with this wall matrix with a variety of surface receptors known as integrins, which bind to specific regions along the fiber. The expression and binding of specific integrins to their ligands along the ECM fiber has been shown to guide lymphatic function[69–71]. During events that trigger lymphangiogenesis, such as injury and inflammation, the type and number of activated integrins change significantly which seems to promote migration and proliferation. In LECs these activated integrins include α9β1 α4β1 α2β1 α1β1[72]. There is no available research looking at the change in LMC integrin expression during lymphangiogenesis or following injury, but literature from VSMCs would suggest that LMCs may also undergo altered integrin expression. For example, VSMCs begin to upregulate the α5β1 integrin isoform in response to arterial injury[73,74]. Similarly blocking α5β1 integrin binding blocked inflammation driven lymphangiogenesis in the airway, although in this study α5β1 integrin expression was associated exclusively with sprouting lymphatic endothelial cells, not muscle cells[75]. Generally, the collecting vessel remodelling

that occurs during lymphatic disease states, such as elevated, dense, type I collagen synthesis, would presumably impact the number and types of adhesive peptides available to the cells of the vessel wall.

Matrix stiffness has a large impact on cell phenotype. It has been shown that matrix stiffness can guide stem cell differentiation, cell migration, protein synthesis and more[76–78]. For example, it has been shown that in development the migration of LEC progenitors from the cardinal vein to the softer surrounding matrix triggers GATA2 transcriptional factors needed to form initial lymphatic vessels[79]. Changes in arterial stiffness with age or disease have been linked to propagating disease states and triggering vascular smooth muscle cells to proliferate and remodel the vessel walls. The ideal stiffness for each cell type is different but it is typically bimodal, with matrices that are too soft preventing adequate traction force generation and matrices that are too stiff often preventing migration or inducing a pathological phenotype[80–82]. Biologically, matrix stiffness is intricately tied to the density of ECM components. A stiff matrix is typically less porous and more heavily crosslinked, requiring higher levels of specific enzyme to degrade the matrix before cell migration is possible. When examining the mechanical properties of the collecting vessel it is important to consider its loading condition. At low transmural pressures, the ECM fibers of the basement membrane will not be engaged and therefore the perceived wall stiffness to the cells will be low. At high transmural pressures the fibers will fully engage increasing the relative stiffness and the necessary force for the muscle cells to contract the vessel[68,83]. Therefore, even without matrix remodeling, elevated loading can alter the stiffness based signaling cues to the embedded cells.

The interstitium is composed primarily of collagens I, III, and V, elastin, and glycosaminoglycans. These components are both mechanically entangled and cross-linked forming a gel-like matrix to provide structural support for tissues and migrating cells. The exact components of the interstitial tissue, and therefore the biomechanical properties, vary greatly across different regions of the body and as such lymphatics have local variability in density, size, and contractility[84–87]. The density of the ECM is dynamic with fluid content playing a large role in the density of fibers, thereby altering porosity, volume, and fiber tension. Two prominent cell populations that reside in the ECM are fibroblasts and tissue resident immune cells (such as macrophages and dendritic cells). Fibroblasts are primarily responsible for both synthesizing ECM components and can release a variety of enzymes to degrade matrix components allowing for migration and remodelling[88,89]. Among these enzymes are the family of matrix metalloproteinase. Both endothelial cells and smooth muscle are capable of excreting many MMPs as well, which allow for their migration and remodelling of vessel basement membranes.

1.2 Specific Aims

The central goal of this work is to better understand how the loading conditions and properties of the extracellular matrix (ECM), regulate the phenotype and regenerative capacity of the lymphatic cells that compose the collecting vessels' walls. This goal is accomplished through the following three aims.

1.2.1 Specific Aim 1: Determine the role of in-vitro mechanical stretch in the remodelling response of lymphatic muscle cells.

While the phenotypic switch of vascular smooth muscle cells (VSMCs) during disease states or 2D culture has been well characterized[90–92], the extent to which lymphatic muscle cells are capable of this phenotypic plasticity is unclear. As outlined, recent studies characterizing isolated lymphatic collecting vessels support the hypothesis that LMCs behave similarly to synthetic VSMCs during lymphedema progression. The synthetic phenotype is characterized by a down-regulation of contractile markers, such as myosin, an up regulation of actins, and elevated synthesis of ECM components[34,91]. We isolate LMCs from a sheep model of lymphatic dysfunction and compare the behaviour of LMCs isolated from the remodelled lymphatic vessel in the surgically insulted limb to an internal control LMC line established from the contralateral limb. We demonstrate a chronic increase in metabolic activity and oxidative stress in the LMCs isolated from the remodelled vessel.

We hypothesize that this remodelled, or "wounded" phenotype impacts the sensitivity of LMCs to loading conditions. We modify and characterize a stretch device platform to apply physiologically relevant levels of cyclic mechanical strain to 2D cultures of LMCs. Stretch profiles are based on contraction metrics of in-vivo lymphatic collecting vessels during a surgically induced lymphedema model in sheep, where the LMCs were derived from.

1.2.2 Specific Aim 2: Characterize sprouting lymphangiogenesis sensitivity to extracellular matrix properties using a modular poly(ethylene glycol) (PEG) hydrogel.

It has been well demonstrated that the components and density of the ECM alone have a significant impact on the phenotype of a cell[76–78], leading to changes in the form and

function of a cell. Fibrosis and inflammation alter the properties of the interstitial ECM following surgically induced lymphedema[49,93], but the sensitivity of lymphatic repair mechanisms such as sprouting lymphangiogenesis, to ECM properties is poorly understood.

In this aim we begin to answer this question by determining the baseline sensitivity of sprouting lymphangiogenesis to various ECM properties. Through implementation of a modular, poly(ethylene glycol) hydrogel, we systematically determine which ECM properties significantly impact sprouting from segments of lymphatic collecting vessels. We hypothesize that a degradable hydrogel that facilitates high affinity adhesion of lymphatic cells, will optimize sprouting as measured by sprout length and abundance. Stiffness, degradability, and adhesive ligands will be independently configured to optimize sprouting and the best performing gel condition will then be used to determine sprouting sensitivity to other drugs and molecular regulators.

1.2.3 Specific Aim 3: Utilize animal lymphatic damage models to study PEG hydrogel facilitated lymphatic tissue transplantation and influence of PEG hydrogels on lymphatic function and regeneration following injury.

Transfer of healthy lymphatic tissue or cells to a region of lymphedema or surgically induced lymphatic dysfunction has shown promising preliminary results in mitigating lymphedema symptoms in both animal models and human patients[94,95]. This field is still growing, and the exact mechanisms and pathways that facilitate successful transfer are still being determined. Given the robust sprouting produced in the degradable 10% PEG – 2mM

RGD gels characterized in aim 2, we wish to determine if these PEG gels could be used to enhance lymphatic regeneration and minimize lymphatic dysfunction *in-vivo*.

We hypothesize that the sprout promoting characteristic of the PEG hydrogel will enhance repair of lymphatic tissue into a region where lymphatics are damaged and surgically resected. In our first animal model we aim to determine if lymphatic tissue transfer is feasible when embedded within our PEG hydrogel formulation. Given the success of this first model, we then use a second animal model to examine the impact of PEG hydrogel facilitated lymph node transfer compared to the innate repair process without intervention and to alternative biomaterial approaches. In the process we also assess the response of upstream lymphatic collecting vessels to lymph node resection surgery.

CHAPTER 2. DETERMINE THE ROLE OF IN-VITRO MECHANICAL STRETCH IN THE REMODELLING RESPONSE OF LYMPHATIC MUSCLE CELLS.

2.1 Overview

Objective: Using primary lymphatic muscle cells (LMCs) in vitro we sought to characterize the impact of LMC remodeling on their functional and molecular response to mechanical loading and culture conditions.

Methods: Primary "wounded leg" LMCs were derived from the hindlimb of three sheep who underwent lymphatic injury six weeks prior, while "control leg" LMCs were derived from the contralateral, unwounded, limb. Functions of the LMCs were characterized in response to media of variable levels of serum (10% vs 0.2%) and glucose (4.5g/L vs 1g/L). Additionally, functional and proteomic data were evaluated in LMCs exposed to cyclic stretch (0.1Hz, 7.5% elongation) for 1 week.

Results: LMCs were sensitive to changes in serum levels, significantly reducing overall activity and collagen synthesis under low serum conditions. LMCs from the remodeled vessel had higher baseline levels of metabolic activity but not collagen synthesis. Cyclic loading induced cellular alignment perpendicular to the axis of stretch and alterations in signaling pathways associated with metabolism. Remodeled LMCs had consistently higher levels of metabolic activity and were more resistant to strain induced apoptosis. **Conclusions:** LMCs exist on a functional spectrum, becoming more active in response to

stretching and maintaining phenotypic remodeling in response to local lymphatic/tissue damage.

2.2 Motivation and Background

As stated previously, the primary driver for lymph transport is the intrinsic contractility of lymphatic muscle cells (LMCs). Despite their unique phenotype and importance in generating fluid transport, the role of lymphatic muscle in mediating or propagating pathologies such as lymphedema has been largely understudied. Functionally, it has been demonstrated that lymphatic collecting vessels become more permeable in inflammatory environments and significantly remodel[96–98]. Vessels removed from lymphedema patients undergoing lymphaticovenous anastomosis displayed a thicker media and intima when the stage of lymphedema was advanced, decreased ratio of myosin-heavy-chain-2 to alpha-smooth muscle actin and increased collagen[49,99]. In the lymphedemic environment, the phenotype of the lymphatic collecting vessel is sensitive to various macrophages and inflammatory signaling that regulate tissue remodeling through fibrosis[49,100]. Understanding the remodeling response of lymphatic muscle to injury and pathology, and the role that the mechanical tissue microenvironment plays in this process, may provide useful insight into the chronic nature of lymphedema.

LMC's response to local injury and disease is likely to be similar in many ways to vascular smooth muscle cells (VSMCs). The behavior of VSMCs have been characterized in much greater detail both in-vivo and in-vitro. Depending on the combination of chemical and mechanical cues, VSMC phenotype is typically described as "contractile" or "synthetic" [91,101,110–112,102–109]. In the contractile phenotype, VSMCs tend to be quiescent;

with little to no migration or proliferation. A contractile VSMC's primary function is to modulate the diameter of a blood vessel through constricting or relaxing in response to biomechanical cues such as endocrine signaling or pressure changes. Commonly in response to pathological stimuli, such as disease or vessel damage, VSMCs convert to a synthetic phenotype. In this phenotype, VSMCs are highly proliferative and migratory. In addition, they begin to excrete a variety of extracellular matrix (ECM) proteins, such as collagen. In combination, proliferation and ECM synthesis from high levels of synthetic VSMCs thicken and alter the walls of blood vasculature in disease states. Studies have demonstrated that the contractile and synthetic phenotypes do not exist exclusively, and in-vitro assays using a variety of different chemical and mechanical cues can induce a VSMC phenotype that exhibit features of both phenotypes[90]. While much of the LMC pathological response could be characterized as existing on this contractile to synthetic spectrum as well, it is unclear how the distinct functions of LMCs may lead to differences in their pathological responses.

At this time, LMC phenotype and function have mostly been explored while part of an intact vessel[23,35,113–115], limiting the opportunity for systematic, high throughput, analysis of multiple factors and stimuli. Therefore, with this study we aim to assess the impact of common biochemical and mechanical culture conditions on the phenotype of LMCs in-vitro. Primarily we explore the chronic phenotypic changes that occur in lymphatic smooth muscle derived from a limb where surrounding lymphatic vessels were surgically removed and compare those responses to LMCs isolated from the contralateral control. We determine the sensitivity of LMC phenotype to common changes in culture media thought to regulate phenotype. Specifically, we examine how changes in medium

serum and glucose levels, in addition to cyclic loading, alter LMC morphology, metabolic activity, and synthesis of collagen. Furthermore, we examine how cyclic stretching of LMCs influence orientation and the expression of various molecular pathways. We further demonstrate that LMCs derived from an inflammatory in-vivo environment, following local tissue damage, chronically alter the state of lymphatic muscle and their response to bio-mechanical cues.

2.3 Materials and Methods

2.3.1 Surgical Overview and Lymphatic Tissue Collection

A total of five, 3 to 5-year-old randomly bred female Suffolk sheep were used in this study; Before the study, 3 of the sheep underwent Gadolinium-Enhanced MR imaging (GE MRI) to structurally map the lymphatic anatomy of the hind limbs. One day after the MRI the sheep underwent a collecting lymphatic ligation surgery on one of the hind limbs, with the contralateral limb remaining intact to act as an internal control. In brief, a 4 cm incision was made on the lateral aspect of the hind limb proximal to the tarsus, exposing 2 collecting lymphatic vessels running in parallel to the saphenous vein, one cranial and one caudal with respect to the animal. A 2 cm portion of the caudal vessel along with the vein was ligated with sutures and resected. The sheep were recovered from anesthesia following the final NIR imaging session and surgery. Near-infrared (NIR) functional lymphatic imaging was conducted prior to the surgery, as well as 7, 14, 28, and 42 days after the procedure. One day before the final NIR imaging session, the 3 sheep that underwent the MR lymphatic imaging underwent a second MR imaging session. On day 42, following the NIR imaging procedure, the sheep were not recovered and were euthanized via

pentobarbital overdose for tissue collection. The cranial collecting lymphatic vessel that was left intact on the wounded leg, and the corresponding cranial vessel on the contralateral control limb, were isolated and excised for cell collection.

2.3.2 Cell Culture

Primary lymphatic muscle cell (LMC) lines were formed from cranial collecting lymphatic vessels isolated from wounded and control hind limbs. Once isolated, the collecting vessels were cleaned from all adipocytes and rinsed in a physiological saline before being transferred to a tissue culture dish where they were attached by gently pressing the ends to the surface with forceps. Vessels were cultured in Dulbecco's Modified Eagle's Medium (ThermoFisher Scientific, Waltham, MA), 4,500mg/L of glucose, with 10% Fetal Bovine Serum (FBS), along with Antibiotic-Antmycotic (ThermoFisher Scientific). Media was exchanged every 2-3 days. Muscle cells began to migrate and proliferate from the vessel around day 3. The vessel was gently discarded, leaving only the newly migrated cells. Cells were split once confluent using Trypsin, 0.25% EDTA, and frozen in liquid nitrogen at passage 3. Experiments were conducted on LMCs between passage 5-6. All following experiments were done with LMCs derived from 3 separate sheep, all who underwent the same lymphatic injury surgery, creating 6 cells lines. For statistical analysis experimental conditions were grouped into cells isolated from the wounded leg (3 sheep) and cells isolated from the control leg (3 sheep).

Lymphatic endothelial cells were isolated by first inverting a segment of the isolated collecting lymphatic vessel so that the luminal endothelial cells would be on the exterior. One end of the collecting vessel was tied to the end of a long glass micropipette and

inverted using suction and removed from the micropipette. The inverted lymphatic vessel was then gently pressed to a petri dish and cultured in Endothelial Basal Medium (Lonza, Basel, CH), supplemented with 20% FBS, 1% penicillin-streptomycin-amphotericin B (Gibco), 1% Glutamax (Gibco), 0.1% DBcAMP (Sigma), and 0.1% hydrocortisone acetate (Sigma), until the LECs began to migrate away from the vessel, usually around day 2-3. The vessel was then discarded and the cells were cultured until confluent. Cells were split using Trypsin, 0.25% EDTA, and frozen in liquid nitrogen at passage 3. Immunohistochemistry was conducted on LECs at passage 5.

2.3.3 Marker Assessment

Purity of the cell culture lines was established through expression of key protein markers including endothelial nitric oxide synthase (Abcam, Cambridge, UK), alpha-Smooth Muscle Actin (Sigma, St Louis, MO), Collagen Type 1 (Sigma), and Tropomyosin (BD Biosciences, San Jose, CA). Samples were permeabilized with methanol (-20C) for 2 minutes then rinsed three times with phosphate buffered saline (PBS). Blocking of samples was done in a PBS solution containing 2% bovine serum albumin, BSA and 10% goat serum for 1 hour at room temperature. Following this, a primary antibody, suspended in the 2% BSA solution (1:100), was applied to the samples for one hour on a plate rocker. The samples were rinsed in PBS before application of a fluorescent secondary antibody solution in 2% BSA (1:200) for 1 hour at room temperature on a shaker. Samples were rinsed two times in PBS before imaging.

2.3.4 Media Assay

To explore the role of serum levels and glucose levels in the phenotype of LMCs, cells were seeded into a cell culture treated 48-well plate at a density of 14800 cells/cm^2 in our standard DMEM formulation. This DMEM contained 4,500mg/L glucose and was supplemented with 10% FBS. Cells were allowed to settle and attach overnight before being serum starved for 24 hours in standard DMEM supplemented with 0.2% serum to arrest cell cycle progression. After serum starvation, cells were grown in one of three types of media for two days; the standard DMEM formulation (4,500 mg/L of glucose and 10% FBS), a low serum DMEM formulation (LS-DMEM) with only 0.2% FBS, or a low glucose DMEM formulation (LG-DMEM) containing only 1000mg/L of glucose.

2.3.5 Cellular Metabolic Activity

A reduction-oxidation indicator known as alamarBlue® (ThermoFisher Scientific) both fluoresces and undergoes a colorimetric change in response to cellular metabolic activity. Specifically, resazurin, a blue cell permeable compound with low fluorescence is reduced to resorufin, a red shifted and highly fluorescent compound. This reduction of resazurin to resorufin is a byproduct of normally occurring reduction reactions in metabolically active cells. Each well from the stretch experiment was incubated in media containing 10% alamarBlue® reagent for 4 hours. After the 4 hours, 100μL of the media from each well was transferred to a 96-well plate. The fluorescent intensity of each sample-including well was measured using a plate reader (Synergy H4) after excitation with a 562nm wavelength laser.

2.3.6 Collagen Expression Assay

A Sirius red/fast green assay (Chondrex, Redmond, WA) was used to determine the amount of collagen produced by cultured LMCs. In short LMCs were cultured on a tissue culture treated 48-well plate. Cells were cultured at a density of 15,000 cells/cm^2. Cells attached overnight and then were serum starved for 24 hours. Following the serum starvation, media of a specific formulation was applied, and the cells were cultured for two days before being fixed in 4% PFA. 75µL of the Sirius red/fast green dye was then incubated with each sample for 30 minutes. Samples were rinsed with 0.5mL of PBS twice, and then 0.3mL of the dye extraction buffer was applied and pipetted briefly to mix. 100µL of the extraction dye was added to a 96-well plate and optical density was analyzed with the Synergy H4 plate reader at 540nm and 605nm.

To calculate the amount of collagen, the OD 540 value was corrected by subtracting the contribution of Fast Green at 540 nm, which is 29.1% of the OD 605 value. The color equivalence (OD values/µg protein) is 0.0378 for collagen and 0.00204 for non-collagenous proteins at OD 540 and 605, respectively.

$$\text{Collagen (ug/section)} = \frac{\text{OD 540 value } - \text{ (OD 605 value x 0.291)}}{0.0378}$$

$$\text{Non} - \text{collagenous proteins (ug/section)} = \frac{\text{(OD 605 value)}}{0.00204}$$

2.3.7 Stretch Device

Hardware from a commercially available Flexcell® system (Flexcell® International Corporation, Burlington, NC) was interfaced with a vacuum pump from Parker Hannifin Corporation and a custom control code using National Instruments LabVIEW program to

cyclically strain a monolayer of cells. In brief, 70,000 LMCs (~7400 cells/cm^2) were seeded into each well of the Uniflex® Culture Plate onto a rubber membrane treated with type I collagen. The plate was loaded above loading posts which allow the cells to be deformed in a uniaxial direction through the manipulation of a vacuum below the wells, see Figure 5.

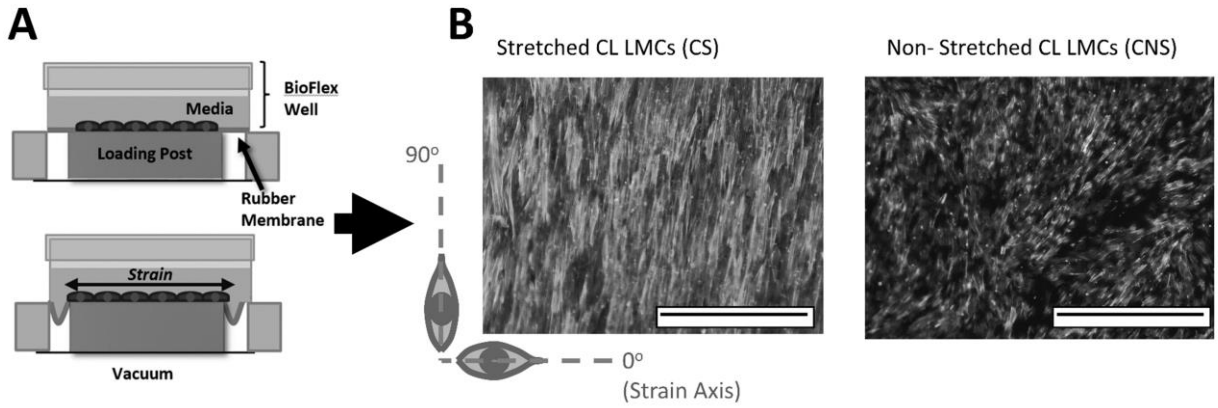

Figure 5: (A) Stretch Device Schematic. (B) Alignment of F-actin fibers for stretch and non-stretched CL LMCs to axis of strain

For all stretch experiments, the membranes which made the basement substrate of the LMCs were stretched to 7.5% elongation at 0.1Hz for 1 week. The deformation profile was roughly a square wave with up to 2% oscillation around the set vacuum pressure. This translates to about a 0.3% variation in the percent elongation (7.5% ± 0.3%). Ultimately there were four stretch conditions; Control Leg LMCs - Non Stretched (CNS) , Control Leg LMCs - Stretched (CS) , Wounded Leg LMCs - Non Stretched (WNS) , Wounded Leg LMCs - Stretched (WS). Cells isolated from all three sheep are present in each of the 4 experimental groups.

Blebbistatin (Abcam), an inhibitor to myosin II, was added to the cell culture media (5μM) to determine the sensitivity of the cyclic stretch induced behavior changes to the cell-matrix adhesion.

2.3.8 Actin Fiber Alignment

Images were taken of the wells post stretching for 1 week. The wells were immediately fixed in 4% paraformaldehyde once the experiment finished and stained with a F-actin stain (Molecular Probes, Eugene OR). Each image was analyzed with a Matlab code that utilizes built-in functions to determine the magnitude and direction of a vector indicating the path of maximum intensity change. In practice, this gradient vector is oriented perpendicular to a fiber at any given point along the fiber. The direction of the vector is given as an angle from -180° to 180°, referred to as the intensity angle. We then calculated an alignment score for each pixel based on how well the intensity gradient vector aligned to an arbitrary angle from 0° to 90° using the following formula:

$$Alignment\ Score_i = abs(\cos(Angle - abs(Intensity\ Angle_i))$$

$$\text{Normalized Alignment Score}_{\ i} = \frac{\text{Alignment Score}_{\ i}}{\min(Alignment\ Score)}$$

Values were normalized to the minimum score in any direction for the specific image to correct for slight variations in brightness from image to image.

2.3.9 Statistical Analysis of Functional Cell Assays

All data was tested using GraphPad prism software. Data was initially tested for normality using D'Agostino & Pearson normality test. The normality test revealed that the

alamarBlue results in the control leg LMCs cultured in the standard DMEM were not normally distributed. In addition, the alamarBlue and the collagen synthesis results for the wounded leg LMCs cultured in the low serum DMEM were not normal. Therefore, multiple one-way, nonparametric, Kruskal-Wallis tests were used to assess statistical differences for a single LMC type across the three media conditions. Dunn's test was used to correct for multiple comparisons. Differences between CL and WL LMCs in a shared media conditions were tested with the Mann-Whitney test.

2.3.10 Proteomic Analysis

One well of LMCs from each stretch condition (CNS, WNS, CS, or WS) was collected at the end of 5 individual stretch experiments to be used as a sample for proteomic analysis, with the cells that made up these samples being derived from 3 different sheep. Each of the 5 samples was run through the protocols listed below in duplicate. To prepare samples for proteomic analysis, monolayers of LMCs were rinsed once with PBS and then trypsinized. The cell solution was centrifuged for 5mins at 4°C and 800RCF. The resulting cell pellet was re-suspended in PBS and then spun down again under the same conditions. After aspirating the PBS, the cell pellet was then suspended in 0.5mL of RIPA lysis buffer (Thermo Scientific) and incubated on ice for 30 minutes. After 30 minutes, the samples were centrifuged at 13,000-14,000 RPM for 10 minutes at 4°C. The protein containing supernatant was collected and the pellet of cell debris was discarded. Protein content of the cell lysate was measured using a microplate BCA protein assay kit (Thermo Scientific) and aliquots containing 20µg of protein were stored in a -20C freezer.

Proteins in the supernatant are reduced, alkylated and digested with trypsin according to the FASP protocol[116]. The peptides were analyzed by high-performance liquid chromatography-coupled tandem mass spectrometry (HPLC-MS/MS), separated on a 2 micron, 15 cm X 75 μm C18 column, and analyzed with a Q Exactive Plus mass spectrometer.

2.3.11 Protein Identification

The protein IDs were assigned by searching the raw files from each technical and biological replicate against the sheep *(Ovis Aries)* Swiss-Prot database (December 2017; 788 entries) after being filtered and "de novo" sequenced in Peaks 8.0 software (Bioinformatics Solutions, Waterloo, Canada). The following search parameters were applied: trypsin restriction for enzyme and one allowed missed cleavages. The parent mass tolerance was set to 15 ppm using monoisotopic mass, and fragment ion mass tolerance was set to 0.05 Da, for the samples run on a *Q Exactive Plus* mass spectrometer. Carbamidomethyl cysteine (+57.0215 on C) was specified in PEAKS 8.0 as a fixed modification. Methionine, lysine, proline, arginine, cysteine and asparagine oxidations (+15.99 on CKMNPR), deamidation of asparagine and glutamine (NQ-0.98) and pyro-Glu from glutamine (Q-18.01 N-term) were set as variable modifications. The results were validated using the FDR method built in PEAKS 8.0 and protein identifications were accepted if they could be characterized with a confidence score (-10lgP)>15 for peptides and (-10lgP)>15 for proteins. The FDR for proteins was further adjusted to less than 1% ($p<0.05$) after removing contaminants like serum albumin, hemoglobin, keratins and immunoglobulin and further allowing a minimum of 1 peptide per protein. An independent validation of the MS/MS-based peptides and protein identification was performed with the Scaffold

(version Scaffold_4.7.3, Proteome Software Inc., Portland, OR) using the compatible ". mzid" files exported from PEAKS 8.0. for each "control" and "wounded" stretched or non-stretched lymphatic muscles samples. The Scaffold built in option "MuDPIT" was used to combine multiple files from technical replicates for each sample defining the "control stretched or non-stretched" and "wounded stretched or non-stretched" samples (see Supplementary Table 1). Peptide identifications were accepted if they could be established at greater than 95.0% probability by the Peptide Prophet algorithm with Scaffold delta-mass correction. Protein identifications were accepted if they could be established at greater than 90.0% probability and contained at least 1 identified peptide. Protein probabilities were assigned by the Protein Prophet algorithm. Proteins that contained similar peptides and could not be differentiated based on MS/MS analysis alone were grouped to satisfy the principles of parsimony as described originally elsewhere[117,118].

2.3.12 Label-free relative peptide quantification (LFQ) and analysis of differential protein expression profiles across the stretch and non-stretched control and wounded sample

Label-free quantitative (LFQ) methods used the raw spectral data from parallel MS runs to determine relative protein abundances. We used both "MS/MS (MS2) spectral counting" and "precursor MS1 area" methods for LFQ analysis and further contrasting the differentially expressed proteomic profiles across the control and wounded lymph (stretched or non-stretch) muscle samples. The label-free quantification based on the precursor intensity (area) was performed using the quantification algorithm supported by the PEAKS Q module (Bioinformatics Solution Inc., version 8.0). The data were filtered, smoothed, and aligned in retention time, followed by feature detection based on peak volume and isotopic

clustering using the algorithm of PEAKS 8.0. An additional LFQ analysis using the spectral counts intensity (MS/MS or MS2) was employed for the same set of samples using the normalized weighted spectrum count option provided in "perSPECtives", (version 2.0.6, Proteome Software Inc., Portland, OR). The corresponding ".mzIdentML" files generated in Scaffold (version 4.7.3) for each "control" and "wounded" in both "stretched and non-stretched" sample categories were imported in "perSPECtives" where the threshold of 1 unique peptide/sample and the significance level of $P<0.05$ were set up with the standard Benjamini-Hochberg procedure.

The relative protein abundances were displayed as heat maps including representative proteins of each protein group after normalization of the corresponding weighted spectral counts using the built-in algorithm from "perSPECtives" (see Figure 5A and 10A). Only proteins, which passed a selected significance statistical threshold (ANOVA, $p<0.05$ and FDR <1% for protein and peptide expression) and are shown in the representative heat maps.

2.3.13 Gene ontology (GO), molecular and cellular pathways enrichment analysis

The biochemical and cellular pathways together with the GO assignments were generated by the ingenuity pathway analysis (IPA; Ingenuity Systems, Redwood City, CA, USA) on the list of differentially abundant proteins extracted from LFQ analyses (weighted and normalized MS2 spectral counts generated in Perspectives software) and presented categorized in the Supplementary Table 2. Specifically, the experimentally determined protein ratios, quantified using ≥ 1 peptides/sample, were used to calculate the experimental fold changes by rescaling their values using a log2 transformation, such that

positive values reflected fold increases while the negative values reflected fold decreases. For network generation, datasets containing gene identifiers (gene symbols) for the "control" and "wounded", for each "stretched" and "non-stretched" sample category samples were uploaded into the IPA application together with their rescaled log2 transformation MS2 normalized spectral counts ratios. The networks with qualified molecules were then algorithmically generated based on their connectivity index using the built-in the IPA algorithm. The probability of having a relationship between each IPA indexed biological function and the experimentally determined genes was calculated by a right-tailed Fisher's exact test. The level of significance was set to a P-value of <0.05. Accordingly, the IPA analysis identified the molecular and cellular pathways from the IPA library of canonical pathways that were most significant to the dataset (-log (p value)>2.0). For the quantitative analysis of protein expression profiles, IPA assigned the "z-score" function to all eligible canonical and cellular pathways (where a "z<-1.5 represent significant down-regulation while a z>1.5 represent a significant up-regulation of the selected pathway) (Figure 10 and Appendix A).

2.4 Results

2.4.1 Characterization of the Primary Lymphatic Muscle Cell Line

Lymphatic cells were isolated from the hindlimb of an adult sheep as outlined in the methods. As shown in Figure 6, the leg in which a section of a parallel lymphatic vessel had previously been resected is referred to as the "wounded leg" (WL). The contralateral limb was left uninjured and referred to as the "control leg" (CL). Cells usually began to migrate away from the vessel after 2-3 days in culture. Cells were initially identified

through morphology; LMCs which migrated off the vessel plated in the non-inverted configuration had a spindle like morphology while lymphatic endothelial cells (LECs) which migrated off the vessel plated in the inverted configuration had a cobblestone-like morphology.

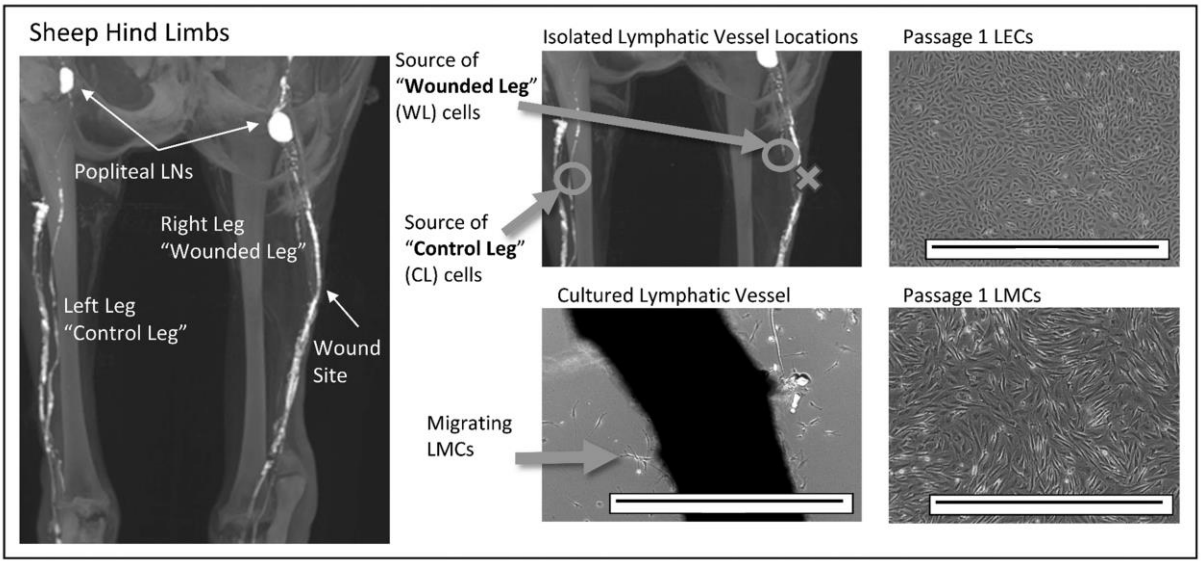

Figure 6: Isolation and morphological identification of lymphatic muscle cells (LMC) and lymphatic endothelial cells (LEC): MRI image of the lymphatics in the hindlimb of an adult sheep using a gadolinium contrast agent. There are two primary collecting lymphatic vessels that drain to the popliteal lymph nodes (LNs). A 1cm section of the caudal vessel in the "wounded leg" (marked with a "X") was removed. The intact, cranial, lymphatic vessel in the wounded leg (WL) and the corresponding intact vessel in the control leg (CL) were isolated at day 42 following surgery and plated in our standard DMEM with 4,500 mg/L of glucose and 10% FBS to produce lymphatic cell lines. Primary LMCs began to migrate from the non-inverted vessel by day 2-3 and had a spindle-like morphology. Primary LECs had a cobblestone-like morphology and were identified using similar methodology to LMCs but the vessel was inverted before plating. Both lines formed a monolayer once passaged. Scale bar is 1mm.

The purity of the primary lymphatic muscle line was determined using expression of four relevant proteins to differentiate endothelial cells from smooth muscle, cells as seen in Figure 7. Wells of lymphatic muscle cells were positive for smooth muscle actin (SMA), collagen type 1 (Col 1), and tropomyosin (TMy), while being negative for endothelial nitic

oxide synthase (eNOS). LECs were positive for eNOS while being negative for the other 3 markers (Figure 7). The differing protein expressions indicate successful separation of LECs and LMCs through the culturing and expansion technique used.

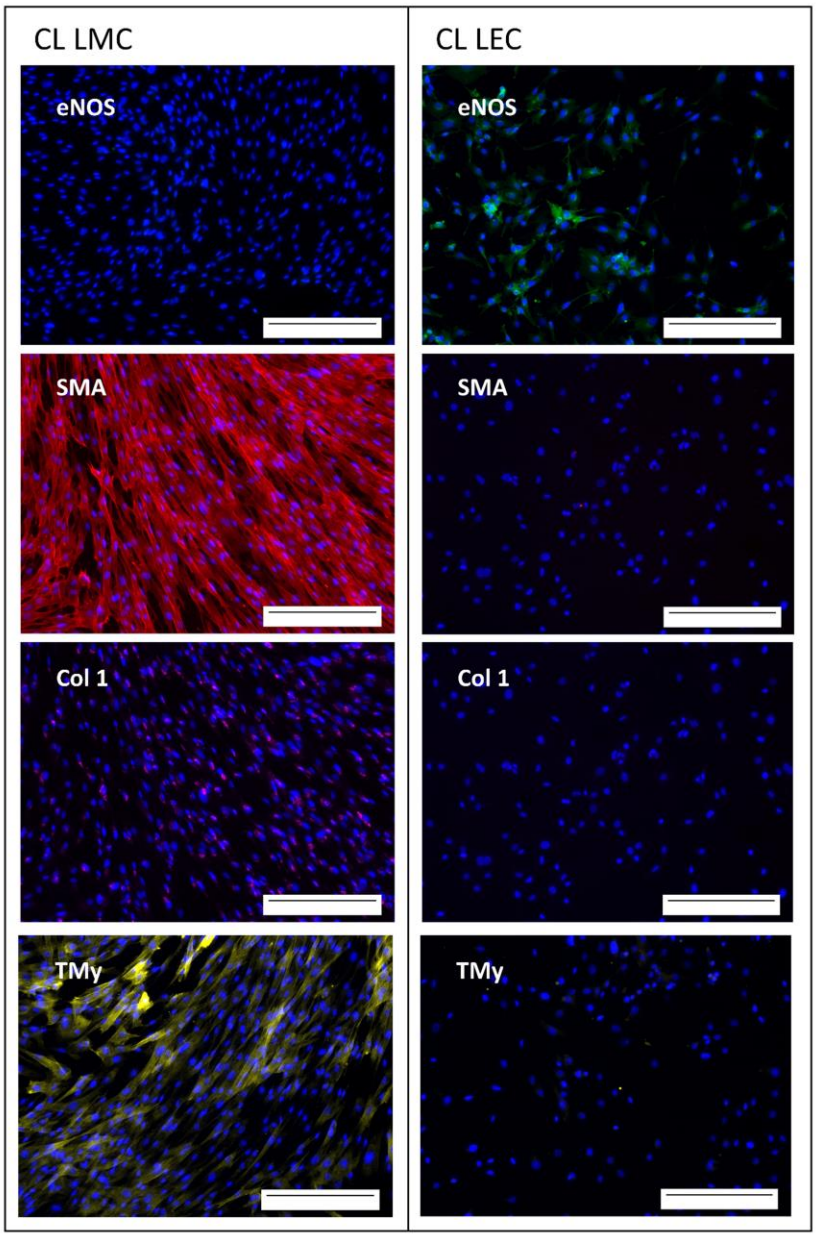

Figure 7: Purity of LMC and LEC lines derived from the control leg of adult sheep. CL LMC (left) had positive expression of smooth muscle actin (SMA) labeled red, collagen type 1 (Col 1) labeled magenta, and tropomyosin (TMy) labeled yellow after one week of culture. CL LEC (right) had positive expression of endothelial nitric

oxide synthase (eNOS) labeled green after one week of culture. Nucleus stained in blue. Scale bar is 0.25mm.

2.4.2 Optimizing Growth Conditions

The impact of changing levels of glucose and serum (FBS) within the DMEM on the phenotype of in-vitro cultured LMCs was systematically explored. Culture in low serum DMEM (LS DMEM), drastically impacted the phenotype of LMCs after two days. The cells took on a shorter spindle morphology and aligned less densely as seen by the SMA staining (Figure 8A & B). Low glucose DMEM (LG DMEM), had a negligible impact on morphology and cell density. Furthermore, metabolic activity and production of collagen were significantly reduced upon reducing serum concentrations but were unchanged when changing glucose levels alone (Figure 8C & D).

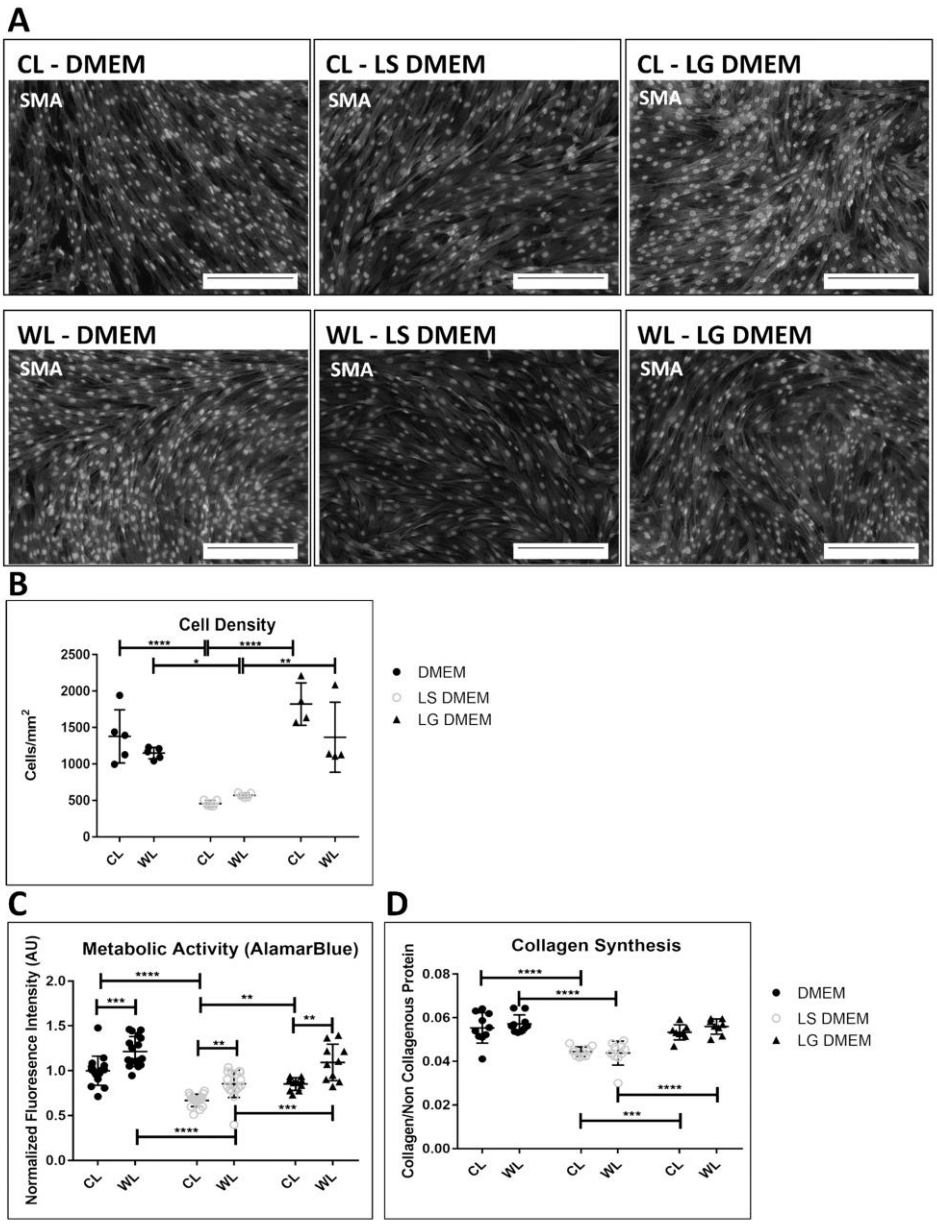

Figure 8: Impact of culture media on non-stretched CL and WL LMC phenotype. (A) CL LMC and WL LMC SMA expression depict shorter spindle morphology and (B) lower cell density after two day culture in low serum DMEM (LS-DMEM) with 0.2% FBS compared to standard DMEM (10% FBS, 4500g glucose/L) or low glucose DMEM (LG-DMEM) with 1000g glucose/L. (C) alamarBlue assay show reduction in fluorescence intensity and by extension, metabolic activity and (D) Sirius red/fast green assay show reduction in collagen production in CL and WL LMCs after two-day culture in LS-DMEM compared to standard DMEM and LG-DMEM. Error bars reflect standard deviation.

***: p<0.05, **: p<0.01, ***: p<0.001, ****: p<0.0001**

Despite similar cell densities (Figure 8B), wounded leg LMCs consistently had higher metabolic activity levels (Figure 8C) than CL LMCs, but their response to changes in the culture media followed a similar trend to the response of the control leg LMCs. The cellular source of the LMCs (WL vs. CL) had no measurable impact on expression of collagen after two-day cultures (Figure 8D).

2.4.3 Cyclic Stretching Impacts Alignment and Viability of LMCs

Cells were cultured in standard DMEM on the stretch device as shown in Figure 5A. After exposure to cyclic stretch for one-week, LMCs from control and wounded legs (CS and WS LMCs, respectively) were fixed and stained for F-actin (Figure 9A). Control leg or wounded leg LMCs that were not stretched (CNS and WNS LMCs respectively), did not align in any particular direction. When LMCs were stretched in media containing blebbistatin (abbreviated as "Bleb"), an inhibitor for myosin, there was not a dominant axis to which the cells regularly oriented. Images were processed and the extent to which all the fibers fell along a specific orientation was assigned a score as outlined in the methods section. Stretched LMCs cultured in standard DMEM were much more likely to be oriented in the 90^{o} direction compared to non-stretched cells and this orientation was lost with blebbistatin (Figure 9B&C).

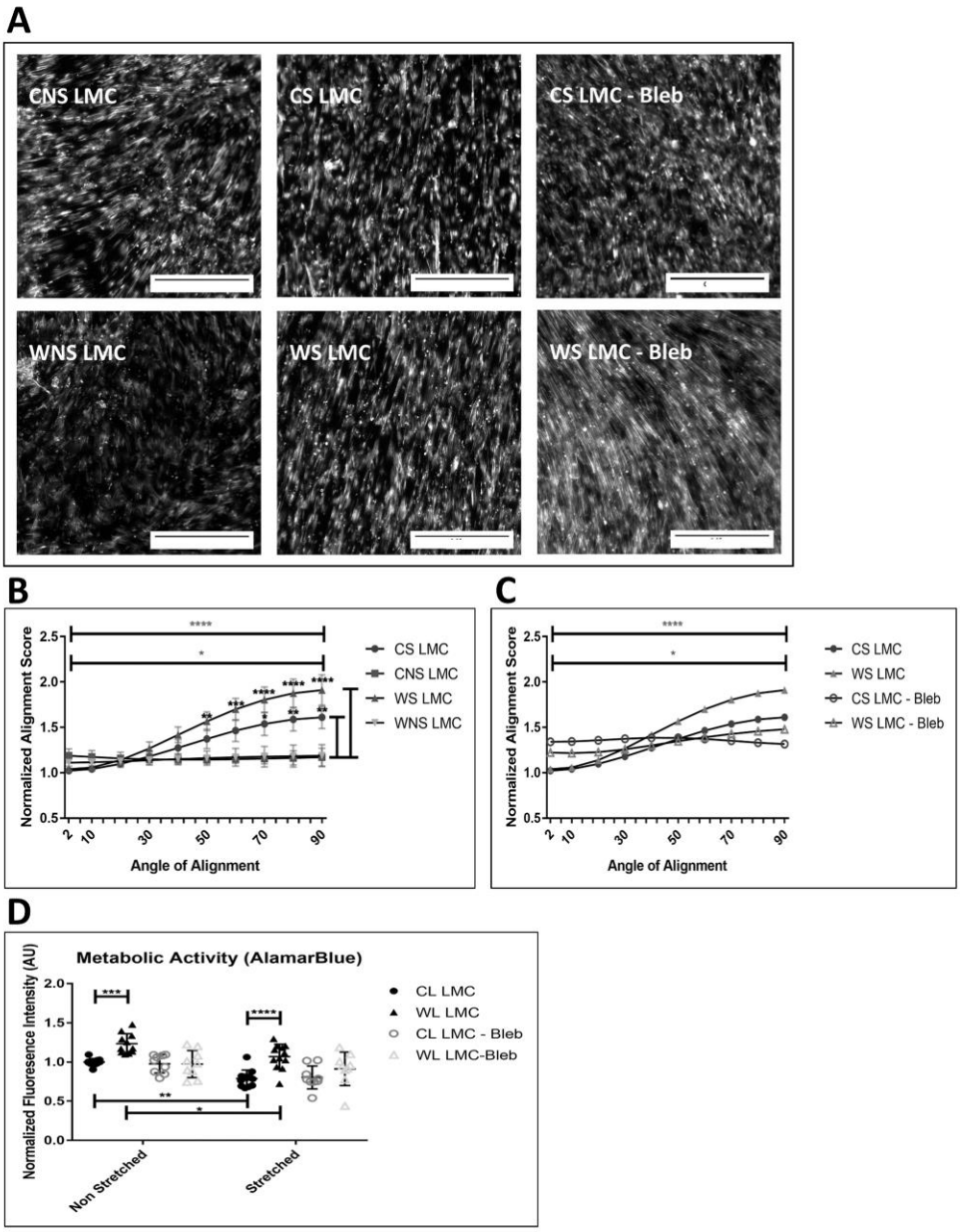

Figure 9: Impact of cyclic stretching on the alignment and metabolic activity in CL and WL LMCs. (A) Representative images of F-actin fiber orientation of stretched (CS) and non-stretched (CNS) CL LMCs and stretched (WS) and non-stretched (WNS) WL LMCs taken after 1 week. Scale bar is 0.25mm. (B) Quantification of F-actin fiber alignment for stretched and non-stretched LMCs. Preferential orientation perpendicular to strain (along 90º axis) is shown by comparing alignment score at 2º to alignment score at 90º for WS LMCs (top bar) and CS LMCs (2nd bar). Comparisons along the side are between the CS vs CNS LMCs and the WNS vs WS LMCs respectively. Error bars reflect standard error. There was no significant difference in the response between control and wounded LMCs (C) Blebbistatin (5μM) inhibited preferential alignment along 90º axis after cyclic strain. Error bars

are removed for clarity. (D) Impact of cyclic stretching on metabolic activity of LMCs cultured in Standard DMEM, and DMEM supplemented with Blebbistatin (5μM). *: p<0.05, **: p<0.01, ***: p<0.001, ****: p<0.0001

Results of alamarBlue assay showed significantly reduced fluorescent intensity, metabolic activity by extension, in both CS and WS LMCs compared to CNS and WNS, respectively. Culture in media containing blebbistatin inhibited any difference between the cell groups and their response to stretching (Figure 9D).

2.4.4 Phenotypic Impact of Cyclic Stretching

Proteomic analysis reveals much about the changing phenotype of the LMCs in response to cyclic stretch. Oxidative phosphorylation and mitochondrial function are displayed as one of the major pathways up-regulated for CL LMCs in response to stretch (Figure 10). "ATP synthase F0 subunit" is one of the highest up-regulated proteins in CS vs CNS (characterized by more than eight-fold increase in the expression profile). The F0 subunit of ATP synthase is a transmembrane, proton powered, rotating motor, which provides the energy to convert ADP to ATP in the F1 subunit. The IPA analysis of cellular networks identified the increased in cellular spreading, transport of metals and organ degeneration up-regulated in the CS vs CNS ($z>1.5$ and orange/red color). By contrast, the down-regulated cellular pathways in the CS vs CNS ($z<-1.5$ and blue/green color) identified the development of connective tissue together with cellular proliferation. Elevation of proteins such as cathepsin B (CTSB) and cathepsin D (CTSB) contribute to pathways associated with tissue degeneration. Reductions in the expression of tissue inhibitor of metalloprotease 1(TIMP1) allow for additional local matrix remodeling.

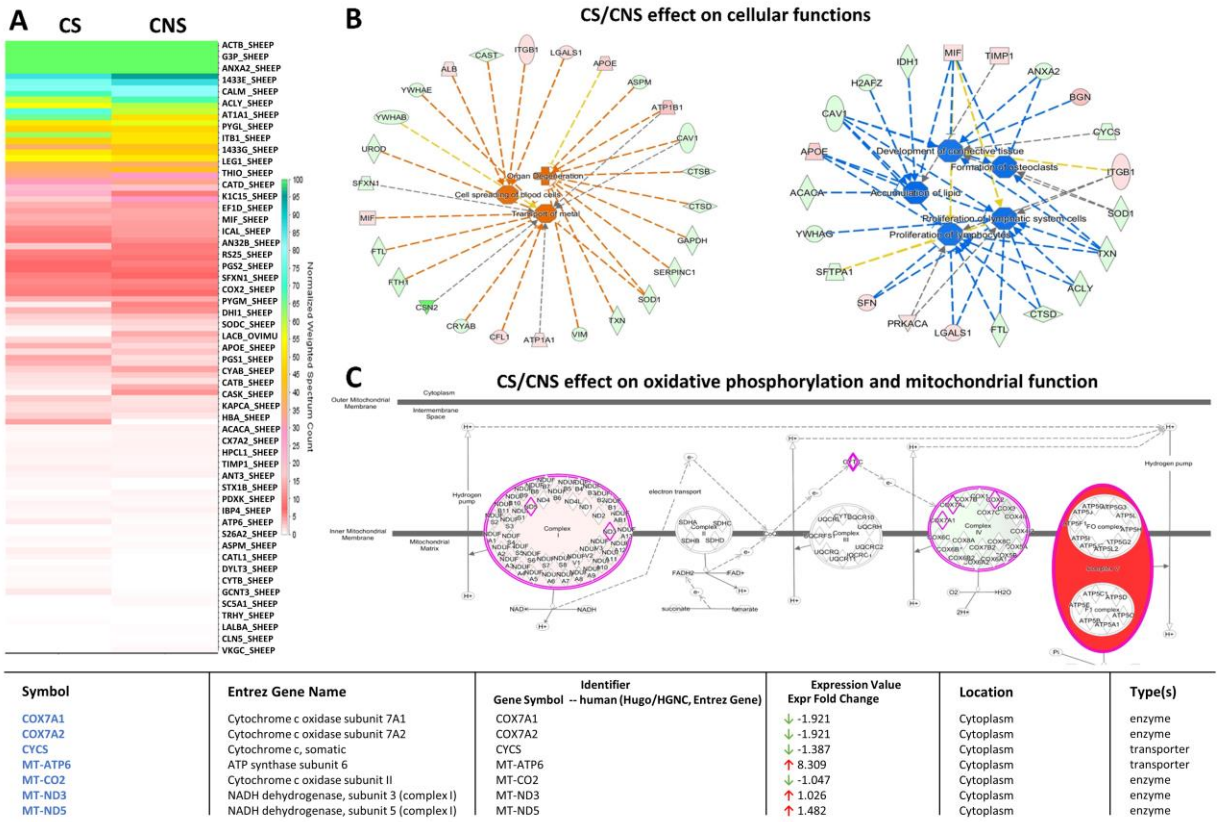

Symbol	Entrez Gene Name	Identifier Gene Symbol -- human (Hugo/HGNC, Entrez Gene)	Expression Value Expr Fold Change	Location	Type(s)
COX7A1	Cytochrome c oxidase subunit 7A1	COX7A1	↓ -1.921	Cytoplasm	enzyme
COX7A2	Cytochrome c oxidase subunit 7A2	COX7A2	↓ -1.921	Cytoplasm	enzyme
CYCS	Cytochrome c, somatic	CYCS	↓ -1.387	Cytoplasm	transporter
MT-ATP6	ATP synthase subunit 6	MT-ATP6	↑ 8.309	Cytoplasm	transporter
MT-CO2	Cytochrome c oxidase subunit II	MT-CO2	↓ -1.047	Cytoplasm	enzyme
MT-ND3	NADH dehydrogenase, subunit 3 (complex I)	MT-ND3	↑ 1.026	Cytoplasm	enzyme
MT-ND5	NADH dehydrogenase, subunit 5 (complex I)	MT-ND5	↑ 1.482	Cytoplasm	enzyme

Figure 10: Comparative protein expression profiling of "control stretched" vs "control non-stretched" in the lymphatic muscle cells. (A) Heat map highlights the change in the protein expression profiles in the "control-stretched (CS))" relative to the "control non-stretched (CNS)" lymph muscle cells. (B) Oxidative phosphorylation and mitochondrial function is displayed as one of the major pathways up-regulated (red-color) in the CS vs CNS sample. The "expression value" associated with each protein found in the experimental data set presented in supplementary table 1 highlights the "ATP synthase F0 subunit" as being top up-regulated protein in CS vs CNS (characterized by more than eight-fold increase in the expression profile). (C) The IPA analysis of cellular networks identified the increased in cellular spreading, transport of metals and organ degeneration up-regulated in the CS vs CNS (z>1.5 and orange/red color). By contrast, the down-regulated cellular pathways in the CS vs CNS (z<-1.5 and blue/green color) identified the development of connective tissue together with the cellular proliferation. The proteins in red and green had a significantly up- or down-regulated expression (p < 0.05), respectively. The shape of symbols denotes the molecular class of the proteins. A solid line indicates a direct molecular interaction, whereas a dashed line indicates an indirect molecular interaction.

As a result of stretch, specific functional pathways associated with protein trafficking, carbohydrate metabolism, cell death/survival, and others were determined for stretched or

non-stretched CL LMCs (CS vs CNS). The up or down-regulation of specific proteins associated with these functions are outlined in Figure 11.

A

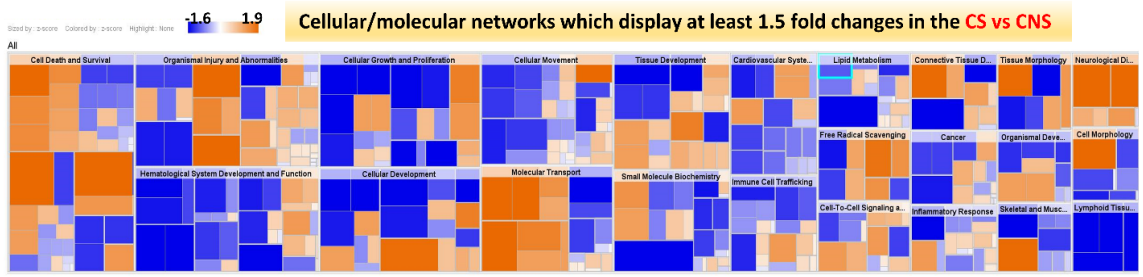

B

Increased activity

Categories	Diseases or Functions Annotation	p-Value	Predicted Activation St	Activation z-score	Molecules	# Molecules
Organismal Injury and Abnormalities	Organ Degeneration	5.90E-05	Increased	2.715	↑APOE, ↓ASPM, ↑ATP1B1, ↓CAV1, ↓CTSB, ↓CTSD, ↓GAPDH, ↓SERPINC1, ↓SOD1, ↓TXN, ↓VIM	all 11	11
Neurological Disease	Neurodegeneration	9.44E-05	Increased	2.637	↑APOE, ↑ATP1B1, ↓CAV1, ↓CTSB, ↓CTSD, ↓GAPDH, ↓SOD1, ↓VIM	all 8	8
Cell Death and Survival	necrosis of prostate cancer cell lines	3.10E-05	Increased	2.567	↓ACACA, ↓CAV1, ↑IGFBP4, ↑ITGB1, ↑LGALS1, ↓SOD1, ↓TXN	all 7	7
Cell Death and Survival	apoptosis of prostate cancer cell lines	1.22E-04	Increased	2.377	↓ACACA, ↓CAV1, ↑IGFBP4, ↑ITGB1, ↑LGALS1, ↓SOD1	all 6	6
Molecular Transport	transport of metal	2.80E-09	Increased	2.339	↑ATP1A1, ↑ATP1B1, ↓CAV1, ↑CFL1, ↓CRYAB, ↓CSN2, ↓FTH1, ↓FTL, ↑MIF, ↓SFXN1, ↓SOD1, ↓UROD, ↓YWHAB, ↓YW...	all 14	14
Molecular Transport	quantity of heavy metal	2.26E-05	Increased	2.200	↓CRYAB, ↓FTH1, ↓FTL, ↓SOD1, ↓UROD	all 5	5
Molecular Transport	quantity of metal	7.94E-08	Increased	2.011	↓ANXA2, ↑APOE, ↓CAST, ↓CAV1, ↓CRYAB, ↑DCN, ↓FTH1, ↓FTL, ↑LGALS1, ↑PRKACA, ↓SFTPA1, ↓SOD1, ↓UROD, ↓Y...	all 14	14
Cell Morphology, Cellular Movement	cell spreading of blood cells	2.87E-04	Increased	2.000	↑ALB, ↓CAST, ↑ITGB1, ↑LGALS1	all 4	4
Cell Death and Survival	cell death of lymphoma cell lines	3.18E-05		1.982	↑ALB, ↓ANXA2, ↓FTH1, ↑IGFBP4, ↑LGALS1, ↓YWHAG, ↓YWHAZ	all 7	7
Cellular Assembly and Organization, Cellular Function and Maintenance	organization of filaments	2.63E-07		1.980	↓ANXA2, ↑BGN, ↑CFL1, ↑DCN, ↓GAPDH, ↑ITGB1, ↓SERPINC1, ↓SOD1, ↓VIM	all 9	9
Neurological Disease, Organismal Injury and Abnormalities	gliosis	2.21E-04		1.969	↑APOE, ↓CAST, ↓CAV1, ↓CTSB, ↓SOD1	all 5	5
Connective Tissue Development and Function, Skeletal and Muscular Sy	quantity of bone cells	6.60E-04		1.910	↑BGN, ↓CAV1, ↑DCN, ↓HSD11B1, ↓SOD1	all 5	5
Cellular Development	differentiation of cells	1.69E-05		1.857	↓ACACA, ↓ACLY, ↑ALB, ↓ANP32B, ↓ANXA2, ↑APOE, ↓ASPM, ↑BGN, ↓CAST, ↓CAV1, ↑CFL1, ↓CTSB, ↑DCN, ↓GAPDH,	all 27	27
Free Radical Scavenging	synthesis of reactive oxygen species	6.81E-09		1.735	↑ACTB, ↑ALB, ↑APOE, ↓CAV1, ↓CRYAB, ↑DCN, ↓FTH1, ↓FTL, ↓IDH1, ↑ITGB1, ↑MIF, ↓MYLK, ↓SFTPA1, ↓SOD1, ↓YW...	all 15	15
Infectious Diseases	quantity of virus	9.41E-05		1.678	↓ANXA2, ↑APOE, ↑MIF, ↓SFTPA1	all 4	4
Carbohydrate Metabolism	synthesis of carbohydrate	1.62E-04		1.633	↓ALDH1A1, ↑APOE, ↓GAPDH, ↑GCNT3, ↑ITGB1, ↑MIF, ↓PGD, ↓PYGL, ↑SFN	all 9	9
Organismal Survival	organismal death	3.60E-08		1.545	↓ACACA, ↓ACLY, ↑ACTB, ↓ALDH1A1, ↑APOE, ↑ATP1A1, ↑ATP1B1, ↑BGN, ↓CAST, ↓CAV1, ↑CFL1, ↓COX7A1, ↓CRYAB,	all 33	33
Cellular Development, Cellular Growth and Proliferation, Nervous Systen	outgrowth of neurites	5.76E-04		1.520	↑APOE, ↑ITGB1, ↑LGALS1, ↑PRKACA, ↓SOD1, ↓TXN, ↓VIM, ↓YWHAZ	all 8	8

C

Decreased activity

Categories	Diseases or Functions Annotation	p-Value	Predicted Activation St	Activation z-score	Molecules	# Molecules
Lipid Metabolism, Molecular Transport, Small Molecule Biochemistry	accumulation of lipid	4.77E-04	Decreased	-2.381	↓ACACA, ↑APOE, ↓CAV1, ↓H2AFZ, ↓IDH1, ↑MIF, ↑TIMP1	all 7	7
Cellular Development, Cellular Growth and Proliferation, Connective Tissue Developme	formation of osteoclasts	1.56E-04		-1.982	↓ANXA2, ↓CAV1, ↑MIF, ↓SOD1, ↓TXN	all 5	5
Organismal Injury and Abnormalities	Fibrosis	4.92E-07		-1.946	↑ALB, ↑APOE, ↓CAV1, ↓CTSB, ↑DCN, ↓IDH1, ↑ITGB1, ↓ITGB6, ↑MIF, ↓SERPINC1, ↓SFTPA1, ↓SOD1, ↑TIMP1,	all 14	14
Cellular Growth and Proliferation, Lymphoid Tissue Structure and Development	proliferation of lymphatic system cells	1.42E-04		-1.893	↓ACLY, ↑APOE, ↓CAV1, ↓CTSD, ↓FTL, ↑ITGB1, ↑LGALS1, ↑MIF, ↑PRKACA, ↑SFN, ↓SFTPA1, ↑TXN, ↓YWHAG	all 13	13
Cellular Development, Cellular Growth and Proliferation, Hematological System Develc	proliferation of lymphocytes	2.43E-04		-1.708	↓ACLY, ↑APOE, ↓CAV1, ↓CTSD, ↓FTL, ↑ITGB1, ↑LGALS1, ↑MIF, ↑PRKACA, ↑SFN, ↓SFTPA1, ↑TXN	all 12	12
Connective Tissue Development and Function, Tissue Development	development of connective tissue	7.10E-04		-1.664	↓ANXA2, ↑BGN, ↓CAV1, ↓CYCS, ↑ITGB1, ↑MIF, ↓SOD1, ↓TXN	all 8	8
Cellular Development, Cellular Growth and Proliferation, Hematological System Develc	proliferation of immune cells	2.49E-05		-1.654	↓ACLY, ↑ALB, ↑APOE, ↓CAV1, ↓CTSD, ↑DCN, ↓FTL, ↑ITGB1, ↑LGALS1, ↑MIF, ↑PRKACA, ↑SFN, ↓SFTPA1, ↓TXNall 14	14
Cellular Growth and Proliferation	colony formation of cells	1.61E-04		-1.614	↓ALDH1A1, ↓CAV1, ↓CTSB, ↓CTSD, ↑DCN, ↓IGFBP4, ↑MIF, ↑SFN, ↓SOD1, ↑TES	all 10	10
Hematological System Development and Function, Inflammatory Response, Tissue Mc	quantity of phagocytes	2.78E-05		-1.606	↑APOE, ↓CTSB, ↑DCN, ↓HSD11B1, ↓ITGB6, ↑LGALS1, ↑MIF, ↓SFTPA1, ↓SOD1, ↑TIMP1	all 10	10
Cellular Development, Cellular Growth and Proliferation, Hematological System Develc	cell proliferation of T lymphocytes	6.05E-04		-1.604	↑APOE, ↓CAV1, ↓CTSD, ↓FTL, ↑ITGB1, ↑LGALS1, ↑MIF, ↑PRKACA, ↓SFTPA1, ↓TXN	all 10	10
Free Radical Scavenging, Small Molecule Biochemistry	metabolism of hydrogen peroxide	7.43E-06		-1.460	↑ALB, ↓CAV1, ↓CYCS, ↓SFTPA1, ↓SOD1, ↓TXN	all 6	6

Figure 11: Protein networks significantly regulated (p< 0.05) in the "control stretched" relative to the "control non-stretched" lymph muscle cells. The proteins were analyzed by Ingenuity Pathways Analysis (IPA, Ingenuity Systems) to determine the cellular pathways impacted by the stretched conditions relative to the non-stretched control in the lymph muscle cells. (A) Significantly regulated protein networks (p< 0.05) in the "stretched control (CS)" relative to the "non-stretched control (CNS)" lymph muscle cells are displayed as IPA predicted diseases and cellular functions map using the z score (down-regulated corresponding to z>-1.5 and blue color; up-regulated, corresponding to z>+1.5 and orange color). The size of each rectangle is proportional with the value of the z score associated to a specific pathway. (B) Increased (z>2.0) organismal injury, cell necrosis, transport of metals and cell spreading are the main cellular pathways characterizing the "CS" vs "CNS" system. (C) IPA predicted also a decreased (z>-2) in the lipid metabolism, molecular transport and small molecule biochemistry together with a decreased in the proliferation of lymphocytes and development of connective tissue characterizing the cellular pathways down-regulated in the CS vs CNS.

As outlined previously, both CL LMCs and WL LMCs generally become less active and more aligned in response to cyclic stretch, but notably the WL LMCs were found to maintain higher levels of oxidative phosphorylation and mitochondrial dysfunction after one week of stretch (Figure 12).

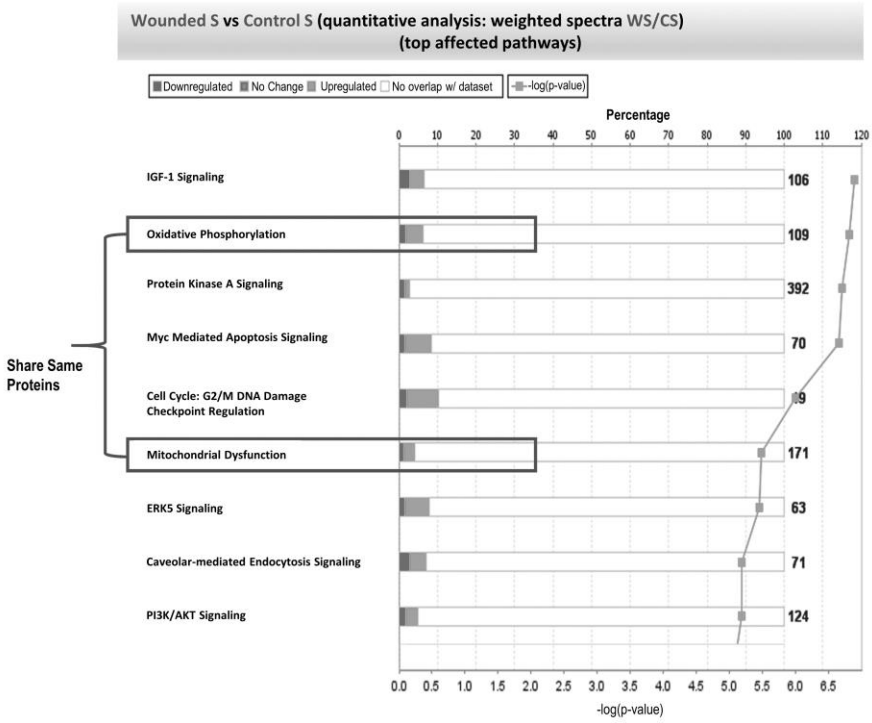

Figure 12: Quantitative analysis of protein expression profiles in the WS vs CS samples. The main canonical pathways affected by the top 105 protein genes presented in the supplementary table 2 for the WS vs CS samples were subjected to the analysis by IPA algorithm. The % of total molecules up- (light gray) or downregulated (dark grey) in each pathway are displayed. White is the total number of proteins in each pathway; which does not appear in our proteome. Each of the square dots on the histograms correspond to the -log(p-value), which act as a scoring function associated with each pathway and reflect the confidence of having the selected number of identified proteins IDs fitted to the IPA Knowledge-based canonical pathways.

Comparing stretched WL and stretched CL LMCs, the stretched WL LMCs are subjected to some biochemical and cellular changes characterized by significant changes in functions related as cell growth, survival, movement, and free radical scavenging (Figure 13A).

Figure 13 B&C indicate proteins contributing to a down-regulation in cellular movement, ions transport and homeostasis and significant up-regulation in some metabolic pathways, related to the generation of energy from lipids and nucleotides as well as activation of reactive oxygen species (ROS) and regulation of ROS (Figure 13).

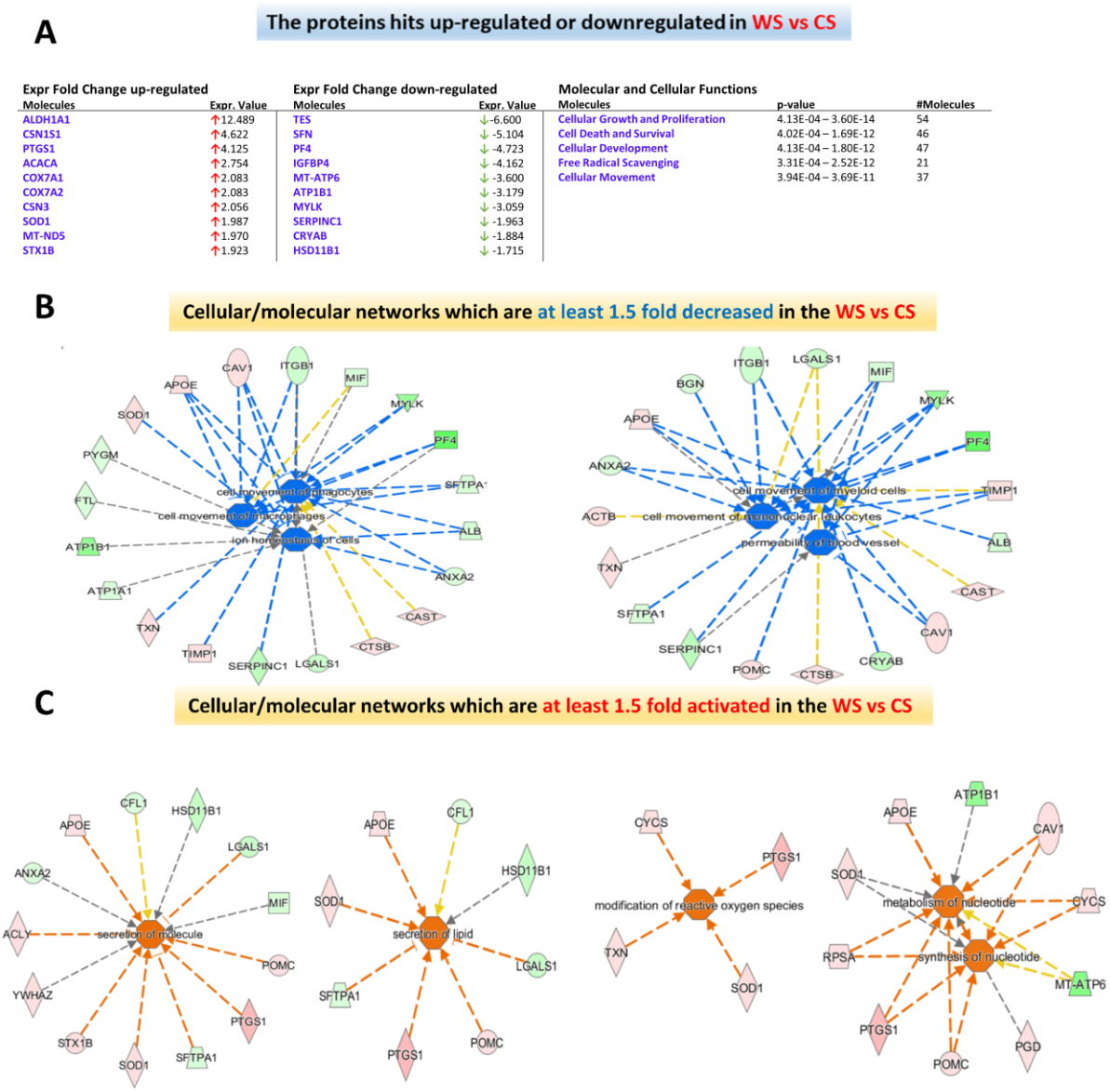

Figure 13: Protein Expression and protein networks of the WS vs CS samples. (A) Top protein hits characterized by at least 1.5-fold up- or down-regulation in the WS vs CS samples are displayed together with the molecular and cellular functions

predicted by IPA to be affected by changes in these protein expression profiles. (B) Significantly down-regulated protein networks (p< 0.05) in the "WS" relative to the "CS" lymph muscle cells are displayed as IPA predicted diseases and cellular functions using the z score (down-regulated corresponding to z<-1.5 and blue color). (C) Significantly up-regulated protein networks (p< 0.05) in the "WS" relative to the "CS" lymph muscle cells are displayed as IPA predicted diseases and cellular functions using the z score (up-regulated corresponding to z>1.5 and orange color).

By normalizing the signaling expression of the WL LMCs by the CL LMCs expression we can further demonstrate the distinct response of WL LMC to stretch when compared to control cells (Figure 14). Overall, proteomic analysis indicates that wounded stretched sample are predicted to be subjected to the loss of many intracellular signaling pathways responsible for preserving the ability of cells to move, proliferate or perform the normal metabolic reactions. Figure 14 outlines variably expressed proteins and canonical signaling pathways. Remarkably, the wounded and stretched state (WS) was characterized by a significant fivefold down-regulation of stratifin (SFN) (Figure 15 A&C), an adapter protein implicated in the regulation of a large spectrum of both general and specialized signaling pathways, including Phosphoinositide 3-kinase (PI3K) and Protein Kinase A (PKA) signalling[24]. In addition, at least a threefold down-regulation of myosin light chain kinase was induced in the WS as compared with the WNS lymph muscle cells (see expression profiles in Figure 15 F). Another important change induced in the WS samples was the threefold down-regulation of the ATP synthase F0 subunit (Figure 14C) that suggests impairment in the mitochondrial ability to couple ATP synthesis with the respiration.

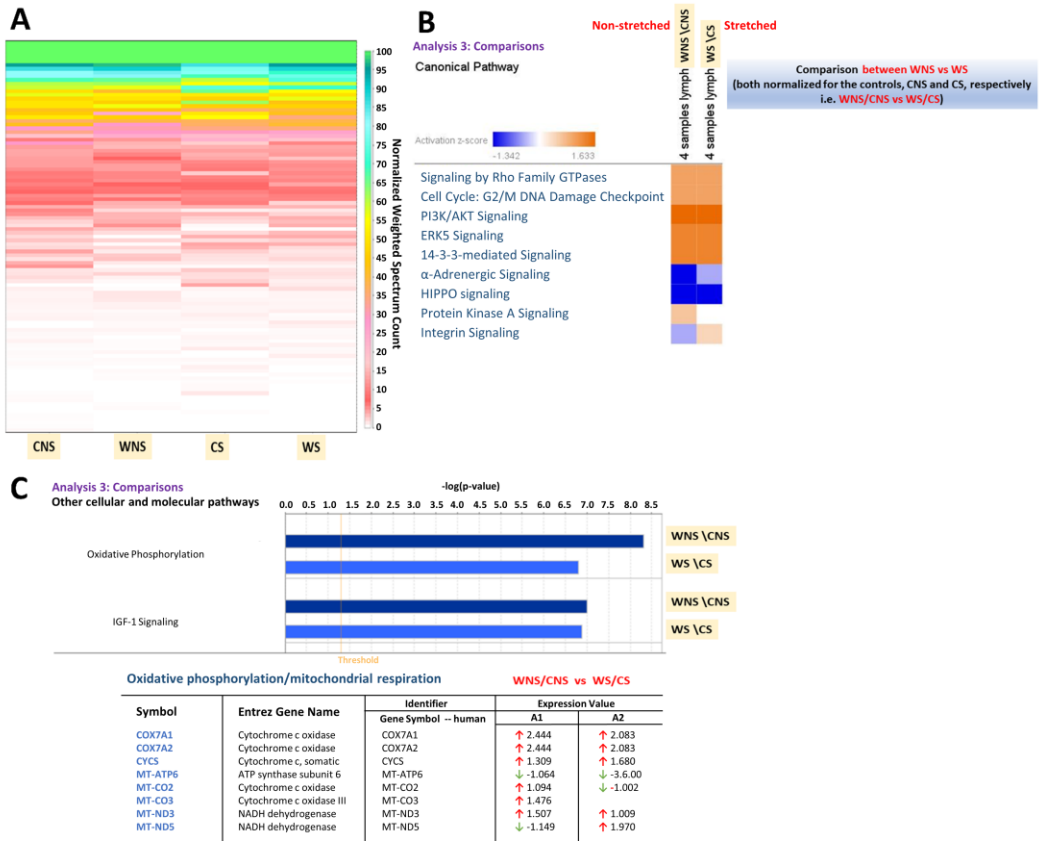

Symbol	Entrez Gene Name	Identifier	Expression Value	
		Gene Symbol -- human	A1	A2
COX7A1	Cytochrome c oxidase	COX7A1	↑ 2.444	↑ 2.083
COX7A2	Cytochrome c oxidase	COX7A2	↑ 2.444	↑ 2.083
CYCS	Cytochrome c, somatic	CYCS	↑ 1.309	↑ 1.680
MT-ATP6	ATP synthase subunit 6	MT-ATP6	↓ -1.064	↓ -3.6.00
MT-CO2	Cytochrome c oxidase	MT-CO2	↑ 1.094	↓ -1.002
MT-CO3	Cytochrome c oxidase III	MT-CO3	↑ 1.476	
MT-ND3	NADH dehydrogenase	MT-ND3	↑ 1.507	↑ 1.009
MT-ND5	NADH dehydrogenase	MT-ND5	↓ -1.149	↑ 1.970

Figure 14: Comparative protein expression profiling of "wounded/control stretched" vs "wounded/control non-stretched" in the lymphatic muscle cells. (A) Un-biased, non-clustered heat map generated in "perSPECtives" using the normalized weighted MS/MS spectral counts highlighting the change in the protein expression profiles in the stretched (CS) and non-stretched (CNS) controls vs stretched (WS) and non-stretched (WNS) wounded lymph muscle cells. (B) IPA generated comparison of the canonical biochemical pathways characterizing the WNS relative to the WS samples, each normalized to the corresponding controls (CNS and CS, respectively). Significantly regulated protein networks ($p < 0.05$) in the "non-stretched WNS" relative to the "stretched WS" lymph muscle cells are displayed as a heat map using the z score (down-regulated corresponding to $z<-1.5$ and blue color; up-regulated, corresponding to $z>+1.5$ and orange color). (C) Comparisons of other cellular and molecular pathways predicted by IPA display the oxidative phosphorylation/mitochondrial function and IGF-signaling as the major possible mechanisms mediating the wounded-stretched (WS) induced changes in the lymph muscle cells.

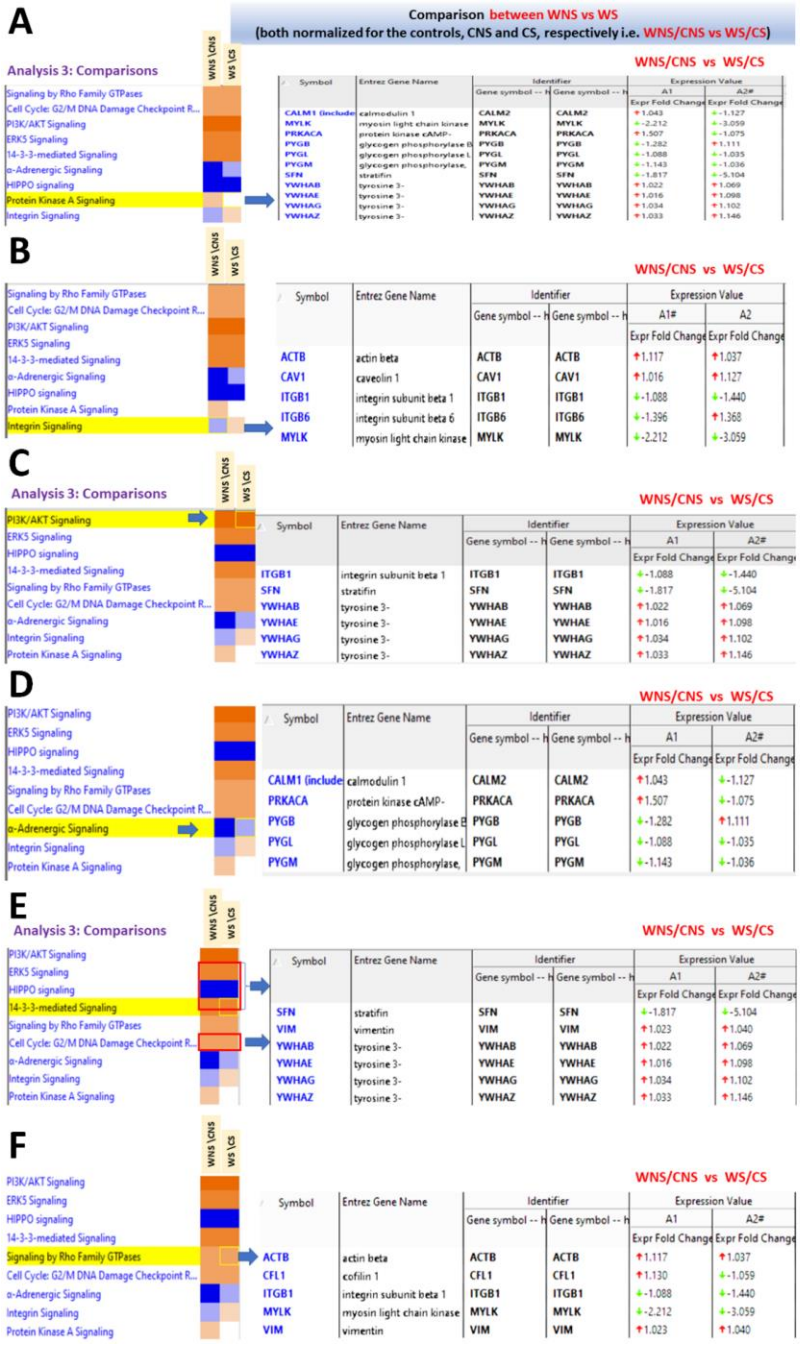

Figure 15: Detailed protein expression profiles analysis inside the biochemical pathways displayed in Figure 14B. (A) Up- regulation of protein kinase A signaling in the WNS conditions as compared with WS (arrow and expanded table). (B) Similarly, the details of the protein expression profiles inside the integrin signaling pathway, which activated in the WS vs WNS samples. (C) Up- regulation of PI3K/AKT signaling in the WNS conditions as compared with WS (arrow and expanded table). (D) Expression profiles inside the alpha- adrenergic signaling pathway which down-regulated in the WNS vs WS samples. (E) Up-regulation of 14-

3-3-mediated Signaling in WNS vs WS samples. (F) Up-regulation of rho family of GTP-ase signaling in the WNS conditions as compared with WS (arrow and expanded table).

2.5 Discussion and Future Work

Studies have begun to show that collecting lymphatic vessels remodel during the progression of disease states such as lymphedema. Collecting vessels isolated from patients with advanced lymphedema have been shown to become stenotic in lymphedemic limbs, with severity of lumen stenosis related directly to the stage of lymphedema[119]. This wall thickening seems to be due to remodeling of the lymphatic muscle cells, increasing in both cell proliferation and collagen synthesis within the walls as well as changing the protein composition of myosin[45]. This study presents a platform to both study the functional and molecular implications of this remodeling and to induce some of the features of the remodeling phenotype for further exploration in-vitro. We were able to successfully isolate LMCs from a lymphatic dysfunction model and established that the LMC lines used for this study were free of eNOS expressing cells such as lymphatic endothelial cells. We demonstrate that LMCs' behavior seems to change from a more quiescent phenotype to a more proliferative and active phenotype after vessel injury and that these differences persist in culture. A more quiescent phenotype seems to be restored partly in culture under low serum, reducing the LMC's metabolic activity, as indicated through the alamarBlue assay, and reducing the production of collagen. The LMC line derived from the wounded leg of the adult sheep seem chronically differentiated, expressing high cell metabolic activity. Functional assay results, in combination with elevated signaling pathways highlighted in the proteomic analysis, indicate the WL LMCs may be in a more dedifferentiated, proliferative phenotype. While collagen expression was not quantifiably higher, other types

of ECM protein synthesis and proteins integral to ECM remodeling should be explored in future studies.

In alignment with other work in smooth muscle cells, LMCs were particularly sensitive to serum levels. Lymph is rich in a variety of growth factors, and lymph spillage in addition to bleeding following lymphatic vessel or node resection may in part contribute to dedifferentiating the LMCs surrounding lymphatic vasculature[120,121]. While very little has been published on the effect of growth factors on LMC, vascular smooth muscle cell (VSMC) are very responsive to components of serum such as platelet-derived growth factor and insulin-like growth factor (IGF), which have been shown to induce proliferation, and migration in VSMCs. VSMC proliferation is accompanied by a loss in contractile force generation and increase in ECM synthesis[32,111,122]. Our work demonstrates that reducing serum levels restores aspects of a quiescent phenotype, similar to what's been documented with VSMCs in-vitro[101]. While growth factors have a beneficial effect on expansion of lymphatic endothelial cells, it is possible that their sustained release could impair LMC function and contractility, although such statements are currently speculative due to the lack of research currently published on LMC signaling. Targeted and strategically timed interventions to conserve or restore the contractile phenotype of LMCs may contribute to treating or preventing future lymphatic complications.

Recent work has thoroughly explored the phenotype of LMCs after being cultured in hyperglycemic and hyperinsulinemic conditions[123]. As the LMCs developed a resistance to insulin they also developed significant impairment to glucose uptake, mitochondrial function, ATP production, and other functional changes. The results from our study are largely in agreement with these findings as the response to changing glucose levels that

were previously observed were only apparent in the presence of insulin. Otherwise, the LMCs behaved quite similarly, regardless of glucose concentration in the media. Initially, introduction of high glucose media (25mM) lead to a short-term increase in glucose uptake, but glucose uptake lowered to initial rates within one-hour. This is slightly divergent to early work that explored in-vitro VSMC response to high glucose concentrations, which demonstrated that glucose levels alone lead to cell cycle progression and growth[124,125].

Exposure to cyclic stretch has been demonstrated to have a complex impact on VSMC phenotype [90] and this seems to hold true for LMCs as well. Cellular response and sensitivity to stretch depends on many factors including the magnitude and frequency of elongation, loading profile, coating of the wells, direction of the strain, duration of stretch, and the phenotypic state of the cell prior to loading[90]. A notable study showed that by using a stretching waveform that replicates the heart pressure waveform proliferation was actually inhibited by cyclic strain[126], despite purely sinusoidal strain typically enhancing proliferation in the majority of other 2D cyclic stretch studies[127–129]. With this in mind, our study attempted to design a waveform that was reflective of lymphatic physiology through choosing a frequency of 0.1 Hz and a percent elongation of 7.5%. These values reflect commonly reported of frequencies of lymphatic pumping in-vivo[130] and the passive diameter changes from pressurizing an isolated collecting vessel from low pressures (~2cmH_2O) to high pressures (≥6cmH_2O)[131]. Furthermore, the initial phenotype of a cell strongly influences its response to stretch. We demonstrate a notable differential response to stretch of the CL LMCs compared to WL LMCs, presumably due to different phenotypes of the LMCs prior to stretch, a phenomena noted in VSMCs as well[132].

Proteomic analysis of the CL LMCs and their response to cyclic stretching outlined in Figure 12-Figure 14, under normal conditions LMC are more quiescent and contractile than the LMC derived from vessels that have undergone active compensation due to a lymphatic injury. Higher expression of signaling pathways associated with oxidative phosphorylation and insulin-like growth factor-1 in WL LMCs, regardless of stretch, indicate that the differentiation of the WL LMCs in response to a local injury persist 6 weeks after the initial insult and are maintained even after several passages in vitro (Figure 14C). Both of these pathways have been found to be critical to the growth, proliferation, and survival of VSMCs[32,122,133,134]. This, in part may explain the increased sensitivity of CL LMCs to tissue degeneration and apoptosis in response to stretch (Figure 13). Furthermore, the WL LMCs consistently expressed lower levels of α-adgrenergic signaling proteins (Figure 14B), a pathway critical for regulation of vascular tone and constriction of vascular smooth muscle[135]. In response to stretch, WL LMCs down regulate MLCK, which may be correlated with a weaker contractile state and increased migration or growth[41]. The changes in PKA signaling further support this notion as PKA signaling has been found to inhibit proliferation in response to vascular injury in VSMC[136]. Down regulation of PKA signaling in the WL LMCs (Figure 14B) further indicate a commitment to growth, a common reaction to vessel damage, in response to cyclic loading.

Given the unique phenotype and function of LMCs, it is still unclear exactly how LMC remodeling impacts the unique lymphatic role of fluid drainage and immune cell regulation. Characterization of this sheep wound model in-vivo and the functional impact on intact lymphatic vessels will be the focus of future studies from our lab. Future experiments can build on this stretch platform to see how LECs influence LMC response

to stretch and to look for specific signaling pathways that can be interrupted to promote a specific response. This platform and the established findings provide a framework to begin to explore how interventions to maintain or restore a given LMC phenotype in the presence of pathological cues. The effect of interventions adopted from vascular research, such as rapamycin or calcium channel agonist, on LMCs can be effectively and systematically explored in future work.

CHAPTER 3. CHARACTERIZE SPROUTING LYMPHANGIOGENESIS SENSITIVITY TO EXTRACELLULAR MATRIX PROPERTIES USING A MODULAR POLY(ETHYLENE GLYCOL) (PEG) HYDROGEL.

3.1 Overview

Objective: After significant lymphatic damage, it is unclear how damaged collecting lymphatic vessels adapt and/or integrate back into the larger lymphatic network. Recent work has demonstrated that segments of lymphatic collecting vessel can be cultured within collagen gels. This causes lymphatic endothelial cells to proliferate from the vessel segment in a sprouting morphology. To engineer a regenerative scaffold to support collecting vessel regrowth, we have isolated and cultured segments of collecting lymphatic vessels within poly(ethylene glycol) (PEG) hydrogels with tunable properties to study the independent contributions of the physicochemical matrix properties to lymphatic collecting vessel regeneration.

Methods: Modular, vessel-encapsulating hydrogels were formed using a four-armed PEG macromer with maleimide groups at each terminus (PEG-4MAL) that are conjugated with cysteine-containing ligands and crosslinker. Lymphatic collecting vessels downstream to the lungs were isolated and then segmented into 1-2 mm segments and individually encapsulated into PEG-4MAL hydrogels. We examined the response of sprouting lymphangiogenesis to the stiffness, adhesive peptides, and protease dependent

degradability of the PEG and compared them to the response of segments cultured within native collagen type I gels of various concentrations.

Results: Fully degradable gels that were 10% PEG-4MAL and presented 2.0 mM RGD maximized branch length and branching number in PEG gels. Proliferation of cells occurred in both collagen gels and synthetic PEG-4MAL gels, with cells growing from the implanted vessel more rapidly in the collagen gels. Sprouts in the synthetic PEG-4MAL were more organized than in collagen and co-stained for ENOS, VEGFR-3, and SMA. The optimized gel was then used to demonstrate that sprouting lymphangiogenesis is sensitive to drugs used clinically in cancer chemotherapy and in lymphatic overgrowth syndromes in a concentration dependent fashion. These PEG gels were demonstrated to support the culture of lymphatic malformation tissue, where the clinical therapeutic rapamycin had a concentration dependent inhibition of cellular activity.

Conclusions: The properties of these synthetic hydrogels can be independently tuned, allowing greater control over the tissue microenvironment. We demonstrate the lymphatic collecting vessels are sensitive to the properties of extracellular matrix such as the relative stiffness, degradability, and adhesive peptides and that sprouting is optimized in a 10% PEG -2mM RGD gel compared to other tested formulations. Finally, a novel tissue-on-a-chip platform of lymphatic malformations with patient-derived tissue is presented for probing the tissue response to rapamycin treatment.

3.2 Motivation and Background

Functional lymphatics are critical for proper fluid homeostasis, immune trafficking, and organ function. For example, appropriate integration of lymphatics have been found to

be important for mediating the initial inflation of postnatal lungs[137] and influence the success of transplanted organs such as lungs or kidneys[138–140]. Despite their importance, our understanding of how lymphatics naturally repair after injury and respond to environmental cues *in-vivo* is lacking. As previously outlined, lymphangiogenesis is the process by which lymphatic endothelial cells (LECs) proliferate and form new vessels. Lymphangiogenesis has many parallels to angiogenesis, the formation of new blood vessels, and is promoted and inhibited by many of the same growth factors and signaling as the blood vasculature[58,72]. Unique to the lymphatic endothelial cells is a high surface expression of vascular growth factor receptor 3 (VEGFR-3), which binds most efficiently to its primary ligands, vascular endothelial growth factor C & D (VEGFC VEGFD)[63,141,142]. Unfortunately, naturally occurring lymphangiogenesis in response to inflammatory cues has often been show to worsen lymphatic dysfunction, in part by producing highly permeable, dysfunctional, initial lymphatics[61,143,144]. Examination of other environmental cues can allow for the promotion of lymphangiogenesis in the absence of other inflammatory signaling and independent of VEGFC to allow for finer control of the rate of lymphangiogenesis and the phenotype of the proliferating LECs.

Most work elucidating the molecular mechanism regulating lymphangiogenesis ex-vivo have cultured isolated LECs either in 2D culture or in collagen gels[63,145–148]. These studies have successfully showed novel pathways, such as the Notch signalling pathway, or signalling proteins involved in lymphangiogenesis[63,145] as well as the role of interstitial flow[149]. While impactful, these assays have several limitations. Most commercially available LEC lines are derived from initial lymphatics and there is evidence that LECs lining a lymphatic collecting vessel are functionally distinct from LECs that compose the

initial lymphatics. This includes a downregulation of LEC specific markers such as Lyve-1[150,151]. Therefore, lone culture of LECs derived from initial lymphatics are phenotypically distinct and may behave differently then LECs of the collecting vessel wall. Furthermore, culture of LECs alone prevents the study of how signalling between other cells of the collecting vessel wall influence lymphangiogenesis and repair mechanisms. While strides have been made in our understanding of mature collecting vessel formation in the developing embryo[152–155], in the context of postnatal lymphangiogenesis it is unclear if and how sprouts mature to include muscle cell coverage and valve development. Lymphangiogenesis originating from an injured collecting vessel is likely in the surgical model of lymph node resection, but this condition has not been well studied *ex-vivo*. This requires researchers to recreate the signalling between the LMCs and LECs, as well as other unique cell populations and components that make up the collecting vessel walls.

Some studies have begun exploring sprouting lymphangiogenesis in response to collecting vessel injury. In these studies, a segment or "ring" of a mature lymphatic collecting vessels can be cultured within hydrogels. Most studies with this approach have been done with a ring of the lymphatic thoracic duct cultured in collagen gels[57,156]. This collecting vessel approach allows us to examine the role of multicellular signalling on the rate and behaviour of sprout formation. Though few in number, these studies have shown the importance of matrix metalloproteinases, growth factors and their inhibitors in sprout formation in lymphatics vasculature.

While relatively new to the lymphatic community, a similar assay has been done to explore angiogenesis from blood vasculature for decades. The arteriole ring assay has contributed much to our understating of sprouting angiogenesis and the formation of new

blood capillaries from existing vasculature. In this assay a segment of artery is implanted within a hydrogel, such as collagen or Matrigel, and typically cultured for 6-10 days. This assay combines the repeatability of in-vitro experiments while allowing multi-cell signaling making it more relevant to the sprouting process in-vivo. These studies have shown how branching is dependent on contributions from a variety of cell types and processes to degrade the surrounding matrix and promote mature, lumen forming, sprouts[157–160]. Sprouting occurs most consistently from damaged areas of the vessel, with uninjured sections or the arterial ring being more quiescent[161]. In addition, sprouting occurs consistently even when the vessel is significantly damaged, with only full denudation of the endothelial cells typically inhibiting sprouting. The type and properties of ECM plays a large role on sprouting angiogenesis for two major reasons. First, the ECM composition plays a role in what proteases will be able to degrade the matrix allowing migration and proliferation of cells[162]. In addition, the integrin/ligand specific binding and consequent mechanotransduction feedback are critical for influencing the behavior and function of the sprouts[163]. Sprouts are generally broken into two states of the endothelial cells, tip or stalk cells. Tip cells are along the leading edge and are more migratory than proliferative. Stalk endothelial cells are more proliferative and less migratory and begin to form early lumens in these assays. Stalk regions of sprouts typically have pericyte cell coverage offering structural stability[164].

Culture of segmented lymphatic collecting vessels within collagen type I based hydrogels has been useful but is inherently limited. The properties of a collagen gel, such as stiffness degradability and availability of matrix binding sites, are all linked to the collagen density and therefore it is impossible to study the impact of these properties on

growth independently. Thus, we have implemented a poly(ethylene glycol) (PEG) based hydrogel to manipulate the microenvironment of lymphatic collecting vessel segments[78]. Specifically, modular, vessel-encapsulating hydrogels were formed using a four-armed PEG macromer with maleimide groups at each terminus (PEG-4MAL) that are conjugated with cell adhesive peptides and crosslinker. These gels are unique in that the density of the PEG, degradability, and adhesive peptides within the gel can be manipulated independently[78]. The modular capability of the PEG gel system allows us to decouple these properties of the ECM. In other studies of this platform, the components and density of the ECM alone have a significant impact on the behavior of tissue through specific integrin-ligand interaction[89,7877165]. Signaling cues from the ECM matrix properties can lead to drastic changes in the form and function of a cell[77]. In this study we systematically explore how matrix stiffness, degradability, and adhesive peptides on the function and response of sprouts from embedded lymphatic collecting vessel segments.

Once optimized to enhance lymphatic sprouting, we then demonstrate the use of this platform as an in vitro screen to assess the impact of a variety of drugs on lymphatic growth. This is done in two clinically relevant contexts: first we investigate the lymphangiogenic effects of chemotherapeutic compounds on collecting vessel sprouting; second, we test the mTOR inhibitor rapamycin on collecting vessel sprouting of both lymphatic vessels culture from segments from the rat as well as on freshly isolated human biopsies of lymphatic malformations, which is a rare lymphatic-specific overgrowth syndrome thought to be driven by somatic mutations in the PI3-AKT signaling pathway. Vascularization by both blood capillaries and lymphatics is critical to allow primary tumors to grow and eventually metastasize. While the target of chemotherapeutic drugs is typically the primary tumor, the

role of chemotherapy on lymphatic behaviour is an area of growing interest[19,69,166,167]. The capacity of these drugs to inhibit or promote "cross-talk" between the tumor and lymphatics is critical to better avoid metastasis to downstream lymph nodes, as well as to reverse the tolerogenic environment of the locally draining lymph node[146,168–170]. We hypothesize that our platform can be used to further explore the role of docetaxel and carboplatin, another common chemotherapeutic drug, on the lymphatic sprouting lymphangiogenesis phenotype.

We also examine rapamycin, a molecular inhibitor of mTOR, which impacts cell cycle progression and cell function. Rapamycin, also known as sirolimus, has been shown to directly impact the phenotype of vascular smooth muscle cells (VSMCs) and keep the muscle cells in previously described "contractile phenotype" in-vitro. This state is associated with lower proliferation, ECM synthesis, and improved expression of contractile molecular mechanisms[32,102,106]. Due to the similar changes observed occurring to LMCs during lymphedema, rapamycin may be useful in understanding the phenotypic changes of these cells. More immediately relevant is the increasingly common use of rapamycin to treat rare lymphatic and other vascular malformations[171,172]. While early clinical use has seemed promising at inhibiting unregulated lymphatic growth, the efficacy across the wide variety of clinical presentation, the long-term impact on lymphatic health, and what cell types within the LM are the primarily target are unknown. Early work in a mouse model of lymphatic dysfunction driven by overexpression of VEGF-C demonstrated that rapamycin reduces overexpression of VEGFR-3 and the lymphangiectasia by 76% within 7 days[171]. We demonstrate that our gels can be used as a high throughput method to culture

human, clinical lymphatic malformation tissue *in-vitro* in order to assess the impact of rapamycin on growth and activity.

3.3 Methods

3.3.1 Poly(ethylene glycol) (PEG)Hydrogel Formation

To prepare PEG hydrogels, PEG-4MAL macromer (MW 22,000; Laysan Bio) was dissolved in 4-(2-hydroxyethyl)piperazine-1-ethanesulfonic acid (HEPES) buffer (20 mM HEPES in DPBS, pH 7.4) at 2.5x the final density. Adhesive and cross-linking peptides were custom synthesized by AAPPTec. Adhesive peptides RGD (GRGDSPC), GFOGER (GYGGGP(GPP)5GFOGER (GPP)5GPC), RDG, or GAOGER were dissolved in HEPES at 10.0 mM (5X final ligand density) and mixed with PEG-4MAL at a 2:1 PEG-4MAL/ligand ratio to generate a functionalized PEG-4MAL precursor. After at least 15 min, the functionalized PEG-4MAL precursor solution was further diluted using HEPES buffer at a 3:1 functionalized PEG-4MAL/HEPES ratio. Bis-cysteine cross-linking peptide GPQ-W (GCRDGPQG↓IWGQDRCG; ↓ denotes enzymatic cleavage site) was dissolved in HEPES at 5X the density that corresponds to 1:1 maleimide/cysteine ratio after accounting for maleimide groups reacted with adhesive peptide. Non-degradable (or 0% degradable) gels were made by exchanging GPQ-W with the non-enzymatically degradable crosslinking agent, PEG-DT (1,4-dithiothreitol).

3.3.2 Lymphatic Isolation and Encapsulation

Isolation of Rat Lung Draining Lymphatic Vessels (LLV)

Lymphatic collecting vessels that drain downstream of the lungs, running alongside the left phrenic nerve, were isolated from surrounding soft tissue in the chest cavity of adult male Sprague Dawley rats. In brief, rats were euthanized and immediately shaved along the chest. The chest cavity was then carefully cut open and the lung and heart were gently pulled to the side, exposing the phrenic nerve located above the lungs. About 5-6mm of lymphatic collecting vessel that travels parallel to the nerve was mechanically separated from the surrounding fat tissue, taking care to keep the vessel from drying out by frequent application of Dulbecco's Phosphate-Buffered Saline (DPBS). After being cleaned from surrounding tissue, the vessel segment was removed and transported to a petri dish of DPBS for further cleaning and to be cut into roughly 300-micron long segments. To form hydrogels, an individual vessel segment was carefully placed into a solution of the cross-linking peptide in a 24 well plate. A solution of the adhesive peptide-functionalized PEG-4MAL macromer was then mixed in and allowed to polymerize for 15 min before the addition of growth medium. All animal procedures were performed in compliance with procedures approved by the Georgia Institute of Technology Internal Animal Care and Use Committee (IACUC).

Collection of Lymphatic Malformation Tissue

All procedures involved with the collection of lymphatic malformation samples were done in accordance with the accepted protocols submitted to the Internal Review Board (IRB) of Emory University and Georgia Institute of Technology. In brief, LM patients underwent percutaneous sclerotherapy of their lesions in Interventional Radiology. This procedure was done as part of the patient's routine care and not for research purposes. During the procedure, a tissue sample, one 18-gauge 2cm specimen, was taken for research

purposes. The tissue sample was not from discarded tissue. Lymphatic malformation segments were immediately transferred into DMEM/F12 solution containing 1% penicillin-streptomycin (p/s) after biopsies were taken from patients. Samples were typically several centimetres in length with a diameter of about 0.8-1mm and segmented into sections about 0.5mm long. In total, sample from 4 patients contributed to the presented work. Patients exhibited LM in a variety of anatomical locations including the neck, arm, left axilla and upper abdomen. Three of the four patients had been treated with rapamycin for some period of time prior to tissue collection. There were 3 females and one male patient ranging in age from 17 months to 19 years old.

3.3.3 Tissue Culture

Culture Protocol for LLV During Optimization of PEG Hydrogel Properties

Segments were cultured in our standard endothelial basal medium (EBM) formulation. This consisted of EBM (Lonza,) supplemented with 20% FBS, 1% penicillin-streptomycin-amphotericin B (Gibco), 1% Glutamax (Gibco), 0.1% DBcAMP (Sigma), and 0.1% hydrocortisone acetate (Sigma). Vessel segments were cultured for a total of 7 days and media was changed on days 3 and 5.

Culture Protocol for LLV to Assess Rapamycin Sensitivity

For lung draining CV experiments involving rapamycin (Sigma R8781), the 20nM or 100nM rapamycin suspended in EBM, was applied to cells starting either immediately after implantation (day 0) or on day 5 of culture. Control tissue segments were treated with

an equal volume of DMSO (0.1μL DMSO/1mL EBM) to control for the independent impact of DMSO on cell growth.

Culture Protocol for LLV to Assess Chemotherapy Drug Sensitivity

Lung draining CVs segments used for the chemotherapy experiments were cultured in the standard EBM formulation until day 5. At this point non-sprouting segments were discarded. Samples were treated with docetaxel (1μM in ethanol) or carboplatin (1μM in PBS) or in a vehicle control of ethanol.

Culture Protocol for LM to Assess Rapamycin Sensitivity

For lymphatic malformation tissue, samples were cultured in the standard EBM formulation until day 5. At day 5 the specified concentration of rapamycin or DMSO was applied to the sample and reapplied at day 8 before fixation at day 10. Samples that had not begun sprouting by day 5 were discarded.

3.3.4 Live/Dead Assay

Calcein-AM and Toto-3 (Thermo Fisher) were used as a live and dead stain, respectively, to determine the viability of the tissue within the hydrogel at day 7. Each stain was mixed with cell culture media at a 1:1000 ratio and incubated with the tissue samples at 37°C for 1 hour. Samples were rinsed with PBS before imaging via confocal microscopy followed by fixation in 4% paraformaldehyde (PFA) for 10 minutes. All stains were imaged with the same (5x) objective. Images that appear to vary in magnification are a 2x2 stitched tile composition, altering the size of the image but maintaining the same resolution for analysis.

3.3.5 Sprouting Analysis

Sprouting from vessel segments were analysed following the live/dead stain using image analysis code developed in MATLAB (Appendix B). Samples were imaged using confocal microscopy. This code binarized the max intensity projections of the live stain determined the sprout length and branching complexity. If samples did not test positive for the live stain they were not included in the sprouting analysis. The code requires the user to manually select the center of the implanted vessel segment and then set concentric squares around the selected point to determine the quantity of tissue along the perimeter. By assessing the percent of tissue vs blank space along the perimeter the max length of sprouts and number of individual sprouts could be assessed.

3.3.6 Cellular Metabolic Activity

Given the large size of the sprouting network for lymphatic malformation tissue, metabolic activity was used to assess the impact of rapamycin on cellular growth and viability. The reduction-oxidation indicator known as alamarBlue® (ThermoFisher) both fluoresces and undergoes a colorimetric change in response to cellular metabolic activity. Each well was incubated in media containing 10% alamarBlue® reagent for 2 hours. After the 2 hours, 100μL of the media from each well was transferred to a 96-well plate. The fluorescent intensity of each sample-including well was measured using a plate reader (Synergy H4) after excitation with a 562nm wavelength laser.

3.3.7 Immunostaining and Imaging

Fixed tissue samples within the gels were permeabilized with 0.5% Triton-X for 20 minutes and then rinsed 3 times. After the third rinse, samples were blocked for 1 hour in a phosphate buffered saline solution containing 10% goat serum and 2% bovine serum albumin. The blocking solution was then removed, and samples were incubated with primary antibodies suspended in a 2% BSA solution (1:200) were incubated with the samples overnight at 4C on a rocker. The samples were then rinsed three times and then rocked in a solution of secondary antibodies (1:400) for two hours at room temperature. After a final three rinses the samples were then imaged using confocal microscopy.

3.3.8 Statistics

GraphPad Prism version 7.01 was used for statistical analysis. Kruskal-Wallis test followed by Dunn's multiple comparisons test were used for comparisons between multiple experimental groups at the end of each culture period. All analyses were considered statistically significant at $p<0.05$. Error bars on all data points are standard deviation. Grubbs test for statistical outliers was used to remove one outlier from the 1.00mg/mL collagen gel condition.

3.4 Results

3.4.1 Assessment of Sprouting Response in Collagen Gels of Various Concentrations

Segments of lung-draining lymphatic collecting vessels were implanted into collagen gels at 4 different concentrations of collagen: 1.00 mg/mL, 1.87 mg/mL, 3.00 mg/mL, and 3.50 mg/mL. Generally, as the collagen concentration increased the resulting

sprout length was reduced (Figure 16). The average number of sprouts was only significantly reduced at the highest tested concentration of 3.50 mg/mL.

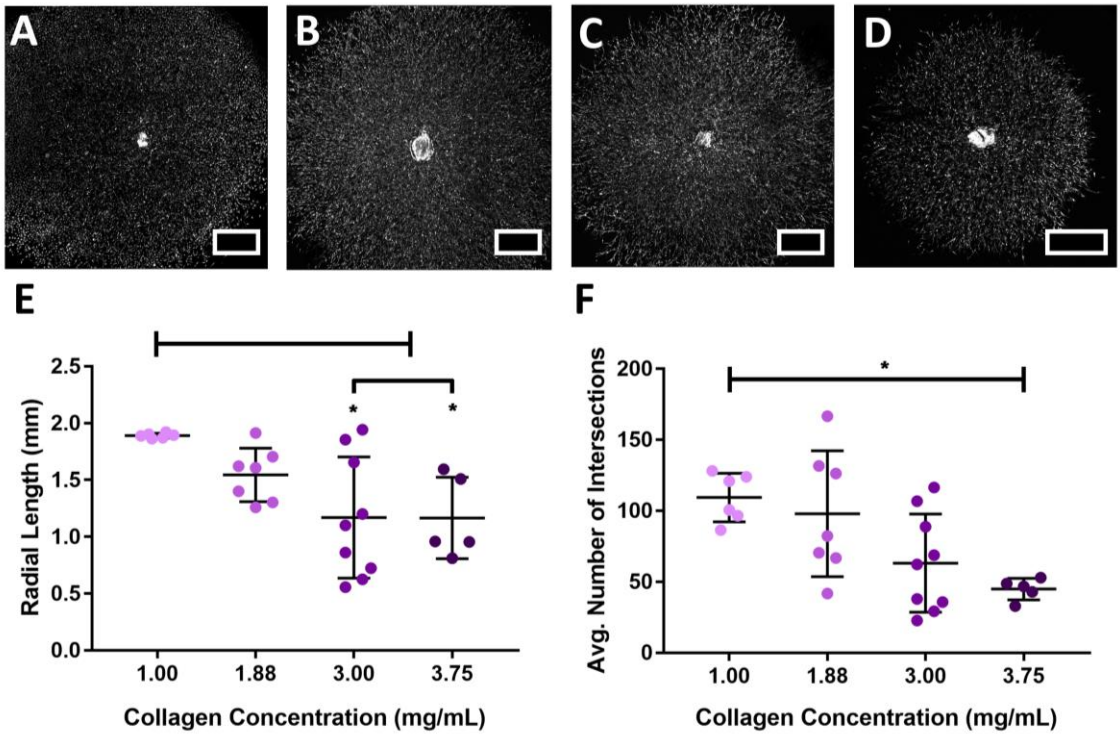

Figure 16: Impact of Collagen Concentration on Sprouting Phenotype. Representative images of collecting vessel segments sprouting at day 7 in A) 1.00 mg/mL, B) 1.88 mg/mL, C) 3.00 mg/mL, and D) 3.75 mg/mL collagen gels, respectively. Images are of intracellular fluorescent calcein indicating live cells. Scale bar = 500μm. E) Collagen concentration of 1.00mg/mL had significantly increased sprout length compared to concentrations of 3.00mg/mL or 3.75 mg/mL. F) There was a significant decrease in the average number of sprouts 3.75mg/mL gels compared to 1.00mg/mL. Significance was determined via Kruskal-Wallis test followed by Dunn's multiple comparisons.
***: p<0.05**

3.4.2 Assessment of Sprouting Response in PEG Hydrogel Formulations

Segments of lung-draining lymphatic collecting vessels were implanted into the hydrogels of different formulations. The sprout properties were quantified to determine

max length of sprouts and the average number of sprout branches formed moving away from the vessel core.

LLV segments were sensitive to the weight percentage of PEG macromers within the synthetic hydrogel. The length of sprouts within the PEG hydrogel was maximum at a 10% weight percentage compared to 6% or 12% weight percentage (Figure 17). The number of sprouts branching from the embedded segment were enhanced at tested values above 6%. All PEG hydrogels used to test various percentages of PEG density contained 2mM concentrations of RGD, which facilitated cell adhesion within the gels and were crosslinked with the enzymatically degradable GPQ-W crosslinker.

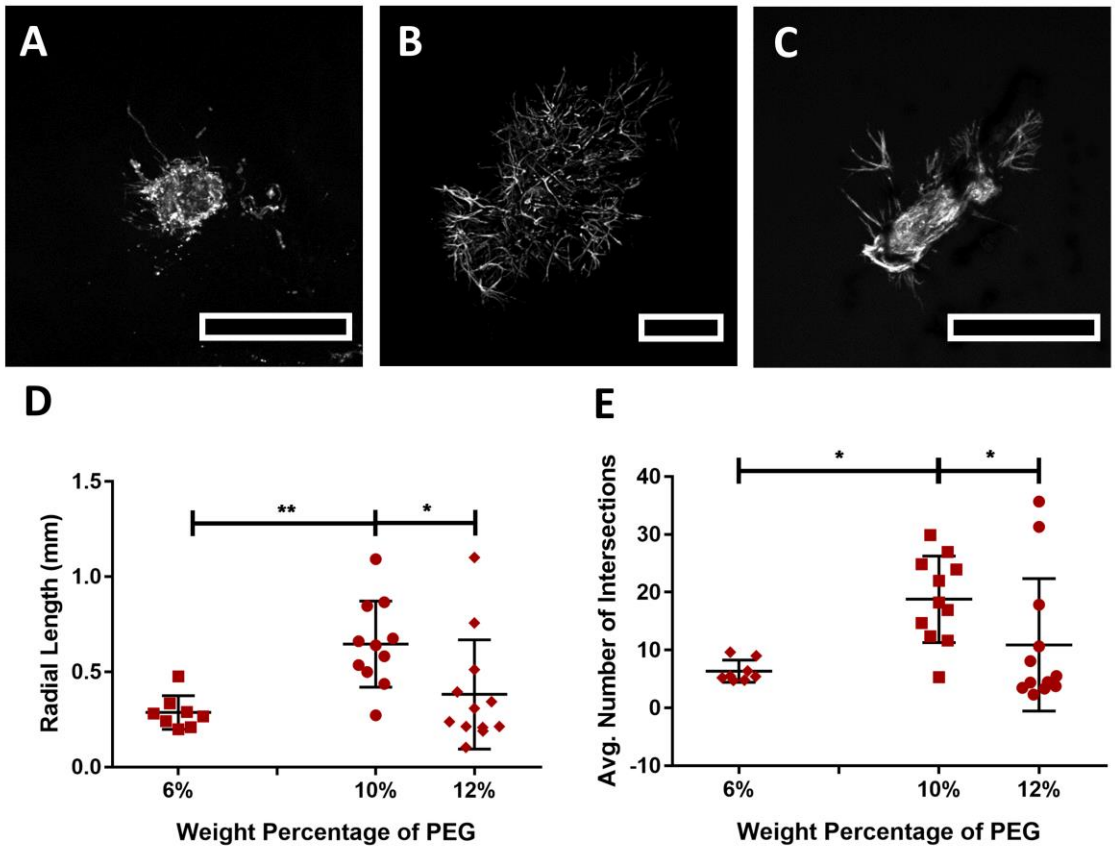

Figure 17: Impact of PEG Weight Percentage on the Sprouting Phenotype in fully degradable, 2mM RGD Hydrogels. Representative images of collecting vessel

segments at day 7 cultured in A) 6% PEG, B) 10% PEG, and C) 12% PEG gel conditions. Images are of intracellular fluorescent calcein indicating live cells. Scale bar = 500μm. D)10% PEG optimized the radial sprout length from imbedded vessel segments at day 7 compared to 6% and 12% PEG. E)10% PEG improved the average number of sprouts. Significance was determined via Kruskal-Wallis test followed by Dunn's multiple comparisons.
***: $p<0.05$, **: $p<0.01$**

LLV segments in PEG hydrogels with tethered RGD peptides, which facilitate cell adhesion and migration, exhibited significantly higher sprouting when compared to the two scrambled negative control peptides, RDG and GAOGER, that do not allow for cell adhesion (Figure 18). PEG hydrogels tethered with the collagen derived GFOGER peptides did not support the same length or complexity of branching sprouts, and in fact produced sprouting that was not statistically different from the scrambled negative controls. Notably, PEG gels with the scrambled peptides allowed for low levels of sprouting seen on day 7 of culture. All adhesive peptides were at a 2.0mM concentration within a fully degradable 10% PEG hydrogel.

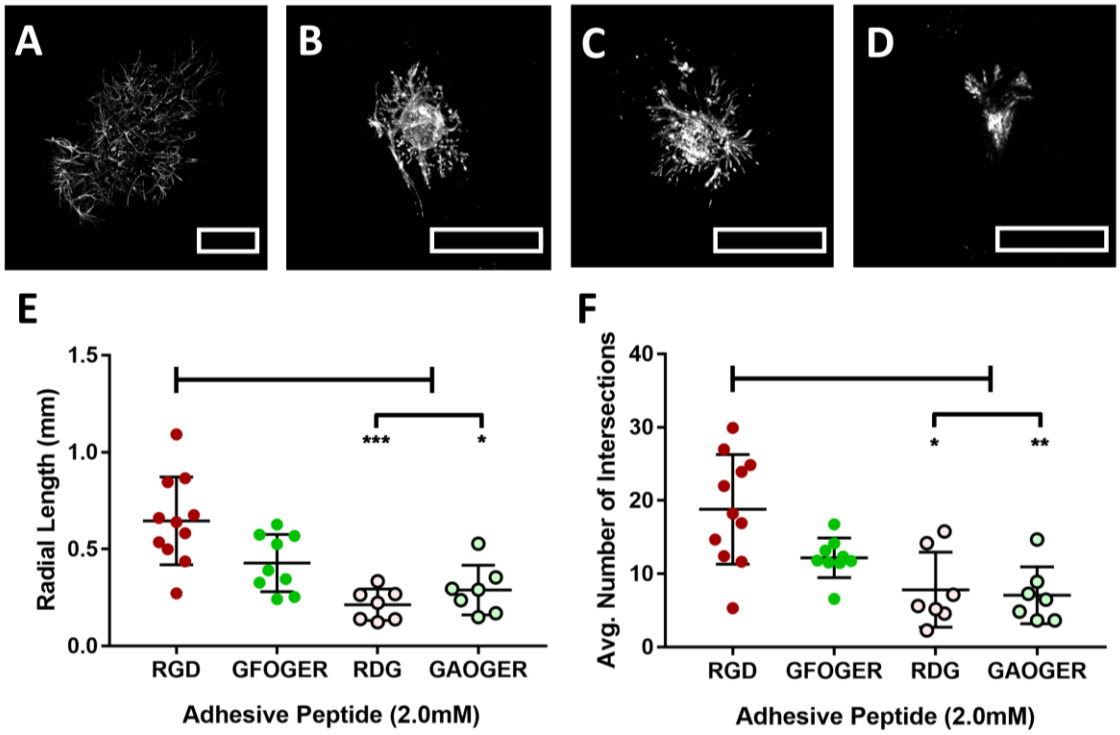

Figure 18: Impact of Adhesive Peptide Type on the Sprouting Phenotype in fully degradable, 10% PEG Hydrogels. Representative images of collecting vessel segments at day 10 cultured in A) 2mM RGD, B) 2mM GFOGER, C) 2mM RDG, and D) 2mM GAOGER conditions. Images are of intracellular fluorescent calcein indicating live cells. Scale bar = 500μm. The RGD adhesive peptide optimized the E) max sprout length and the F) average sprout number from the imbedded tissue on day 7 compared the GFOGER adhesive peptide and the 2 scrambled, negative control peptides, RDG and GAOGER. Significance was determined via Kruskal-Wallis test followed by Dunn's multiple comparisons.
***: p<0.05, **: p<0.01, ***: p<0.001**

Concentration of RGD was gradually reduced from 2.0mM to 0.0mM. To maintain full crosslinking of maleimide groups, RDG was used to replace the RGD as the concentration was stepped down such that the total concentration of both peptides combined was always 2.0mM. All tested concentrations of RGD above 0.0mM had statistically equivalent levels of sprouting by day 7 (Figure 19). Sprout length and average number of sprouts were not significantly different at tested concentrations. All hydrogels

used to determine optimal RGD concentration were fully degradable and were 10% PEG by weight volume.

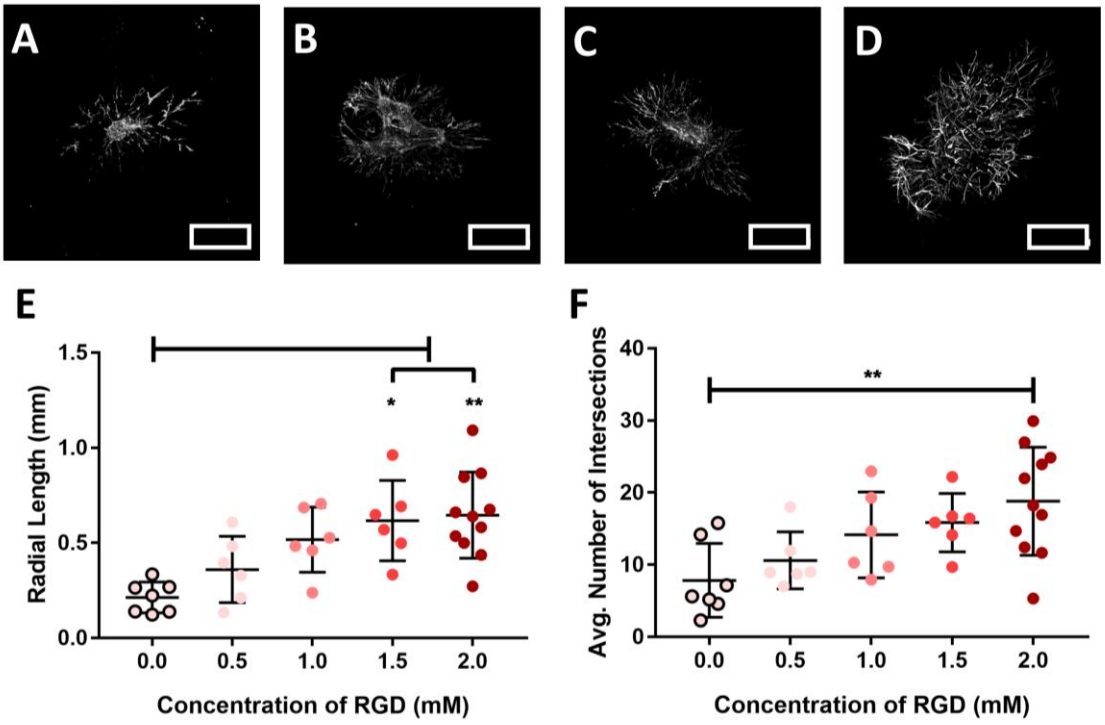

Figure 19: Impact of RGD Concentration on the Sprouting Phenotype in fully degradable, 10% PEG Hydrogels. Representative images of collecting vessel segments at day 10 cultured in A) 0.5mM RGD, B) 1.0mM RGD, C) 1.5mM RGD and D) 2.0mM RGD conditions. Images are of intracellular fluorescent calcein indicating live cells. Scale bar = 500μm. There was no significant change in E) radial sprout length or F) sprout number at tested concentrations above 0.0mM RGD. Significance was determined via Kruskal-Wallis test followed by Dunn's multiple comparisons.
***: p<0.05, **: p<0.01**

Finally, the impact of gel degradability on sprouting phenotype was explored (Figure 20). By altering the ratio of the fully degradable, GPQ-W, crosslinker, with a non-degradable, PEG-DT, crosslinker we could alter the overall degradability of the gel. Fully, 100% degradable gels were crosslinked entirely with GPQ-W while 0% degradable gels were crosslinked with PEG-DT. Fifty percent degradable gels were crosslinked with a 1:1

ratio of GPQ-W and PEG-DT. The fully degradable gel allowed for significantly longer and more numerous sprouts than a 50% less degradable hydrogel or completely non-degradable gel. This property was explored in 10% PEG hydrogels with 2mM RGD.

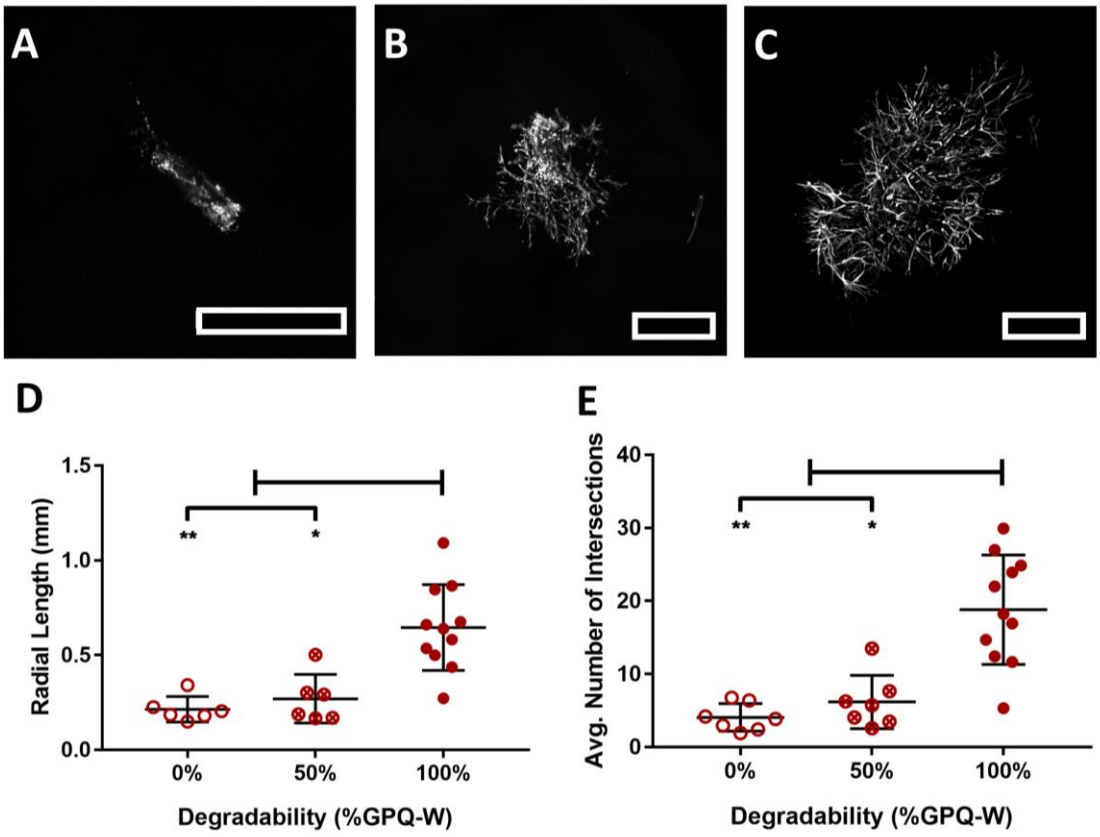

Figure 20: Impact of Gel Degradability on the Sprouting Phenotype in 10% PEG – 2mM RGD Hydrogels. Representative images of collecting vessel segments at day 10 cultured in A) 0% degradable, B) 50% degradable, and C) 100% degradable conditions. Images are of intracellular fluorescent calcein indicating live cells. Scale bar=500μm. D) Lymphatic collecting vessels cultured with 0% of 50% degradability had significantly reduced max sprout length by day 7 compared to the fully (100%) degradable condition. E) Lymphatic collecting vessels cultured with 0% of 50% degradability had significantly reduced average number of sprouts coming from the implanted vessel segment by day 10 compared to the fully (100%) degradable condition. Significance was determined via Kruskal-Wallis test followed by Dunn's multiple comparisons.
***: p<0.05, **: p<0.01, ***: p<0.001, ****: p<0.0001**

3.4.3 Phenotype of Segment and Sprouting Tissue

Compared to the collagen gels, sprouts in the PEG hydrogels appear to be more organized, with multiple cells aligning into a single sprout extension (Figure 21). Cells in the collagen gel do not appear to organize into any complex, organized, structures. Sprouting lymphatic segments were stained for a variety of markers to assess cell type and phenotype. Alpha-smooth muscle actin (SMA) should stain either LMCs or myofibroblast that reside within the wall, while vascular endothelial growth factor 3 (VEGFR-3) and endothelial nitric oxide synthase (eNOS) staining was used to identify lymphatic endothelial cells (LECs). In the collagen gel (1.88mg/mL), the vessel core remained positive for VEGFR-3 and eNOS positive lymphatic endothelial cells. While cells away from the vessel core were generally not eNOS positive in the collagen gels, they were generally positive for either SMA or VEGFR-3. VEGFR-3 and SMA cells were generally not organized along a "sprout" but spread out along the gel. In the 10% PEG – 2mM RGD hydrogels sprouts expressed eNOS at a much higher intensity and uniformity than in the collagen gel (Figure 21). In addition, the SMA, VEGFR-3, and eNOS positive cells colocalize along the sprouts.

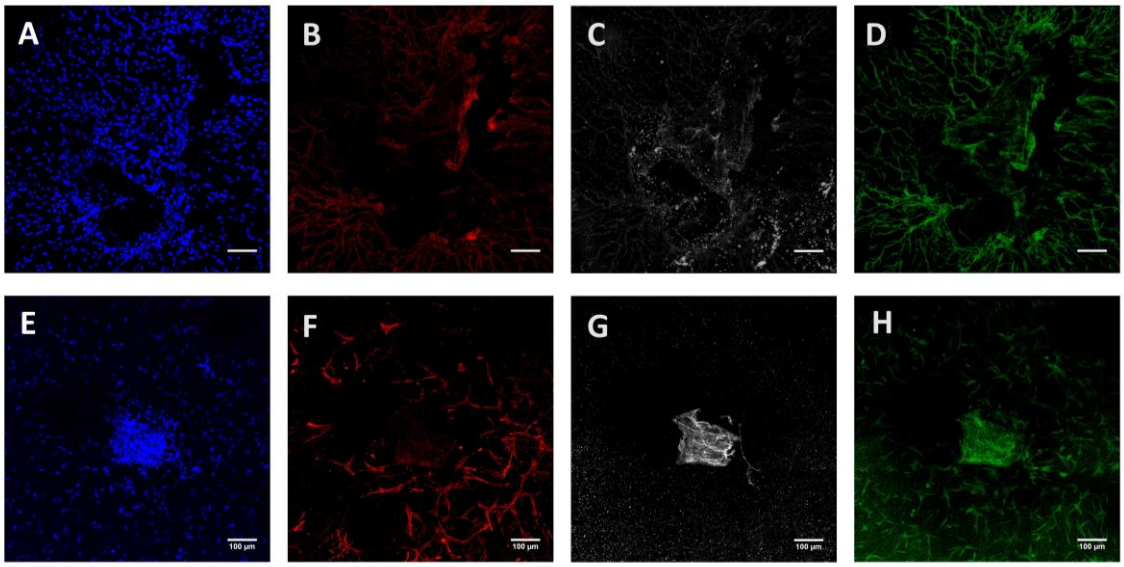

Figure 21: Representative Stains and Images of Lymphatic Vessel Segments Cultured in hydrogels. A-D) Stains of vessel segments cultured in fully degradable, 10%PEG – 2mM RGD hydrogels for nuclei (blue), α-smooth muscle actin (red), endothelial nitric oxide synthase (gray), and vascular endothelial growth factor receptor-3 (green), respectively. E-H) Similar staining for vessel segments cultured in collagen gels (1.88mg/mL). Scale bars=100µm

3.4.4 Impact of Chemotherapy Drugs on Sprout Phenotype

Lymphatic collecting vessels cultured in the fully degradable, 10%PEG – 2mM RGD, hydrogel conditions were cultured in the established endothelial basal media until day 5. At day 5, sprouting segments were treated with docetaxel (doc), carboplatin (carb), or a vehicle control as outlined in the methods until day 10. Docetaxel significantly halted lymphatic sprout growth (Figure 22). In contrast, carboplatin had no consistent impact on sprout formation compared to the control.

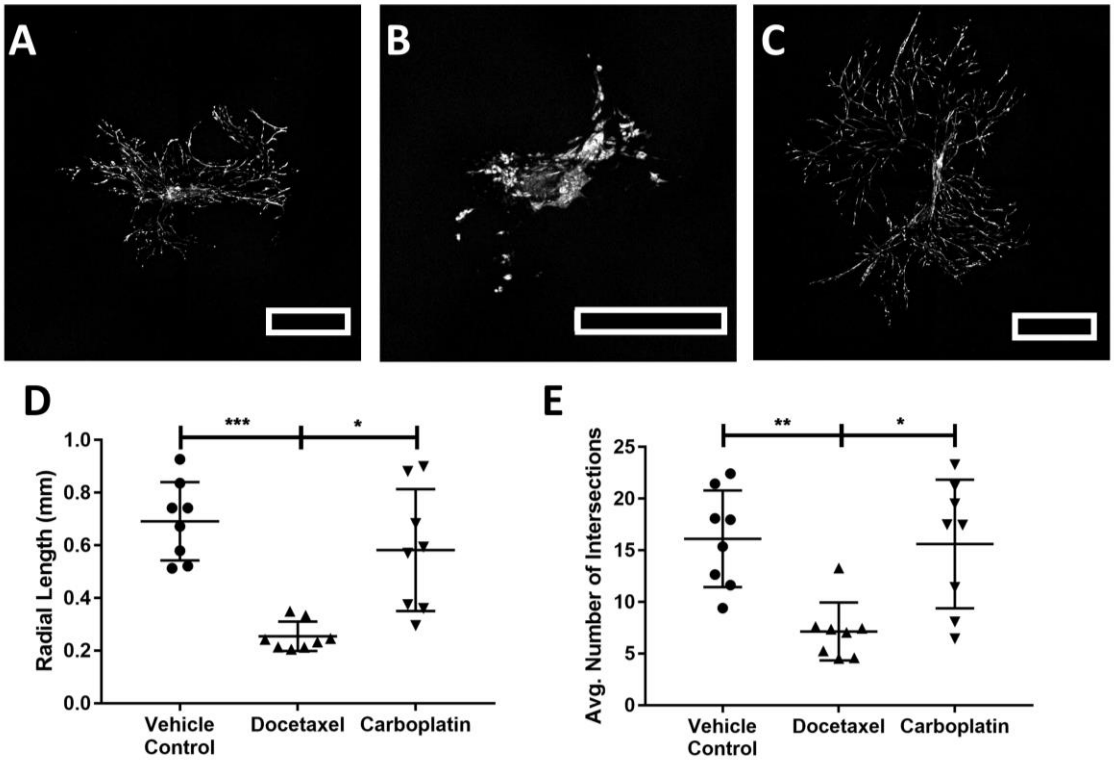

Figure 22: Impact of Chemotherapy Drugs on the Sprouting Phenotype in fully degradable 10% PEG – 2mM RGD Hydrogels: Representative images of collecting vessel segments at day 10 cultured in A) ethanol (vehicle control), B) docetaxel, and C) carboplatin conditions. Images are of intracellular fluorescent calcein indicating live cells. Scale bar = 500μm. D) Lymphatic collecting vessels cultured with docetaxel (1mM concentration) at day 5 had significantly reduced max sprout length by day 10. E) Lymphatic collecting vessels cultured with docetaxel (1mM concentration) at day 5 had significantly reduced average number of sprouts coming from the implanted vessel segment at day 10. There was no impact on sprout length or number from treatment with carboplatin. Significance was determined via Kruskal-Wallis test followed by Dunn's multiple comparisons.
***: p<0.05, **: p<0.01, ***: p<0.001**

3.4.5 Impact of Rapamycin on Sprout Phenotype

The mTOR inhibitor, rapamycin, was applied to this sprouting assay to determine its impact on the sprouting response (Figure 23). When gels were cultured with rapamycin (20nM) from day 0 to day 7, sprouting was largely inhibited with only a few, short sprouts emerging (D0R20). Rapamycin at 20nM, but not 100nM, applied at day 5 reduced

continued sprout growth compared to vehicle-controlled segments by day 7 (D5R20 and D5R100 respectively). Only sprouting in the vehicle control and the D0R20 condition were statistically different.

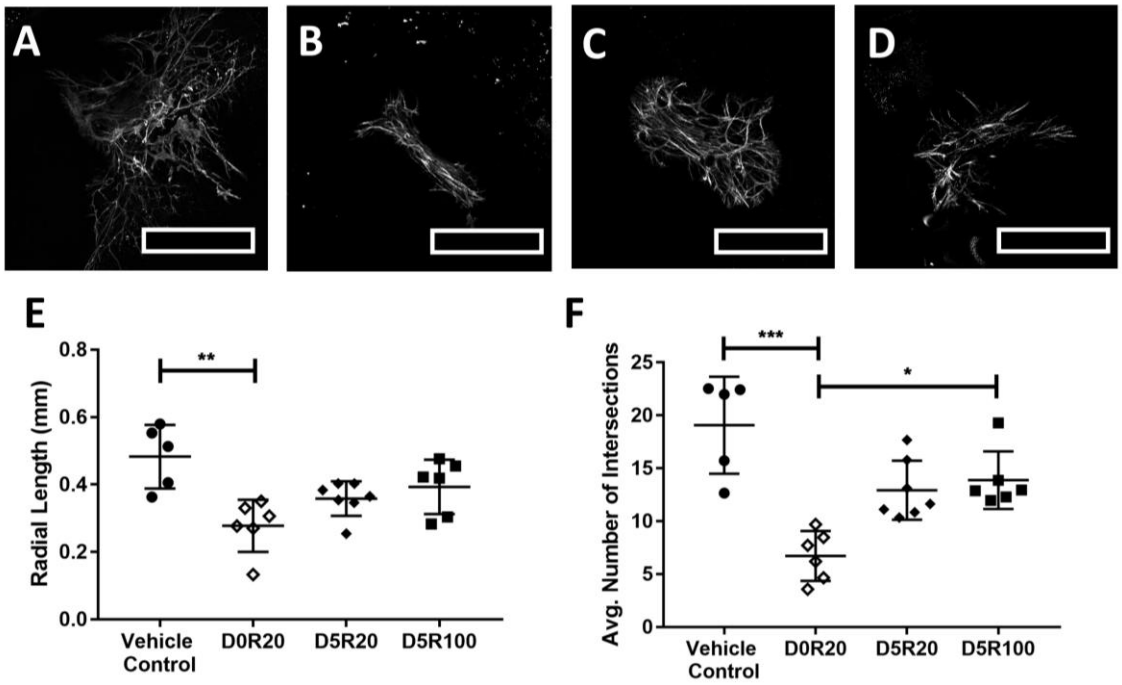

Figure 23: Impact of Rapamycin on Sprouting Phenotype in fully degradable 10% PEG – 2mM RGD Hydrogels: Representative images of collecting vessel segments at day 7 cultured in A) DMSO (vehicle control), B) 20nM of rapamycin from day 0 (D0R20) C) 20nM of rapamycin from day 0=5 (D5R20), D) 100nM of rapamycin from day 5 (D5R100). Images are of intracellular fluorescent calcein indicating live cells. Scale bar = 500μm. E) D0R20 condition had significantly reduced max sprout length compared to control. B) D0R20 condition had a significantly reduced average number of sprouts coming from the implanted vessel segment compared to control and the D5R100 condition. Significance was determined via Kruskal-Wallis test followed by Dunn's multiple comparisons.
***: p<0.05, **: p<0.01, ***: p<0.001**

3.4.6 Culture of Lymphatic Malformation tissue in PEG Hydrogel

Segments of lymphatic malformation tissue collected from human paediatric patients were cultured within the gels for 5 days in our EBM formulation. At day 5

sprouting segments were treated with various concentrations of rapamycin, an inhibitor of mTOR. Compared with the control, tissue treated with 100nM rapamycin had significantly reduced metabolic activity by day 10, but no effect was observed on tissue treated with 20nM rapamycin (Figure 24).

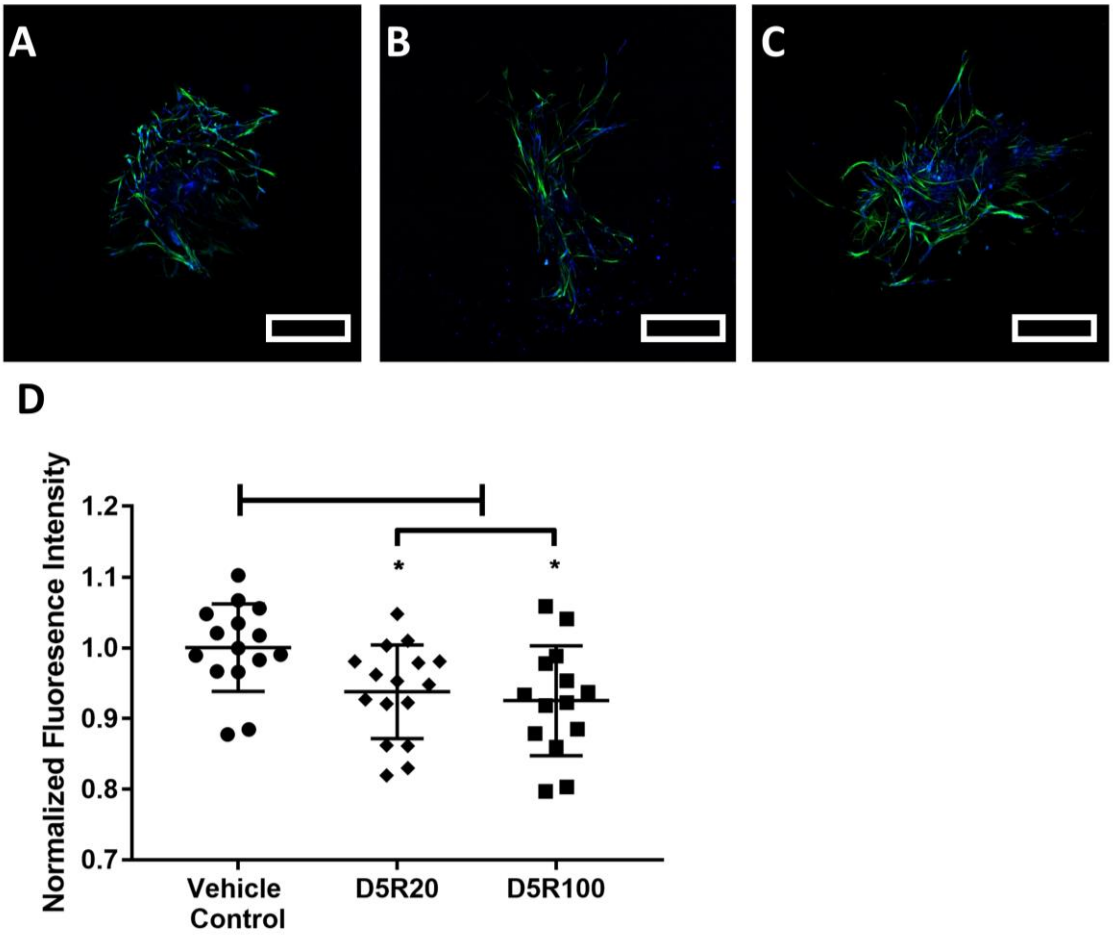

Figure 24: Lymphatic malformation tissue cultured in fully degradable, 10%PEG – 2mM RGD hydrogels. Representative images of LM tissue at day 10 of culture. From day 5 until day 10 tissue was cultured with either A) DMSO (vehicle control), B) 20nM rapamycin (D5R20), or 100nM rapamycin (D5R100). D) Metabolic activity of LM tissue at day 10 in various rapamycin concentrations. Images are of an F-Actin stain in green and DAPI in blue. Scale bar = 500μm. Significance was determined via Kruskal-Wallis test followed by Dunn's multiple comparisons.
***: $p<0.05$**

3.5 Discussion and Future Work

Here we have further demonstrated the sensitivity of lymphatic health and function on the unique biomechanical cues of the microenvironment. We demonstrated that culture of implanted segments of lymphatic collecting vessels within synthetic PEG hydrogels produce an "organized" lymphatic network with cells within the sprouts staining for both SMA positive cells and eNOS/VEGFR-3 positive LECs. Furthermore, we systematically demonstrate that the binding cues and biomechanical properties of the synthetic PEG gels significantly alter the growth rate and abundance of lymphatic sprouts. 10% PEG hydrogels, associated with a Young's modulus of 1.5kPa[173], lead to a relative maxima in sprout length and branching compared to other stiffnesses. This is around the physiological stiffness for healthy lung tissue, with a reported stiffnesses between 1-5kPa[174,175]. In comparison, collagen gels (2mg/mL) have a young's modulus of roughly 0.2kPa[176] stiffness and fibrotic lung tissue exceed 17kPa stiffness[177]. RGD adhesive peptides at a concentration of 1mM to 2mM facilitated the formation of an intricate lymphatic network. PEG hydrogels embedded with GFOGER or that were not fully degradable had significantly reduced sprouting. We show high levels of α-smooth muscle actin positive cells in our sprouts in both PEG and collagen hydrogel conditions. This has not been documented in similar studies using segments of mouse thoracic duct in collagen gels[57]. This could be due to a unique composition of lung draining lymphatic vessels or the media formulation they were grown in (Figure 25). Both LMCs and myofibroblasts are capable of expression αSMA[178] and it is unclear which cell type is integrated in the sprouts in our hydrogel formulations. Finally, we demonstrated that this optimized PEG gel can be used

as a platform to explore the impact of drugs and on the function of healthy or pathological lymphatic tissue.

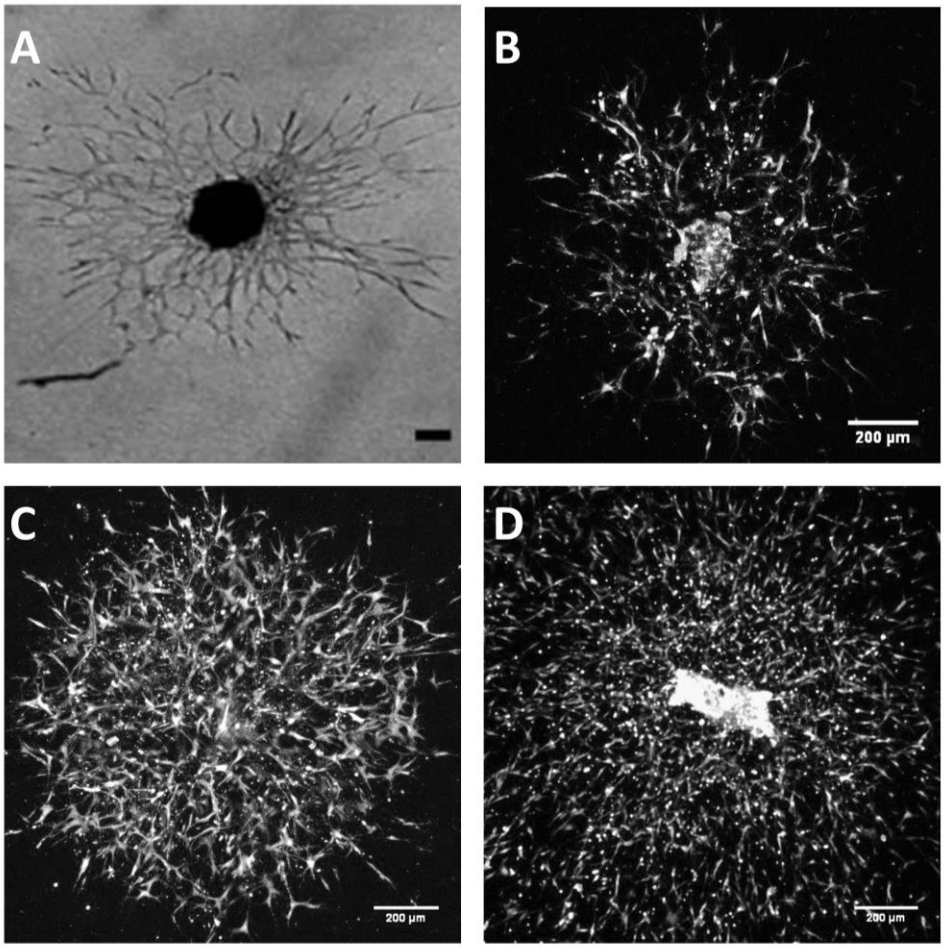

Figure 25: Representative sprouting from various lymphatic tissues in variable media formulations culture in collagen gels. A) Mouse TD sprouting network after 9 days culture in 2mg/mL collagen gels with media containing 10% FBS. Modified from Bruyère, 2008. B) Mouse TD sprouting network after 7 days of culture in 1.88mg/mL collagen gels with media containing 10% FBS. C) Rat LLV sprouting network after 7 days of culture in 1.88mg/mL collagen gels with media containing 20% FBS. C) Mouse TD sprouting network after 7 days of culture in 1.88mg/mL collagen gels with EBM-20% FBS. D) Rat LLV sprouting network after 7 days of culture in 1.88mg/mL collagen gels with media containing 20% FBS.

We demonstrate that the synthetic RGD peptide allowed for the most robust sprouting phenotype. RGD is a fairly conserved adhesive peptide found in fibronectin,

vitronectin, fibrinogen, as well as others, and has been demonstrated to bind with high affinity to a variety of integrins[179–181]. For future work two integrins of interest that have been shown to bind to RGD are αvβ3 and α5β1 integrin for their demonstrated role in lymphangiogenesis or angiogenesis. As previously detailed, α5β1 has been shown to be upregulated in sprouting lymphangiogenesis of the airway[75]. The αvβ3 integrin has been shown to be upregulated in angiogenesis, and critical for lumen formation, but the specific impact on lymphangiogenesis has not been studied[182]. This work would imply that these integrins play a role in sprouting lymphangiogenesis but additional staining and blocking via antibodies during culture would be needed.

Additional adhesive proteins within the serum and produced by synthetic muscle cells and resident fibroblasts of the collecting vessel wall are likely to become integrated into the gel during the 7-day culture. Deposition of adhesive proteins from these sources is likely what allows for sprouting lymphangiogenesis in the RDG and GAOGER containing hydrogels. RDG and GAOGER peptides have been scrambled in in order to significantly impair their binding affinity to any native integrin, but deposition of these binding proteins from the media could allow for the limited sprouting that is observed in these conditions. GFOGER, a binding region primarily expressed in type I and IV[183], did not significantly enhance sprouting compared to the scrambled negative controls. GFOGER has been shown to bind with high affinity to α1β1, α2β1, and α11β1 intigrins[184,185]. Interestingly, activation of α1β1 and α2β1 integrins have been correlated with elevated lymphangiogenesis in the presence of tumors[186,187], but it is unclear what the role of these integrins are during lymphangiogenesis in the absence of tumor cells. Binding motifs that form other common

ECM proteins, such as laminin, or combining multiple adhesive peptides should be the focus of future work to determine novel or synergistic effects.

In addition to seeing how properties of the surrounding matrix influence lymphatic tissue sprouting, this PEG gel platform allows for a reliable method to determine the impact of various small molecule regulators on lymphatic viability. We show how common chemotherapy drugs, docetaxel and carboplatin, impact sprouting lymphangiogenesis directly. Research on these chemotherapy drugs and lymphatics have primarily focused on how to target these drugs for lymphatic uptake and eventually into the lymph nodes to act on metastasizing tumors[166,167,188]. Recent work demonstrating that, *in-vitro*, docetaxel may improve the ability of tumor cells to invade through the lymphatics is important to consider as we continue investigating alternative delivery methods[146]. This change in permeability may also explain why docetaxel has been shown to transiently increase fluid retention in the limbs of some cancer patients[189]. We show that docetaxel has a significant impact on lymphangiogenesis in this assay, while carboplatin seems to maintain base levels of sprouting. Future work could focus on how culture with these chemotherapeutics impact tumor invasion or alters sprout junction permeability within our PEG sytem. Furthermore, we demonstrate that, on healthy rat LLV, rapamycin reduces sprouting attained at day 7 when added to the media at the time of tissue implantation. Two days of rapamycin application at 20nM or 100nM was not sufficient to elicit a measurable effect on sprouting but future work could look at later time points or increased concentrations. Based on the lymphatic malformation results, 5 days or culture with rapamycin was able to illicit a measurable reduction in metabolic activity of the embedded segments. In blood vasculature, rapamycin has been used to maintain VSMCs in a contractile phenotype in-

vitro, partially inhibiting the increase in proliferation, migration, and matrix synthesis in response to 2-D tissue culture[102,106]. Clinically, rapamycin eluting stents have been successfully used to reduce restenosis, avoiding the invasive nature of synthetic vascular smooth muscle cells[190]. Due to a somewhat similar behaviour of lymphatic muscle during lymphedema, future work could explore if targeted rapamycin treatments could maintain a healthy, functional, collecting vessels under lymphedema-like conditions.

Overall, there are many directions that this work could go in in the future. Quantifying sprout length and complexity gives us a limited understanding of sprouting. As previously mentioned, it has been shown that inflammatory induced lymphangiogenesis produces leaky lymphatic vessels and therefore optimizing sprout length and complexity may or may not be "ideal". Future work should focus on examining the exact phenotype and functional capacity of theses sprouts. A gel formulation that maintains junction integrity of newly formed initial lymphatics or mediates remodelling and stenosis of collecting vessels when implanted in-vivo would have large translational impact in breast cancer related lymphedema. Lymphatic malformation tissue can be successfully cultured in these gels and we show how rapamycin impact malformation behaviour specifically, but the PEG hydrogel implemented was not formulated for malformation tissue specifically. It is currently unknown how ECM properties may impact lymphatic malformation behaviour and before we can fully explore therapeutic interventions for the LM phenotype, it is important to demonstrate that the cultured LM tissue is functionally similar to the initial biopsy. While rapamycin has been shown to be generally effective at inhibiting unregulated LM tissue growth, the permanency of its effect once removed is an area of interest that could be easily studied with this platform.

CHAPTER 4. UTILIZE ANIMAL LYMPHATIC DAMAGE MODELS TO STUDY PEG HYDROGEL FACILITATED LYMPHATIC TISSUE TRANSPLANTATION AND INFLUENCE OF PEG HYDROGELS ON LYMPHATIC FUNCTION AND REGENERATION FOLLOWING INJURY.

4.1 Overview

Objective: Determine the capacity of the 10% PEG – 2mM RGD hydrogel, characterized in chapter 3, to transfer healthy lymphatic tissue to a wound site and to enhance native lymphatic repair and regeneration mechanisms in a translatable animal model.

Methods: To assess the capacity of PEG hydrogels to deliver lymphatic vessels, a popliteal draining collecting vessel was isolated from a ubiquitously expressing GFP rat and transferred to a non-GFP expressing rat where the local lymphatics had been resected. Lymphatic regeneration was monitored with non-invasive NIR imaging over the course of 28 days and then engraftment of the donated tissue was determined through tissue staining. In addition, a separate rat model was used to assess the impact of PEG hydrogels implantation after axillary lymph node dissections (ALND). The impact of PEG alone was compared to autologous lymph node segment transplant back into the resection site after encapsulation in either the PEG or collagen gel.

Results: PEG gels were capable of transferring collecting vessel segments into the lymphatic network upstream of the popliteal lymph node. Transferred tissue became

functionally engrafted into the host as shown by co-staining of fluorescently labeled lectin delivered via intradermal injection within GFP-positive lymphatic vasculature. In the ALND model there was an initial increase in lymphatic function at 1 week after lymph node removal followed by long term dysfunction of upstream collecting vessels at 4 weeks, even though there was partial regeneration of lymph draining tissues in the site where the node was removed. However, no biomaterial intervention significantly outperformed native repair mechanisms in the ALND model.

Conclusions: PEG gels are a promising vehicle to transplant lymphatic tissue into an area of lymphatic damage. Further work to use the hydrogel platform in conjunction with growth factor delivery needs to be done to further encourage native tissue to engraft within the gel. There is also a pressing need to create and characterize a translationally relevant animal model, that has limited regeneration capacity, to assess the impact of PEG gels on the function of the remaining intact lymphatic vessels and the invasion of new lymphatic networks.

4.2 Motivation and Background

Lymphedema is a common side-effect of treatment for patients recovering from a variety of cancers including breast, prostate, and oral cancer. It is the blockage of lymphatic vessels, leading to fluid retention and swelling of the arms or legs. The exact pathogenesis of breast cancer related lymphedema (BCRL) following initial surgery is not fully understood, but it is believed that the severity of the surgery, in combination with the type and duration or cancer treatments increases the risk of eventual lymphedema development[191]. Two of the most promising emerging surgical therapies for lymphedema

are vascularized lymph node transfers or lymph node flap transfers. These techniques transfer one or multiple functional lymph nodes from one region of the patient into the dysfunctional limb or region. Early application and assessment of these techniques have had promising results permanently treating symptoms of lymphedema but did not work for all patients[94,95,192,193]. Unfortunately, the molecular mechanisms that contribute to these beneficial outcomes are not well understood. It is unclear exactly how the lymph node reconnects to the local lymphatic network, if the full lymph node is needed or if any lymphatic tissue would be beneficial, or how we can enhance the success and integration rate. As researchers we must select the most appropriate animal models to begin studying these questions.

The most commonly used animal model to study lymphedema is the mouse tail lymphedema model. This model has been incredibly useful to our understanding of the lymphatic system and disease pathology but remains limited in its translational applicability. The mouse tail is drained by two primarily lymphatic collecting vessels that run in parallel and a hexagonal crisscrossing of initial lymphatic vessels. In the tail lymphedema model a ring around the mouse tail is cauterized, damaging initial lymphatic capillaries and the collecting vessels without damaging the major veins and artery of the tail. As a result, the tail of the animal swells significantly (2-3 times the typical diameter at the peak of swelling) [93,194,195]. This model has been used to show the importance of VEGF-C in swelling management[51,60,143] and demonstrate the role of fibrosis and various immune cells at regulating swelling outcomes[48,49,93]. One drawback to this model is that swelling in all animals, even without intervention, is self-resolving. Unlike the presentation of lymphedema in humans, swelling in the mouse tail occurs immediately after surgery and

is not chronic. Below we outline alternative animal models to this full tail lymphatic ligation model that we use to inform the studies outlined later in this chapter.

A criticism of the tail model with respect to its relevance to breast cancer related lymphedema (BCRL) in humans is the fact that all collecting vessels of the tail are severed during the surgery, leaving no intact functional vessel to drain the distal limb where swelling occurs. In BCRL, some functional lymphatics that drain the arm remain following lymph node biopsies and subsequent cancer treatments[196]. To address this, novel animal models for lymphedema are being developed which better recreate the conditions that cause BCRL in humans and the chronic symptoms found in humans. For example, a single vessel ligation has been used in the tail lymphedema model and has been used to characterize the functional response of the intact collecting vessel after local damage to the lymphatic network[47]. This model revealed that the intact vessel has reduced contractility following isolation of the parallel lymphatic vessel that persists long after swelling resolves. This model would allow us to look at how transplanting tissue or biomaterials after injury of a single vessel improves regeneration and impacts function of nearby intact lymphatics. However, the taut skin cannot be easily sutured close making it a challenging location for transplantation. The sheep model outlined in chapter 2, presents results similar to the single lymphatic vessel ligation tail model, and would allow for easy transplantation of biomaterials, but large animal models have a low throughput and require special accommodations which were not feasible for this study.

Tumor draining lymph nodes typically reside in the axillar of breast cancer patients, and therefore are typically removed when primary tumor metastasis is assessed. Another promising animal model for studying lymphedema progression and onset is the removal of

axillary lymph nodes. In rats, it was found that lymphatic vessels are chronically impaired following axillary lymph node dissection (ALND), months after the initial swelling has resolved. Oxazolone, which is used as a model of contact hypersensitivity due to repeated application inducing fibrosis when applied to the skin, was applied repeatedly to the forelimb of rats 2 months after surgery. Animals that had undergone ALNDs had significantly increased swelling compared to unoperated controls, despite the absence of physical symptoms at that time oxazolone application commenced. This would imply chronic, underlying dysfunction of the lymphatics needed to drain the limb which is only seen once the limb is challenged with a new inflammatory insult. This is much more in line with our current understanding of what happens in human patients[41,42]. Mouse models of ALND have also shown that VEGF-C delivery can enhance incorporation of a transferred lymph node[60].

In addition to working with a clinically relevant animal model, we sought to acquire preclinical data on the efficacy of PEG hydrogels to enhance lymphatic regrowth and function following surgical damage. While certain therapies, such as the injection of collagen into wound sites, have been demonstrated to reduce negative symptoms of inflammation and swelling[49,197] , the mechanism by which this impacts lymphatic repair, inflammation, and the functional response they elicit from intact lymphatics has not been thoroughly examined. Furthermore it is unclear if a whole lymph node must be transferred to achieve benefits, or if any healthy lymphatic cells/tissue would be beneficial, For example, cell transplantation of healthy human LECs into an animal model after surgical induction of secondary lymphedema showed reduced swelling and fibrosis as a result[198]. The goal of this study is two part: 1) To demonstrate that the synthetic PEG hydrogel

characterized in chapter 3 can be used to deliver lymphatic vessel segments into a host animal and become functionally incorporated. 2) Determine if the PEG hydrogels outperform natural healing mechanisms or alternative biomaterial approaches at preventing dysfunction of existing lymphatic vessels and promoting integration of transferred lymph node segments. To do this in a translationally meaningful way we first recreate the rat lymphatic dysfunction model via axillary lymph node dissections. We then measure the natural lymphatic responses to this surgical insult and compare it to three intervention conditions. We implant the degradable 10% PEG -2mM RGD gel with and without an imbedded lymph node segment, as well as a type I collagen gel containing a lymph node segment.

4.3 Methods

4.3.1 GFP Tissue Transplantation with PEG Hydrogels

Surgical Procedure

Ubiquitously green fluorescent protein (GFP) expressing Sprague Dawley rats (RRRC:0065 [SD-Tg(UBC-EGFP)2BalRrrc]) were purchased from the Rat Resource & Research Center. Animals were anesthetized via injections of ketamine (40mg/kg) and dexdomitor (0.13mg/kg) and the left hindlimb was shaved of hair. A near infrared (NIR) dye, conjugated to 20kDa PEG polymers, were injected into the footpad. Due to the size of the polymer this NIR tracer is drained from the footpad interstitium exclusively by the lymphatic system. Imaging through the skin revealed two lymphatic collecting vessels that drain lymph formed in the foot pad to the popliteal lymph node and travel parallel to the saphenous vein. A 1-2cm long segment of the two parallel collecting vessels was resected

proximal to the ankle (Figure 26). These vessels were segmented into 3-5mm long segments and stored in sterile saline solution. In non-fluorescent Sprague Dawley rats, the same segments of collecting vessel were isolated and discarded. One segment of the GFP expressing collecting vessel was placed along the lateral side of the saphenous vein where the host's collecting vessel was removed. Ten microliters of 10%PEG – 2mM RGD gel was carefully polymerized over the vessel segment and the skin sutured close over the gel and wound. Gels were fabricated as outlined in section 3.2.1. The animals were risen with antisedan (1.3mg/kg) and carefully monitored following recovery. Lymphatic repair in the wound site was assessed using NIR imaging on days 7, 14, and 28 following surgery. This procedure was carried out on 2 adult male rats. All animal procedures were performed in compliance with procedures approved by the Georgia Institute of Technology Internal Animal Care and Use Committee (IACUC).

Tissue Collection and Staining

On day 28, the animal was administered an intradermal injection of fluorescent lectin, wavelength 649, that was passively drained by the lymphatics due to size exclusion from the blood vasculature. After 10 minutes, animals were then euthanized and the entire wound site, including the saphenous vein, was isolated and immediately frozen in optimal cutting temperature (OCT) compound. Tissue slices were stained with a nuclear DAPI stain, for GFP expressing cells, and VEGFR-3 expressing cells. Samples were fixed using a 4% paraformaldehyde (PFA) suspended in a physiological saline solution for 10 minutes then rinsed three times with phosphate buffered saline (PBS). Sections were permeabilized with a 0.5% Triton-X solution at room temperature for 10 minutes and rinsed again three times in PBS. Blocking of samples was done in a PBS solution containing 2% bovine serum

albumin, BSA and 10% goat serum for 1 hour at room temperature. Following this, primary antibodies for GFP and VEGFR-3, suspended in the 2% BSA solution (1:100), were applied to the samples for one hour on a plate rocker. The samples were rinsed in PBS (3x) before application of a fluorescent secondary antibody solution in 2% BSA (1:200) for 1 hour at room temperature on a shaker. Samples were rinsed two times in PBS before imaging. Additional sections were also stained with isotype control antibodies for the GFP antibody (chicken IgY) and VEGFR-3 (polyclonal rabbit IgG). The maximum intensity from these controls were subtracted from the actual stains to eliminate background and non-specific fluorescence.

4.3.2 Axillary Lymph Node Dissection Procedures

Surgery and Conditions

Axillary lymph nodes (ALNs) were isolated from adult female Sprague Dawley rats. In brief, a surgical incision through the dermis was made across the axilla of a rat. This exposes a fat pad in which the axillary lymph nodes reside. The axillary lymph nodes, as well as a short segment of the pre- and post- nodal collecting vessels, were isolated with care to minimize damage to surrounding muscle and tissue. If a lymph node segment was to be returned to the wound site, one of the lymph nodes was stored in a sterile saline solution. All animal procedures were performed in compliance with procedures approved by the Georgia Institute of Technology Internal Animal Care and Use Committee (IACUC).

There were 4 conditions in total to determine the impact of various interventions. The negative control animals simply had the axillary lymph node dissection (ALND) performed and immediately had the dermis over the isolation site sutured close. The PEG

gel group (labelled as PEG) had 20μL of the fully degradable, 10%PEG-2mM RGD, hydrogel polymerized directly into the site where the nodes initially were located and then the wound was sutured shut. The final two conditions had a segment of one of the isolated ALNs encapsulated into 20μL of either a type-1 collagen gel (CG/LN) or the previously described PEG gel (PEG/LN). The collagen gel was at a concentration 1.85 mg collagen/mL. In total there were 5 rats in the ALND condition, 6 in the PEG/LN condition, 4 in the PEG condition, and 4 in the CG/LN condition.

Lymphatic Functional Imaging via Near infrared (NIR) Imaging

The forelimb was shaved of hair before each imaging session. Anesthetized animals were injected with 15μL of NIR-labelled 20kDa PEG in either the foot-pad or between the fingers of the forepaw. The imaging window was downstream of the injection along the collecting vessels that drain the injection site. After a 5-minute adjustment period following the injection NIR images of dynamic lymphatic transport were captured at a rate of 10 fps with a 50ms exposure time for a total of 5 minutes. Lymphatic pumping measurements, such as contraction frequency and fluorescence transport (a proxy for lymph transport) were measured via a custom MATLAB code outlined in a previous publication[130]. In brief, the average fluorescent intensity of a small, manually selected, region of a collecting vessel could be calculated over time, with dips or peaks in fluorescence intensity corresponding with a contraction or an influx of lymph, respectively.

Wrist Swelling Measurements

Accompanying each imaging session, outlined above, and including the day of the surgery, an image of the paw/wrist was taken with the stereoscope. The diameter of the wrist was manually recorded from each image.

Oxazolone Application

After two months of recovery from the initial ALND surgery, the rats were challenged with a topical oxazolone application. First, animals were sensitized by applying 300µl of 2%oxazolone in ethanol to a 1"x1" shaved section of the abdomen using a micropipette. Animals remained anesthetized until the applied oxazolone had dried. Sensitization occurred on day 56.

To initiate dermatitis, 300µl of a 1.6% oxazolone solution of acetone and olive oil (4:1) was applied to the shaved forelegs of anesthetized animals beginning on day 63. The oxazolone solution was applied to the entire foreleg up to the shoulder using a micropipette and allowed to dry before the rats regained consciousness. Oxazolone was applied again on day 66 and 70, 73, and 77.

Terminal Procedures and Tissue Collection

Following the final imaging session on day 98, which required an injection of NIR dye, animals were awoken from their anaesthesia and allowed to move around their cage for 20 minutes. Following this period, animals were euthanized and the brachial lymph node (BLN) and any dye containing tissues within the axillary pocket were isolated. The BLN and axillary tissue were imaged using the NIR scope and the intensity of NIR dye was measured in each.

4.3.3 Statistics

GraphPad Prism version 7.01 was used for statistical analysis. For the data grouped into a single experimental group a one-way ANOVA followed by Tukey's multiple comparisons test was used to determine significant differences at different time points. A two-way ANOVA test followed by Sidak's multiple comparisons test were used for comparisons between differemt experimental groups at each time point following surgery. Error bars on all data points are standard deviation. All analyses were considered statistically significant at $p<0.05$.

4.4 Results

4.4.1 Use of PEG Hydrogel to Implant Lymphatic Tissue for Lymphatic Repair

A segment of GFP expressing collecting vessel was implanted into the wound site of a non-fluorescent host after the two lymphatic collecting vessels that drain the foot pad were resected (Figure 26 A). After just one week, lymph flow, as tracked with NIR dye, seemed to have been established through flow through a network of smaller collateral vessels. By day 28, flow through a single mature collecting vessel was restored across the wound site (Figure 26 B-E). During the injection on day 14 the needle hit a blood vessel and caused bleeding, which prevented drainage of the NIR lymphatic tracer to the collecting vessels downstream (Figure 26 D). On day 28, 20uL of fluorescent lectin was injected into the foot pad and drained into the lymphatics due to size exclusion from the blood capillaries. Imaging the fluorescent lectin through the skin matched perfectly with NIR fluorescence confirming lymphatic specific drainage. Skin above the wound site was carefully removed and tissue below the skin along the gold square was removed, sectioned,

and stained. The draining lymphatic collecting vessel was easily identified due to the lectin stain (Grayscale in Figure 26 G). GFP expressing cells had become incorporated in much of the vasculature including the saphenous vein (indicated with the red arrow). The draining lymphatic collecting vessel stained as GFP positive, but weakly for VEGFR-3 (Figure 26 J&I).

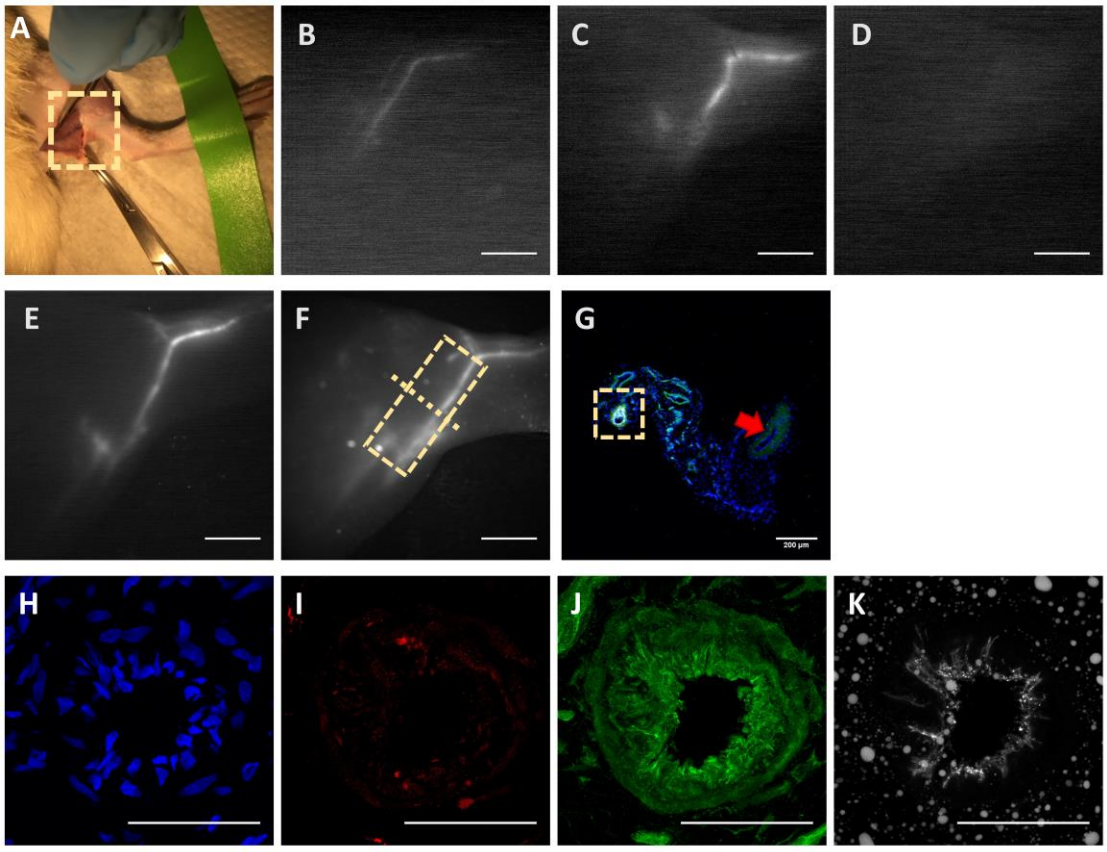

Figure 26: Representative images from the popliteal tissue transfer surgery. A) Brightfield image of rat hindlimb with exposed saphenous vein. The dashed yellow box is the approximate location along the hindlimb shown in panels B-F. B) Presurgical NIR imaging of the two collecting vessels running parallel along the saphenous vein which are isolated during the surgery. Scale bar=0.5cm. C-E) NIR Imaging of the collecting vessels following the surgery at days 7, 14, and 28 respectively. Scale bar=0.5cm. F) Imaging of fluorescent lectin (wavelength 649) through the skin which is selectively up-taken by the lymphatic collecting vessels. The tissue within the yellow box is selectively isolated and sliced into 10µm cross-sections. Scale bar=0.5cm. G) One cross section of the isolated tissue located along the dotted

line of panel F. The red arrow indicates the location of the saphenous vein. The yellow box indicated the only vessel which was passively bound with lectin. Scale bar=100µm. H-K) Close-up of the DAPI, VEGFR-3, GFP positive tissue, and lectin stains, respectively, of the lectin stained collecting vessel. Scale bar=50µm.

4.4.2 Use of biomaterial interventions to improve outcomes of ALND

Generally, animals had a mild response to the surgery itself which is outlined in Figure 27. When grouping animals from all conditions, we see a statistically significant increase in fluorescent transport in response to surgery immediately following the surgery. There is a significant decrease in transport by day 28 compared to pre-surgical levels. This indicates that while the surgery did not induce swelling, it is impacting lymphatic function directly. The exact mechanism of this increase and eventual decrease in lymphatic function was not explored.

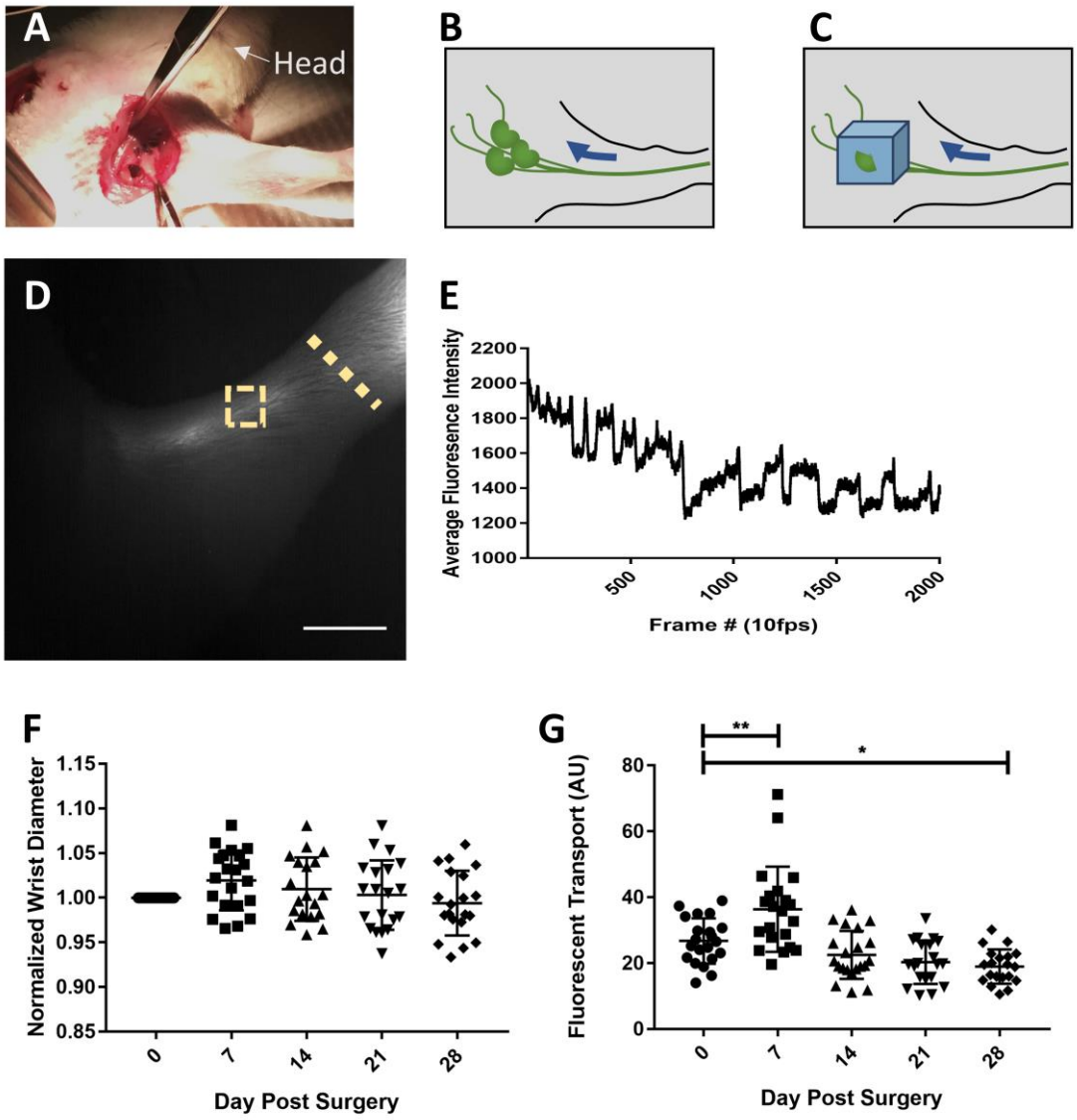

Figure 27: ALND Surgery: A) An anesthetized rat with an incision across the axilla. Muscle is loosely separated to gain access to the axillary lymph nodes (ALNs). B) Cartoon of the lymph nodes in the axillary pocket and their connection to upstream collecting vessels. C) An example of an intervention condition where a biomaterial (blue) is inserted after the nodes are removed. In some conditions a segment of the isolated lymph nodes was embedded into the biomaterial in-situ. D) Representative image of functional near infrared (NIR) imaging. The paw (out of the image at the top right) is injected with 15µL of 20kDa NIR dye which is selectively drained by the collecting vessel along the rat forelimb. Wrist diameter measurements were measured along the gold dashed line. A region of interest (ROI), such as the example shown with the gold dashed box, was selected along the forearm to measure dye transport. Scale bar=0.5cm. E) An example of average NIR fluorescent intensity in the ROI over time is shown. Contractions of the collecting vessel are seen as transient drops in average

intensity. F) Wrist diameter normalized to the initial diameter of the wrist for each rat at day 0. G) Transport of NIR dye through the ROI prior to (day 0) and following the ALND surgery (transport is in arbitrary units). All animal conditions are combined for the measurements in panels F and G. Significance was determined via one-way ANOVA followed by Tukey's multiple comparisons test.
***: $p<0.05$, **: $p<0.01$**

When breaking animals down by the intervention condition, there is generally not a large response to the surgery or a discernible difference from each other in most conditions. There was no significant swelling produced at the wrist in the month following the initial surgery (Figure 28A). Swelling as a result of the oxazolone challenge to the forearm of animals was measured, starting at day 63, only on animals from the ALND and PEG/LN conditions. While there is a significant impact of oxazolone on the wrist diameter on day 66, swelling resolved by the following time point, despite an additional application of oxazolone being given on day 66. Furthermore, there was no difference in the response to oxazolone between the two conditions (Figure 28B). The only measurable impact of the surgery on lymphatic function is a slight increase in fluorescent transport on day 7 in the ALND condition (Figure 28C). Oxazolone did not significantly alter lymphatic function at timepoints 70 and 77 after its twice weekly application which began on day 63 (Figure 28D). Implanting any biomaterial as an intervention did reduce the magnitude of the transient increase in fluorescent transport at day 7 compared to the ALND condition (Figure 28F).

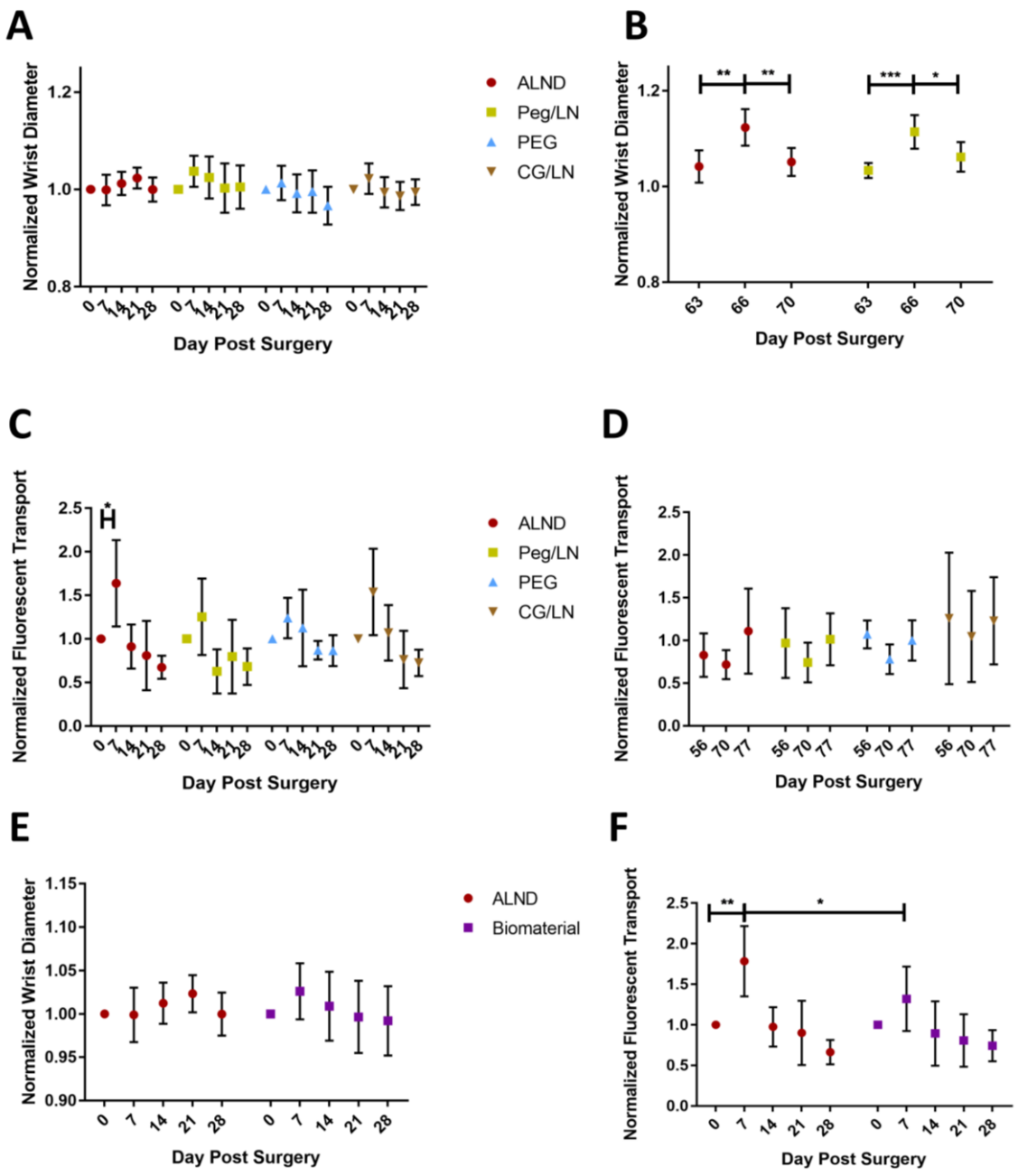

Figure 28: Impact of Interventions on Swelling Lymphatic Function (day 0 reflects presurgical measurements in all panels): A) Wrist diameter did not significantly change in any condition in the month following ALND surgeries. B) As a result of oxazolone application to the forearm, wrists did transiently swell in the ALND and PEG/LN conditions after 3 days but returned to pre-application levels by day 70 (One week after the initial application began). Extent of swelling was not different between the two conditions. C) Florescence transport in the month following ALND surgery revealed that in the absence of any intervention, transport significantly increases after one week before returning to initial levels. D) Oxazolone application did not

significantly impact transport. E) Wrist diameter did not significantly change when comparing the negative control, ALND, to the pooled results all biomaterial interventions. F) There is a significant increase in fluorescence transport in ALND negative control at day 7 compared to conditions where a biomaterial was embedded. Significance was determined via two-way ANOVA followed by Sidak's multiple comparisons test.
***: p<0.05, **: p<0.01, ***: p<0.001**

After the final functional NIR imaging, we collected tissue from animals after letting the animals rest for 30 minutes. We found that many animals had developed lymph node-like tissue in the axilla pocket where the ALNs where initially removed. This axillary, lymph draining, tissue (ALDT) formed in both the ALND and PEG/LN conditions. We removed this tissue, as well as the brachial lymph node (BLN), upstream of the ALNs, and assessed them for NIR dye as seen in Figure 29. In all conditions, both the ALDT and BLN have roughly equal fluorescent intensity signals, implying that both tissues were downstream of lymph formed at the injection site in the paw.

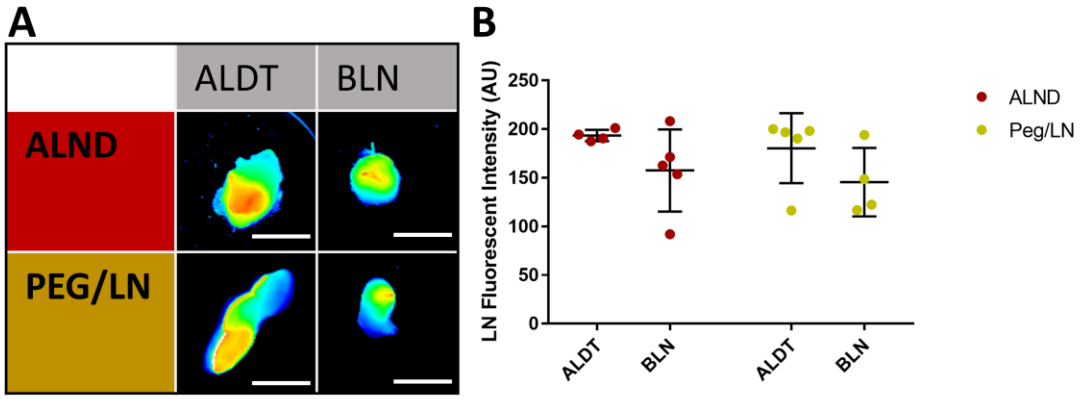

Figure 29: NIR Dye Uptake of Lymph Nodes and Tissue at Day 98: A) Representative NIR images of the axillary lymph draining tissue (ALDT) and the brachial lymph node (BLN). Scale bar=0.2cm. B) Quantification of the fluorescent intensity of these tissues revealing no significant difference in dye uptake. Significance was determined via two-way ANOVA followed by Sidak's multiple comparisons test.

4.5 Discussion and Future Work

In this study we explore lymphatic damage and dysfunction animal models to attempt to determine if the degradable 10% PEG -2mM RGD gels can be used to transfer lymphatic tissue into a host. Our results expand on our understanding of lymphatic repair and regeneration mechanisms. After GFP-expressing lymphatic vessels were transferred to a host it appears that some cells migrated and become incorporated in a variety of the host vasculature within the wound site, most evident through the weak GFP fluorescence of the host saphenous vein. Tissue from the GFP expressing lymphatic vessels were shown to be functionally integrated into the host's lymphatic vasculature via fluorescent lectin injection. The fact that this lectin coated vessel was over 50 microns and was 1-2inches downstream from the injection site would imply that it is a mature lymphatic collecting vessel but staining for LMC coverage remains to be done. Several GFP positive vessels, presumably smaller vessels that branched from the implanted segment, were found near the lectin stained collecting vessel but did not contain lectin. This likely indicates that these smaller vessels are initial lymphatics that do not drain from the injection site at the footpad.

The scope of this aim was simply to show the feasibility of using PEG hydrogels to transplant lymphatic vessels segments but the innate repair response to the surgery alone was not been characterized. The individual contributions of the lymphatic vessel transplant or the PEG hydrogel alone remain to be studied as well. There has been work showing that application of collagen gel to the wound of a mouse tail lymphedema model improves lymphatic repair rate, reduces fibrosis, and alters immune cell recruitment[199–201]. Quantifications of these metrics in future studies will allow for a better understanding of how the PEG gel alone is impacting functional restoration of the injured lymphatic network. A future area of interest would be to determine if the transfer of tissue in this

lymphatic damage model impacts the abundance of host lymphatic vessels following surgery or improves metrics of lymphatic contractility. It has been shown that in a rat tail model of lymphedema injection of human LECs increased the number of rat lymphatic vessels in the wound site and reduced skin thickening and swelling from the surgery[198].

When using the axillary lymph node dissection animal model, we demonstrate the ability for lymphatics to maintain lymph flow and repair following surgery. The power of this study was low, limiting our ability to discern differences that may have existed. For example, comparisons of transport in the ALND animals between day 7 and 14 has a power of 0.6404. To explore some effects we combined conditions, as explained, in order to assess specific effects of surgery or intervention. Combining the results for all animals revealed some measurable impacts of the surgery across all conditions. Specifically, removal of the axillary lymph nodes induces a short-term increase in lymph transport measured at day 7 but resolves by day 14. At the 28-day time point there is a reduction in fluorescence transport, but flow returned to presurgical levels by day 56 prior to oxazolone application (not shown). Implanting any biomaterial, with or without the lymph node segment, had a mitigating impact on this transient lymph transport spike seen in the ALND negative control. These results would seem to indicate that removal of the node reduces lymph flow resistance across the lymphatic network. This could lead to maladaptive remodelling of the collecting vessels to adjust to the elevated flow, explaining the reduction in flow at day 28. Future work isolating and characterizing the structure and force generation of the forelimb lymphatic collecting vessels following the surgery could reveal more insight into these results.

Delivering lymph node segments encapsulated in the PEG hydrogel did not alter lymphatic function of the forelimb lymphatics compared to implanting the PEG gel alone or using a type-1 collagen gel to encapsulate the node. It is important to note that in our model, ALN segments returned to the wound site were not vascularized which may have led to some of the ALN segments dying before revascularization could be achieved. We did find regenerated lymph node-like tissues in the axillary pocket that drained lymph in all experimental conditions. In our study, the wrists of animals undergoing ALND did not swell chronically similar to the results reported by Mendez et al, and future work could focus on how the regenerated lymph node-like tissue in our model contributed to mitigating lymphatic dysfunction[202]. It is unclear how or if our model varied from others and if other ALND models developed these lymph-node like tissues as well.

Lymph node regeneration and enhancing the lymph node repair has been studied with some promising results. As early as 1957, a study explored the lymphatic response after partial lymph node damage, partial lymph node resection, or full lymph node resection with results consistent with our findings[203]. This study looked at 4 different conditions of damaging or removing the single iliac lymph node. When the node was only mildly damaged, but still connected to the lymphatic network, the iliac lymph node repaired fairly robustly after 1-2 months. In conditions when lymph flow was disrupted through segmentation of the node or removal of the afferent or efferent vessels, 3-4 “lymphoid tissues” were found. As in our study, these lymphoid tissues contained dye from their injection upstream but lacked the clear structure of a mature lymph node. They also found that these regenerated nodes contained macrophages and drained lymph in the absence of the native, single iliac lymph node. Recent studies performing axillary lymph node

dissections have not reported the spontaneous formation of this type of lymphoid tissue, but it is unclear if these studies were designed in a manner to determine their presence[60,202,204]. Factors to promote lymph node regeneration have been explored recently, with it being demonstrated that implanting stromal cell–embedded biocompatible scaffolds can induce synthetic lymph node-like lymphoid tissue. These "artificial lymph nodes" can induce immune responses in addition to draining lymph[205,206].The extent to which our implanted gels helped to facilitate the "ALDT" formation, or altered them compared to the non-intervention control is unclear and future work could explore how PEG hydrogels can be tuned to promote lymph node-like tissue formation and functionality.

Perhaps the largest drawback of the lymphatic dysfunction models explored in this chapter are their inability to induce a chronic, negative, impact on lymphatic function or ensure LN segment engraftment. In the case of the ALND negative control, there were few measurable impacts on lymphatic function, and the few measured changes in lymphatic function were transient. The increased lymph transport resolved within a week and the oxazolone induced swelling resolved within a few days. A model with chronic lymphatic dysfunction and swelling would give us a better "baseline" to assess any beneficial effects of the biomaterial interventions. This could be accomplished by increasing the amount of lymphatic tissue resected or damaged, like what was done in a study that used diphtheria toxin injections in a transgenic animal model to locally ablate lymphatics[207]. Ultimately the goal would be to create a wound that slightly surpasses the ability of the lymphatics to naturally overcome. This is similar to studies in bone repair, where fractures are created that are slightly larger than what can heal naturally in order to assess the benefit of biomaterials and growth factors[208]. Alternative metrics, such as measuring fluid content at

the wound site via bioimpedance or lymphatic vessel density in collected tissue have been shown to successfully determine lymphatic function in response to surgery models[204]. The transplanted LN segment was rarely found in the transplant conditions and we were not able to determine the extent to which they either became necrotic or became a part of the "ALDT". Engraftment of the LN segments could be enhanced through either vascularization to the venous system or including VEGF-C, as has be done in similar studies[60].

In summary, our results contribute to our understanding of how lymphatics repair after surgical damage and how transplanted tissue and biomaterials influence this repair. We demonstrate that PEG hydrogels can facilitate transfer of lymphatic tissue and lay the ground work for an ALND model to determine the benefits of a PEG hydrogel. PEG gels tuned for lymphatic growth and regeneration could be used to minimize the amount of tissue needed for lymph node transfers in-vivo and improve their engraftment success rate. As it stands, the results we do gain from this ALND model further show how lymphatics transiently respond to lymph node removal, adjusting to changes in network resistance and loading. PEG hydrogels have the benefit of biocompatibility and modular design, without drawbacks involving sourcing, batch-to-batch variability, and immunogenicity that must be overcome with the clinical use of collagen gels[209–211]. Synthetic, maleimide cross-linked PEG hydrogels have greatly improved consistency in their biomechanical properties are easier to scale up for clinical use[173]. In the future I would propose repeating the ALND procedure but including resection of the brachial lymph node and nearby collateral vessels to induce chronic dysfunction in lymph transport and lymphatic contractility.

CHAPTER 5. CONCLUSIONS AND FUTURE DIRECTIONS

5.1 Conclusion

We have presented multiple studies utilizing engineering tools to better understand how the biomechanical properties and loading of the extracellular matrix regulate lymphatic function. In chapter 2 we establish a healthy and disease lymphatic muscle cell line and explore how this initial phenotype of the LMC influence their response to 2D culture conditions. For the first time the influence of cyclic stretch on lymphatic muscle cell function and protein synthesis is characterized. Through proteomic analysis we revealed that healthy, control, LMCs appeared to be more sensitive to stretch induced apoptosis, where remodelled LMCs were more resistant to apoptosis and upregulated pathways associated with oxidative stress, metabolic activity, and migration in response to cyclic strain. These results demonstrate the chronic nature of LMC remodelling after localized lymphatic damage and set the ground work for future studies in manipulating this phenotype.

Modular poly(ethylene glycol) (PEG) based hydrogels were effectively used to explore the sensitivity of sprouting lymphangiogenesis to properties of the extracellular matrix. We show that sprouting is enhanced around a local optimal stiffness associated with the 10% PEG hydrogel stiffness of about 1.5kPa. Sprouting is extremely sensitive to the type of adhesive peptides available to the embedded tissue, with the adhesive peptide RGD significantly increasing the length and abundance of sprouts compared to the collagen based GFOGER peptide. Furthermore, we demonstrate that embedding collecting vessel segments in PEG gels allows for the study of the effects of clinically relevant

chemotherapeutics and drugs on lymphatic sprouting morphogenesis. Human lymphatic malformation tissue was successfully cultured within the 10% PEG-2mM hydrogels. This platform has been used to begin understanding the role of rapamycin on LM tissue and could act as a platform to screen a variety of microenvironment cues, drugs, and molecular regulators of lymphatic health and function.

Finally, we present results on the application of PEG gels to enhance lymphatic transplantation and regeneration after damage to local lymphatic collecting vessel or lymph nodes. We show that PEG encapsulated lymphatic vessel segments can become incorporated into the host lymphatic network when transplanted and transport lymph from the interstitium by at least day 28. The impact of the axillary lymph node dissection rat model on the function of upstream lymphatic collecting vessel was explored and shown to lead to a transient increase in transport after one week but an eventual decrease in transport at day 28 day following the initial surgery. While the specific formulation of PEG hydrogel used did not outperform collagen gels at improving lymphatic function or engraftment, PEG hydrogels can be modified in a variety of ways to improve their impact for a specific application or function.

5.2 Future Work

While the work of this thesis demonstrates the feasibility of several platforms to study lymphatic function and regulation, many mechanistic and relevant biological questions remain unanswered. With regard to chapter 2, we demonstrate that our stretch waveform induces cellular responses consistent with vascular smooth muscle cell response to vascular damage and elevated loading. Stretch levels imposed were physiologically

relevant, but it remains unclear how slightly lower or higher amplitudes or frequencies would impact the response of LMCs. In addition, now that this platform is in place and the base response to a stretch waveform has been explored, future experiments could also look at how regulators found to be important in chapter 3 impact LMC response. Studies with VSMC would imply that pre-treatment with rapamycin, and culture with rapamycin during culture, may play a critical role in 2-D LMC phenotype in response to stretch. To create a more physiological phenotype of the LMCs, the impact of coculture and straining of LECs and LMCs could be explored to determine if LECs have a mitigating effect on LMC phenotypic changes.

There are many directions that the work with PEG hydrogels to better understand lymphatic sprouting and function. Considering the literature indicating that lymphangiogenesis can exacerbate lymphedema in some conditions, it is critical to gain a better understanding of the phenotype of the sprouts produced in our PEG hydrogels. Our hydrogels were formulated to enhance the length and number of sprouts from the embedded tissue, but stains for junctional proteins or quantification of chemokine levels could give some indication of the functionality of these induced sprouts. Whether or not these sprouts contain lumens and if they can functionally transport fluid, proteins or cells has yet to be determined but is critical to determining how these results may translate to outcomes *in-vivo*. Creating a gel that truly optimizes lymphatic healing *in-vivo* may require slightly different properties and embedded ligands. Along the same rationale, much more work also remains to be done to fully assess the impact of molecular regulators on sprout phenotype. Unanswered questions include how much these drugs alter sprout proliferation vs migration, junctional integrity, and pro- or anti-inflammatory signalling.

Culture of lymphatic malformation (LM) tissue presents a clinically relevant application of these gels. The degradable, 10% PEG – 2mM RGD hydrogel formulation was not optimized to for culture of lymphatic malformation tissue, and a systematic exploration of gel properties on these tissues may be needed to better recreate the behaviour of LM tissue *in-vivo*. Once sprouting within the gel is optimized several clinically relvant questions can be explored. For treatment it is important to know both how quickly rapamycin impacts LM growth and the optimal frequency of dosing. It is also unclear if patients can ever stop taking rapamycin or if LM growth would quickly resume after administration ends. This PEG gel platform allows for these questions to be explored in a somewhat high number and even on a patient specific manner. Finally alternative drugs and molecular regulators can be explored as alternatives to the non-specific administration of rapamycin.

In the GFP study there is a significant amount of work to be done to determine the mechanism of the demonstrated repair and the contributions of each aspect of the presented work. While the PEG gel facilitated successful engraftment of the donated GFP lymphatic collecting vessel, several questions remain unanswered. It is unclear how the lymphatics of the hindlimb would naturally repair without intervention or if this lymphatic injury model would have induced swelling or lymphedema. Future work would need to determine if the PEG was necessary for the tissue to engraft, or if transferring vessel segments alone would naturally become incorporated into the local lymphatic network. Also, the impact of PEG injection alone, on both lymphatic repair and regulation of inflammatory cell recruitment to the wound site, remains to be studied.

A major shortcoming of the ALND in-vivo model was the inability to elicit a large chronic dysfunction of the lymphatics in the animal models as a negative control. Animals seemed to be able to naturally regenerate lymphatic function without intervention. Increased damage or resection of lymphatics near the node site is feasible and could be used to exacerbate the impact of the surgery on the function of upstream lymphatics. Efforts should be made to worsen lymphatic dysfunction as a result of lymph node dissection and to ensure lymph node engraftment. Tethering growth factors within the hydrogel, such as VEGF-C, or vascularizing the transplanted lymph node could improve the engraftment rate of the node, ensuring the tissue does not become necrotic. Culturing the lymph node segment in-vitro to form a lymphatic network around the node before implanting the gel into the animal could also improve successful engraftment.

APPENDIX A.

Protein Name Perspective analysis	gene name	control NS	control S	wounded NS	wounded S	WNS/CNS	WS/CS	CS/CNS	WS/WNS
14-3-3 protein beta/alpha (Fragments) OS=Ovis aries GN=YWHAB PE=1 SV=2	YWHAB	60.13477	55.06828	61.46037	58.85832	1.022043819	1.068824376	0.915747745	0.957662962
14-3-3 protein epsilon OS=Ovis aries GN=YWHAE PE=1 SV=1	YWHAE	95.39869	86.04667	96.886154	94.447655	1.01559208	1.097632889	0.901969094	0.974831295
14-3-3 protein gamma (Fragments) OS=Ovis aries GN=YWHAG PE=1 SV=1	YWHAG	42.181866	36.28367	43.621338	39.96991	1.034125375	1.101595015	0.860172236	0.916292618
14-3-3 protein sigma OS=Ovis aries GN=SFN PE=2 SV=1	SFN	12.538171	13.270233	6.9023533	2.600086	0.550507191	0.195933711	1.058386666	0.376695583
14-3-3 protein zeta/delta OS=Ovis aries GN=YWHAZ PE=1 SV=1	YWHAZ	86.278076	77.1485	89.12907	88.44494	1.033044246	1.146424623	0.894184288	0.992324278
40S ribosomal protein S25 OS=Ovis aries GN=RPS25 PE=2 SV=1	RPS25	9.5323305	9.766068	10.219987	11.17911 6	1.072139389	1.144689552	1.024520499	1.093848358
40S ribosomal protein S26 OS=Ovis aries GN=RPS26 PE=3 SV=3	RPS26	2.869465	2.015385 4	3.255005 4	3.548758 7	1.134359 68	1.760833784	0.702355805	1.090246 64
40S ribosomal protein SA OS=Ovis aries GN=RPSA PE=2 SV=1	RPSA	36.107384	37.199856	38.596302	38.29242	1.068930998	1.029370114	1.030256194	0.992126655
60S ribosomal protein L10 OS=Ovis aries GN=RPL10 PE=2 SV=1	RPL10	18.873259	20.466877	23.824865	23.556015	1.262360941	1.150933 53	1.084437881	0.988715571
6-phosphogluconate dehydrogenase, decarboxylating OS=Ovis aries GN=PGD PE=1 SV=4	PGD	80.90127	68.262245	81.381874	75.74477	1.005940624	1.109614 4	0.843772 23	0.930732684
Abnormal spindle-like microcephaly-associated protein homolog (Fragment) OS=Ovis aries GN=ASPM PE=2 SV=1	ASPM	0.262237 85	0.110565 23	0.146091 74	0.182589 56	0.557096315	1.651419348	0.421621936	1.249828087
Acetyl-CoA carboxylase 1 OS=Ovis aries GN=ACACA PE=2 SV=1	ACACA	0.713675 44	0.529133 6	0.127830 27	1.457347 3	0.179115411	2.754214248	0.741420498	11.40064321

Acidic leucine-rich nuclear phosphoprotein 32 family member B OS=Ovis aries GN=ANP32B PE=2 SV=1	ANP32B	10.813922	8.903204	12.533083	11.374314	1.158976641	1.27755289	0.823309434	0.90754318
Actin, cytoplasmic 1 OS=Ovis aries GN=ACTB PE=2 SV=1	ACTB	1689.8059	1713.0104	1886.9027	1776.7825	1.116638722	1.037228087	1.013732051	0.941639704
Alpha-1-antiproteinase OS=Ovis aries PE=1 SV=1	AHSG	45.39586	50.535717	23.948465	42.045753	0.527547336	0.832000721	1.113223034	1.755676324
Alpha-2-HS-glycoprotein OS=Ovis aries GN=AHSG PE=1 SV=1	AHSG	49.366257	65.00938	41.023277	54.392723	0.830998327	0.836690382	1.316878855	1.325899026
Alpha-crystallin B chain OS=Ovis aries GN=CRYAB PE=2 SV=1	CRYAB	4.0516715	2.0832436	0.8640072	1.1054637	0.213247101	0.530645432	0.51416893	1.279461213
Alpha-lactalbumin OS=Ovis aries GN=LALBA PE=1 SV=2	LALBA	0.10878014 6	0	0	0	0		0	
Alpha-S1-casein OS=Ovis aries GN=CSN1S1 PE=1 SV=3	CSN1S1	28.465424	2.198274	14.381121	10.159937	0.505213659	4.621779178	0.077226111	0.706477402
Alpha-S2-casein OS=Ovis aries GN=CSN1S2 PE=2 SV=1	CSN1S2	0.21756029	0	0	0	0		0	
Annexin A2 OS=Ovis aries GN=ANXA2 PE=1 SV=1	ANXA2	376.9804	314.353	202.86124	289.05273	0.538121451	0.919516372	0.833870939	1.424879045
Antithrombin-III OS=Ovis aries GN=SERPINC1 PE=2 SV=1	SERPINC1	0.5738152	0.46555862	0.41879633	0.23711282	0.729845306	0.509308194	0.811338947	0.566176929
Apolipoprotein E OS=Ovis aries GN=APOE PE=2 SV=1	APOE	1.6457238	3.48241	0.113626905	3.698163	0.069043727	1.061955083	2.11603551	32.54654344
ATP synthase subunit a OS=Ovis aries GN=MT-ATP6 PE=3 SV=1	MT-ATP6	0.10878014 6	0.9038708	0.10226422	0.25106063	0.940100044	0.277761634	8.309152297	2.455019263
ATP-citrate synthase OS=Ovis aries GN=ACLY PE=2 SV=1	ACLY	67.77852	59.312595	65.95057	72.757065	0.973030541	1.226671418	0.875094278	1.103206007
Beta-1,3-galactosyl-O-glycosyl-glycoprotein beta-1,6-N-acetylglucosaminyltransferase 3 OS=Ovis aries GN=GCNT3 PE=3 SV=1	GCNT3	0.10878014 6	0.9950871	0	0	0	0	9.14769042 5	

Beta-casein OS=Ovis aries GN=CSN2 PE=1 SV=3	CSN2	10.178004	0.72933567	1.6573298	1.044492	0.162834461	1.432114242	0.071658025	0.630225801
Beta-lactoglobulin OS=Ovis orientalis musimon GN=LGB PE=1 SV=1	LGB	6.837664	0.06633914	1.3120588	0.10042425	0.191886995	1.513800902	0.009702018	0.076539443
Beta-lactoglobulin-1/B OS=Ovis aries PE=1 SV=1	LGB	6.837664	0.06633914	1.3120588	0.10042425	0.191886995	1.513800902	0.009702018	0.076539443
Biglycan OS=Ovis aries GN=BGN PE=2 SV=1	BGN	1.4060187	3.914379	0.24835597	3.4658687	0.176637743	0.885419807	2.784016315	13.95524617
Bombesin receptor subtype-3 OS=Ovis aries GN=BRS3 PE=2 SV=1	BRS3	0	0	0.10226422	0				0
Calmodulin OS=Ovis aries GN=CALM2 PE=2 SV=3	CALM2	79.45418	78.31891	82.85869	69.47363	1.042848721	0.887060737	0.985711639	0.838459189
Calpain-3 OS=Ovis aries GN=CAPN3 PE=2 SV=1	CAPN3	0.122377664	0	0	0	0		0	
Calpastatin OS=Ovis aries GN=CAST PE=2 SV=1	CAST	12.392495	10.422696	10.489923	11.650951	0.846473894	1.11784427	0.841049038	1.110680264
Calponin-1 OS=Ovis aries GN=CNN1 PE=2 SV=1	CNN1	50.05764	45.873264	55.72783	46.533695	1.113273219	1.014396861	0.916408844	0.835017172
cAMP-dependent protein kinase catalytic subunit alpha OS=Ovis aries GN=PRKACA PE=1 SV=3	PRKACA	1.2972032	1.5234311	1.9551946	1.4166994	1.507238496	0.929939923	1.174396656	0.7245823
Cathepsin B (Fragment) OS=Ovis aries GN=CTSB PE=1 SV=1	CTSB	1.2975322	1.2130586	2.662522	1.7741619	2.051989153	1.46255251	0.934896722	0.666346381
Cathepsin D (Fragment) OS=Ovis aries GN=CTSD PE=1 SV=1	CTSD	33.409035	29.17774	28.538147	26.031916	0.854204469	0.89218411	0.873348781	0.912179617
Cathepsin L1 OS=Ovis aries GN=CTSL PE=1 SV=1	CTSL	0	0.359337	0.25566053	0		0		0
Caveolin-1 OS=Ovis aries GN=CAV1 PE=2 SV=1	CAV1	12.361296	9.575319	12.558119	10.788072	1.015922521	1.126654057	0.774620962	0.859051582
Ceroid-lipofuscinosis neuronal protein 5 OS=Ovis aries GN=CLN5 PE=2 SV=1	CLN5	0.08900194	0	0	0	0		0	
Cholesterol side-chain cleavage enzyme, mitochondrial OS=Ovis aries GN=CYP11A1 PE=1 SV=1	CYP11A1	0	0	0.12783027	0.223165				1.745791509

Cofilin-1 OS=Ovis aries GN=CFL1 PE=2 SV=3	CFL1	136.27386	156.10307	153.9459	147.43892	1.129680336	0.944497248	1.145510005	0.957732034
Corticosteroid 11-beta-dehydrogenase isozyme 1 OS=Ovis aries GN=HSD11B1 PE=2 SV=3	HSD11B1	4.8993206	3.2537522	3.277668	1.8976998	0.669004596	0.583234273	0.664123144	0.578978652
Cystatin-B OS=Ovis aries GN=CSTB PE=1 SV=1	CSTB	0	0.24877177	0	0		0		
Cytochrome c OS=Ovis aries GN=CYCS PE=1 SV=2	CYCS	8.357846	6.02657	10.940993	10.127319	1.309068509	1.68044493	0.721067366	0.925630699
Cytochrome c oxidase subunit 2 OS=Ovis aries GN=MT-CO2 PE=3 SV=1	MT-CO2	5.732361	5.4741645	6.2722054	5.4631586	1.094174878	0.997989483	0.954958088	0.871010793
Cytochrome c oxidase subunit 3 OS=Ovis aries GN=MT-CO3 PE=3 SV=2	MT-CO3	0.24864034	0	0.3668895	0.28692645	1.475583166		0	0.782051408
Cytochrome c oxidase subunit 7A1, mitochondrial (Fragment) OS=Ovis aries GN=COX7A1 PE=1 SV=1	COX7A1	0.45143762	0.23495111	1.1033984	0.48940518	2.44418797	2.08300888	0.520450888	0.443543493
Cytochrome c oxidase subunit 7A2, mitochondrial (Fragment) OS=Ovis aries GN=COX7A2 PE=1 SV=1	COX7A2	0.45143762	0.23495111	1.1033984	0.48940518	2.44418797	2.08300888	0.520450888	0.443543493
Decorin OS=Ovis aries GN=DCN PE=2 SV=1	DCN	5.675286	7.364075	7.015649	13.083026	1.23617541	1.776601406	1.297568968	1.864834743
Dynein light chain Tctex-type 3 OS=Ovis aries GN=DYNLT3 PE=3 SV=1	DYNLT3	0	0.24166402	0.14609174	0		0		0
Elongation factor 1-delta OS=Ovis aries GN=EEF1D PE=2 SV=1	EEF1D	12.224083	14.133897	15.035321	13.340025	1.229975369	0.943832051	1.156233723	0.887245773
Ferritin heavy chain OS=Ovis aries GN=FTH1 PE=1 SV=3	FTH1	3.5039217	0.9101888	0.9933613	0.9627363	0.283499857	1.057732528	0.259762882	0.969170331
Ferritin light chain (Fragment) OS=Ovis aries GN=FTL PE=1 SV=1	FTL	8.255258	6.636257	8.691646	5.991618	1.052861825	0.902861056	0.803882447	0.689353662
Fructose-bisphosphate aldolase B OS=Ovis aries GN=ALDOB PE=2 SV=2	ALDOB	2.6293826	1.6470271	1.5554088	3.004298	0.591549058	1.824073204	0.626393093	1.931516653

Galectin-1 OS=Ovis aries GN=LGALS1 PE=1 SV=2	LGALS1	51.00698	54.712975	45.853653	34.161606	0.898968 2	0.624378 514	1.072656 625	0.745013 838
Glyceraldehyde-3-phosphate dehydrogenase (Fragment) OS=Ovis aries GN=GAPDH PE=2 SV=4	GAPDH	428.3631 6	415.0821 2	470.5562 7	473.0590 2	1.098498 456	1.139675 735	0.968995 84	1.005318 705
Glycogen phosphorylase, brain form OS=Ovis aries GN=PYGB PE=2 SV=3	PYGB	5.315074 4	5.126995	4.146975	5.697503 6	0.780228 965	1.111275 435	0.964613 967	1.373893 887
Glycogen phosphorylase, liver form OS=Ovis aries GN=PYGL PE=2 SV=3	PYGL	56.45109 6	51.15137 5	51.90483	49.42345 4	0.919465 408	0.966219 461	0.906118 368	0.952193 736
Glycogen phosphorylase, muscle form OS=Ovis aries GN=PYGM PE=2 SV=3	PYGM	3.585047 5	3.357161 8	3.135253 4	3.240696	0.874536 084	0.965308 255	0.936434 399	1.033631 285
Hippocalcin-like protein 1 OS=Ovis aries GN=HPCAL1 PE=2 SV=1	HPCAL1	0.448718 07	0.608108 76	0.568134 55	0.481000 3	1.266128 083	0.790977 423	1.355213 442	0.846630 961
Histone H2A.Z OS=Ovis aries GN=H2AFZ PE=2 SV=3	H2AFZ	13.41878 5	12.71933 1	11.86877 4	12.69501 3	0.884489 468	0.998088 107	0.947875 013	1.069614 52
Insulin-like growth factor-binding protein 4 OS=Ovis aries GN=IGFBP4 PE=1 SV=1	IGFBP4	0.560217 74	0.348280 5	0.170440 36	0.083686 88	0.304239 491	0.240285 862	0.621687 739	0.491003 891
Integrin beta-1 OS=Ovis aries GN=ITGB1 PE=2 SV=1	ITGB1	49.99510 6	61.77921 7	45.93357 5	42.90258	0.918761 428	0.694450 045	1.235705 291	0.934013 518
Integrin beta-6 OS=Ovis aries GN=ITGB6 PE=2 SV=1	ITGB6	2.570425 7	1.509323 1	1.840767 6	2.064023	0.716133 363	1.367515 676	0.587187 99	1.121283 86
Isocitrate dehydrogenase [NADP] cytoplasmic OS=Ovis aries GN=IDH1 PE=2 SV=1	IDH1	47.38142	46.567204	49.8917	56.306087	1.052980 261	1.209136 091	0.982815 711	1.128566 214
Kappa-casein OS=Ovis aries GN=CSN3 PE=1 SV=2	CSN3	4.613054 8	0.232617 77	0.241457 16	0.478210 75	0.052342 14	2.055779 101	0.050425 972	1.980520 064
Macrophage migration inhibitory factor OS=Ovis aries GN=MIF PE=3 SV=1	MIF	13.21317	14.127926	9.948515	12.054569	0.752924 166	0.853244 064	1.069230 624	1.211695 313
Metalloproteinase inhibitor 1 OS=Ovis	TIMP1	0.339937 96	0.432389 05	0.259718 66	0.694938 24	0.764017 823	1.607205 918	1.271964 596	2.675734 735

aries GN=TIMP1 PE=2 SV=1									
Myosin light chain kinase, smooth muscle (Fragment) OS=Ovis aries GN=MYLK PE=2 SV=1	MYLK	7.826611 5	5.750217 4	3.538261 2	1.879766 8	0.452080 853	0.326903 605	0.734700 758	0.531268 523
NADH-ubiquinone oxidoreductase chain 3 OS=Ovis aries GN=MT-ND3 PE=3 SV=1	MT-ND3	0.407925 58	0.418568 37	0.614802 7	0.422419 5	1.507144 269	1.009200 719	1.026090 028	0.687081 4
NADH-ubiquinone oxidoreductase chain 5 OS=Ovis aries GN=MT-ND5 PE=3 SV=1	MT-ND5	0.195804 27	0.290233 76	0.170440 36	0.571860 4	0.870462 937	1.970344 18	1.482264 713	3.355193 57
Platelet factor 4 OS=Ovis aries GN=PF4 PE=1 SV=1	PF4	0	4.036815 6	0	0.854801 7		0.211751 486		
Pro-opiomelanocortin OS=Ovis aries GN=POMC PE=1 SV=3	POMC	0	0.124385 886	0	0.125530 32		1.009200 674		
Prostaglandin G/H synthase 1 OS=Ovis aries GN=PTGS1 PE=1 SV=3	PTGS1	0	0.234951 11	0.248355 97	0.969173 7		4.125001 58		3.902357 169
Proteolipid protein 2 (Fragment) OS=Ovis aries GN=PLP2 PE=2 SV=1	PLP2	1.567928 6	1.444491 9	0.624947 97	1.119810 2	0.398581 906	0.775227 746	0.921274 03	1.791845 488
Pulmonary surfactant-associated protein A OS=Ovis aries GN=SFTPA1 PE=2 SV=1	SFTPA1	0.576534 75	0.433548 84	0.993423 8	0.376590 97	1.723094 402	0.868624 098	0.751990 821	0.379083 902
Pyridoxal kinase OS=Ovis aries GN=PDXK PE=1 SV=1	PDXK	0.306562 24	0.252720 53	0.227253 81	0.251060 63	0.741297 461	0.993431 875	0.824369 4	1.104758 728
Retinal dehydrogenase 1 OS=Ovis aries GN=ALDH1A1 PE=1 SV=2	ALDH1A1	1.436555 5	0.284310 6	4.815346	3.550715 4	3.352008 328	12.48886 042	0.197911 323	0.737374 926
Secreted phosphoprotein 24 OS=Ovis aries GN=SPP2 PE=2 SV=1	SPP2	0	0.124385 886	0	0		0		
Serine hydroxymethyltransferase, cytosolic OS=Ovis aries GN=SHMT1 PE=1 SV=3	SHMT1	0.108780 146	0	0	0	0		0	
Serum albumin OS=Ovis aries GN=ALB PE=1 SV=1	ALB	372.1639 4	475.9249 6	358.9995	378.1712 6	0.964627 309	0.794602 704	1.278804 604	1.053403 306
Sideroflexin-1 OS=Ovis aries	SFXN1	6.804692	5.672725	6.178905 5	8.200552	0.908036 029	1.445610 707	0.833649 047	1.327185 211

GN=SFXN1 PE=2 SV=1									
Sodium/glucose cotransporter 1 OS=Ovis aries GN=SLC5A1 PE=2 SV=1	SLC5A1	0.23115781	0	0	0	0		0	
Sodium/potassium-transporting ATPase subunit alpha-1 OS=Ovis aries GN=ATP1A1 PE=1 SV=1	ATP1A1	58.59616	73.71313	56.236767	70.158	0.959734682	0.951770736	1.257985677	1.247546823
Sodium/potassium-transporting ATPase subunit beta-1 OS=Ovis aries GN=ATP1B1 PE=2 SV=1	ATP1B1	0.108780146	0.29023376	0.25566053	0.09129478	2.350249925	0.314556032	2.668076581	0.35709376
Solute carrier family 2, facilitated glucose transporter member 1 (Fragment) OS=Ovis aries GN=SLC2A1 PE=2 SV=1	SLC2A1	0	0.24877177	0	0		0		
Solute carrier family 2, facilitated glucose transporter member 3 OS=Ovis aries GN=SLC2A3 PE=2 SV=1	SLC2A3	0.108780146	0.65276563	0	0	0	0	6.000779131	
Sorbitol dehydrogenase OS=Ovis aries GN=SORD PE=1 SV=1	SORD	0.47591314	0	0.485755	0.223165	1.02067995		0	0.459418843
Sulfate transporter OS=Ovis aries GN=SLC26A2 PE=3 SV=1	SLC26A2	0.22027978	0	0	0.7308654	0		0	
Superoxide dismutase [Cu-Zn] OS=Ovis aries GN=SOD1 PE=1 SV=2	SOD1	1.901357	1.5162627	3.6077287	3.0131266	1.897449401	1.987206175	0.797463443	0.835186582
Syntaxin-1B OS=Ovis aries GN=STX1B PE=2 SV=1	STX1B	0	0.3206392	0.25971866	0.61649334		1.922701092		2.373696753
Testin OS=Ovis aries GN=TES PE=3 SV=1	TES	0.48640266	0.7364434	0.3875489	0.1115825	0.796765585	0.151515378	1.51406121	0.287918505
Tetraspanin-9 OS=Ovis aries GN=TSPAN9 PE=2 SV=1	TSPAN9	0.24475533	0.47661513	0	0.3486953	0	0.731607702	1.947312567	#DIV/0!
Thioredoxin OS=Ovis aries GN=TXN PE=3 SV=2	TXN	41.847206	36.3977	27.918917	40.35974	0.667163227	1.108854131	0.869776109	1.445605501
Trichohyalin OS=Ovis aries GN=TCHH PE=2 SV=2	TCHH	0	0	0.20452844	0				0
Ubiquitin-60S ribosomal protein L40 OS=Ovis aries	UBA52	27.616163	33.900013	30.464231	34.658737	1.103130475	1.022381 23	1.227542472	1.137686259

GN=UBA52 PE=2 SV=2									
Uroporphyrinogen decarboxylase OS=Ovis aries GN=UROD PE=1 SV=1	UROD	2.369853 3	1.399081 1	2.367534 6	1.373660 4	0.999021 585	0.981830 431	0.590366 121	0.580207 107
Vimentin (Fragment) OS=Ovis aries GN=VIM PE=2 SV=3	VIM	563.8526 6	540.6947	576.9602 7	562.5079	1.023246 516	1.040342 914	0.958929 058	0.974950 84
Vitamin K-dependent gamma-carboxylase OS=Ovis aries GN=GGCX PE=2 SV=1	GGCX	0.326340 44	0	0	0	0		0	

Supplementary Table 1: Protein Identification and Expression

Categories	Diseases or Functions Annotation	p-Value	Predicted Activation State	Activation z-score	Molecules	# Molecules
Molecular Transport	secretion of molecule	2.78E-06	Increased	2.281	ACLY,ANXA2,APOE,CFL1,HSD11B1,LGALS1,MIF,POMC,PTGS1,SFTPA1,SOD1,STX1B,YWHAZ	13
Lipid Metabolism, Molecular Transport, Small Molecule Biochemistry	secretion of lipid	1.58E-06	Increased	2.033	APOE,CFL1,HSD11B1,LGALS1,POMC,PTGS1,SFTPA1,SOD1	8
Free Radical Scavenging	modification of reactive oxygen species	6.39E-07		1.953	CYCS,PTGS1,SOD1,TXN	4
Molecular Transport	transport of molecule	4.21E-09		1.812	ACLY,ALB,ANXA2,APOE,ATP1A1,ATP1B1,CAV1,CFL1,CRYAB,CSN2,FTH1,FTL,HSD11B1,ITGB1,LGALS1,MIF,PLP2,POMC,PRKACA,PTGS1,SFTPA1,SFXN1,SOD1,STX1B,UROD,YWHAB,YWHAE,YWHAZ	28
Nucleic Acid Metabolism	metabolism of nucleic acid component or derivative	6.77E-06		1.778	ACACA,ACLY,APOE,ATP1B1,CAV1,CYCS,MT-ATP6,PGD,POMC,PTGS1,RPSA,SOD1	12
Nucleic Acid Metabolism, Small Molecule Biochemistry	metabolism of nucleotide	0.00004		1.778	APOE,ATP1B1,CAV1,CYCS,MT-ATP6,PGD,POMC,PTGS1,RPSA,SOD1	10
Nucleic Acid Metabolism, Small Molecule Biochemistry	synthesis of nucleotide	0.000277		1.778	APOE,CAV1,CYCS,MT-ATP6,POMC,PTGS1,RPSA,SOD1	8
Lipid Metabolism, Molecular Transport, Small Molecule Biochemistry	concentration of lipid	5.81E-07		1.611	ACACA,ACLY,AHSG,ALB,ALDH1A1,APOE,ATP1A1,CAV1,CTSD,HSD11B1,IDH1,MIF,POMC,PTGS1,SFTPA1,SOD1,TIMP1	17
Lipid Metabolism, Small Molecule Biochemistry	synthesis of lipid	2.25E-10		1.6	ACACA,ACLY,ALB,ALDH1A1,APOE,ATP1A1,CAV1,COX7A2,HSD11B1,IGFBP4,ITGB1,MIF,PGD,POMC,PTGS1,SERPINC1,SOD1,TXN,VIM,YWHAG	20
Lipid Metabolism, Small Molecule Biochemistry, Vitamin and Mineral Metabolism	metabolism of terpenoid	7.94E-06		1.595	ACLY,ALDH1A1,APOE,CAV1,HSD11B1,IGFBP4,POMC,VIM,YWHAG	9
Lipid Metabolism, Molecular Transport, Small Molecule Biochemistry	quantity of steroid	8.85E-05		1.507	ALB,APOE,ATP1A1,CAV1,HSD11B1,IDH1,MIF,POMC,PTGS1,TIMP1	10
Lipid Metabolism, Small Molecule Biochemistry	binding of lipid	1.66E-05		1.505	ANXA2,APOE,RPSA,SFN,SFTPA1	5
Lipid Metabolism, Small Molecule Biochemistry	synthesis of fatty acid	1.94E-07		1.474	ACACA,ACLY,ALB,APOE,CAV1,MIF,PTGS1,SERPINC1,SOD1,TXN,VIM	11
Inflammatory Response	inflammation of body cavity	2.12E-06		-1.475	ACTB,ALB,APOE,ATP1B1,CAV1,CTSB,CTSD,DCN,GAPDH,HSD11B1,ITGB6,LGALS1,MIF,PF4,PTGS1,SFTPA1,SOD1,TIMP1	18
Inflammatory Response, Organismal Injury and Abnormalities	inflammation of organ	9.5E-09		-1.492	ACTB,ALB,APOE,ATP1A1,ATP1B1,BGN,CAV1,CFL1,CTSB,CTSD,DCN,GAPDH,HSD11B1,ITGB6,LGALS1,MIF,MYLK,PF4,POMC,PTGS1,SFN,SFTPA1,SOD1,TIMP1,VIM	25

Cellular Movement, Hematological System Development and Function, Immune Cell Trafficking	cell movement of antigen presenting cells	4.66E-05	-1.55	APOE,CAV1,ITGB1,LGALS1,MIF,MYLK,PF4,SFTPA1,TIMP1	9
Neurological Disease	Neurodegeneration	0.000114	-1.554	APOE,ATP1B1,CAV1,CTSB,CTSD,GAPDH,SOD1,VIM	8
Cell-To-Cell Signaling and Interaction, Hematological System Development and Function	binding of leukocytes	0.000121	-1.58	APOE,DCN,ITGB1,PF4,POMC,SFTPA1	6
Hematological System Development and Function, Tissue Development	accumulation of myeloid cells	1.19E-05	-1.586	APOE,CRYAB,ITGB1,MIF,POMC,SOD1,TIMP1	7
Organismal Development	growth of vessel	6.72E-05	-1.606	APOE,CTSB,HSD11B1,ITGB1,LGALS1,TIMP1	6
Cellular Movement	migration of cells	3.69E-11	-1.607	ACTB,AHSG,ALB,ANXA2,APOE,ASPM,BGN,CAST,CAV1,CFL1,CRYAB,CTSB,DCN,FTH1,IDH1,IGFBP4,ITGB1,ITGB6,LGALS1,MIF,MYLK,PF4,POMC,PRKACA,RPSA,SERPINC1,SFN,SFTPA1,SOD1,TIMP1,TXN,VIM,YWHAE,YWHAZ	34
Cancer, Organismal Injury and Abnormalities	tumorigenesis of tissue	0.000253	-1.611	ACLY,ACTB,AHSG,ALB,ALDH1A1,ALDOB,ANP32B,ANXA2,APOE,ASPM,ATP1A1,ATP1B1,BGN,CALM1 (includes others),CAST,CAV1,CNN1,COX7A1,COX7A2,CRYAB,CSN1S1,CSN2,CSN3,CTSB,CTSD,CYCS,DCN,EEF1D,FTH1,FTL,GAPDH,H2AFZ,HSD11B1,IDH1,IGFBP4,ITGB1,ITGB6,LGALS1,MIF,MT-ATP6,MT-CO2,MT-ND3,MT-ND5,MYLK,PDXK,PF4,PLP2,POMC,PRKACA,PTGS1,PYGB,PYGL,PYGM,RPL10,RPS25,SERPINC1,SFN,SFTPA1,SFXN1,SOD1,STX1B,TES,TIMP1,TSPAN9,TXN,UROD,VIM,YWHAE,YWHAG,YWHAZ	70
Endocrine System Disorders, Metabolic Disease	insulin resistance	0.00002	-1.644	ACACA,AHSG,APOE,CAV1,HSD11B1,MIF,POMC,PTGS1,SOD1	9
Cellular Movement, Hematological System Development and Function, Immune Cell Trafficking	cellular infiltration by mononuclear leukocytes	1.12E-06	-1.658	APOE,BGN,ITGB1,LGALS1,MIF,MYLK,PF4,TIMP1	8
Cellular Development, Connective Tissue Development and Function, Tissue Development	differentiation of connective tissue	0.000362	-1.671	APOE,BGN,CAST,HSD11B1,ITGB1,MIF,PRKACA,SFXN1,SOD1,TIMP1,VIM,YWHAZ	12
Protein Synthesis	quantity of IL-6 in blood	0.000331	-1.732	APOE,CAV1,POMC,SOD1	4
Cellular Movement, Hematological System Development and Function, Immune Cell Trafficking	cell movement of leukocytes	1.28E-09	-1.742	ACTB,ALB,ANXA2,APOE,BGN,CAST,CAV1,CRYAB,CTSB,DCN,ITGB1,LGALS1,MIF,MYLK,PF4,POMC,SERPINC1,SFTPA1,TIMP1,TXN	20
Cell Death and Survival	apoptosis of prostate cancer cell lines	0.000141	-1.758	ACACA,CAV1,IGFBP4,ITGB1,LGALS1,SOD1	6
Cellular Movement, Immune Cell Trafficking	leukocyte migration	2.03E-09	-1.788	ACTB,ALB,ANXA2,APOE,BGN,CAST,CAV1,CRYAB,CTSB,DCN,ITGB1,LGALS1,MIF,MYLK,PF4,POMC,SERPINC1,SFTPA1,SOD1,TIMP1,TXN	21
Cellular Movement	cell movement	5.11E-11	-1.805	ACTB,AHSG,ALB,ANXA2,APOE,ASPM,BGN,CAST,CAV1,CFL1,CNN1,CRYAB,CTSB,DCN,FTH1,GAPDH,IDH1,IGFBP4,ITGB1,ITGB6,LGALS1,MIF,MYLK,PF4,POMC,PRKACA,RPSA,SERPINC1,SFN,SFTPA1,SOD1,TIMP1,TXN,VIM,YWHAE,YWHAZ	36
Hematological System Development and Function, Immune Cell Trafficking, Inflammatory Response, Tissue Development	accumulation of leukocytes	2.65E-05	-1.843	APOE,BGN,ITGB1,MIF,POMC,SERPINC1,SOD1,TIMP1	8
Cellular Movement	chemotaxis	0.000367	-1.876	ANXA2,APOE,CAV1,ITGB1,LGALS1,MIF,MYLK,PF4,SFTPA1,TXN	10

Organismal Survival	morbidity or mortality	1.68E-09		-1.896	ACACA,ACLY,ACTB,ALDH1A1,APOE,ATP1A1,ATP1B1,BGN,CAST,CAV1,CFL1,COX7A1,CRYAB,CTSB,CTSD,CYCS,DCN,FTH1,H2AFZ,IDH1,ITGB1,MIF,POMC,PRKACA,PTGS1,RPSA,SERPINC1,SFN,SFTPA1,SOD1,STX1B,TIMP1,TXN,UROD,VIM,YWHAE	36
Cell Death and Survival, Organismal Injury and Abnormalities	necrosis of epithelial tissue	4.54E-10		-1.917	ALDH1A1,CAV1,CRYAB,CTSB,CYCS,DCN,GAPDH,ITGB1,LGALS1,MIF,MYLK,POMC,PRKACA,PTGS1,SERPINC1,SOD1,TIMP1,TXN	18
Cellular Movement, Hematological System Development and Function, Immune Cell Trafficking, Inflammatory Response	migration of neutrophils	9.27E-05		-1.927	ALB,ITGB1,MYLK,SERPINC1,TXN	5
Cellular Movement, Skeletal and Muscular System Development and Function	migration of smooth muscle cells	0.000385		-1.932	APOE,IGFBP4,ITGB1,TIMP1,TXN	5
Cell Death and Survival	cell death of leukemia cell lines	2.21E-06		-1.956	CAV1,CTSB,CTSD,CYCS,FTH1,GAPDH,ITGB1,LGALS1,PRKACA,YWHAG	10
Hematological System Development and Function, Immune Cell Trafficking, Inflammatory Response, Tissue Development	accumulation of phagocytes	0.000365		-1.959	APOE,ITGB1,MIF,SOD1,TIMP1	5
Cardiovascular Disease	Infarction	3.01E-05		-1.992	APOE,ATP1A1,CAV1,MIF,PTGS1,SERPINC1,SOD1,TIMP1,TXN	9
Protein Synthesis	quantity of TNF in blood	0.000242	Decreased	-2	APOE,CAV1,MIF,SOD1	4
Cell Morphology, Cellular Movement	cell spreading of blood cells	0.000317	Decreased	-2	ALB,CAST,ITGB1,LGALS1	4
Cell Death and Survival	necrosis of prostate cancer cell lines	3.67E-05	Decreased	-2.022	ACACA,CAV1,IGFBP4,ITGB1,LGALS1,SOD1,TXN	7
Organismal Survival	organismal death	4.9E-09	Decreased	-2.058	ACACA,ACLY,ACTB,ALDH1A1,APOE,ATP1A1,ATP1B1,BGN,CAST,CAV1,CFL1,COX7A1,CRYAB,CTSB,CTSD,CYCS,DCN,FTH1,H2AFZ,IDH1,ITGB1,MIF,POMC,PRKACA,PTGS1,RPSA,SERPINC1,SFTPA1,SOD1,STX1B,TIMP1,TXN,UROD,VIM,YWHAE	35
Cellular Movement	cell movement of myeloid cells	1.5E-09	Decreased	-2.189	ALB,ANXA2,APOE,CAST,CAV1,CRYAB,CTSB,ITGB1,LGALS1,MIF,MYLK,PF4,POMC,SERPINC1,SFTPA1,TIMP1,TXN	17
Cardiovascular System Development and Function, Tissue Morphology	permeability of blood vessel	2.8E-06	Decreased	-2.19	APOE,CAV1,MIF,MYLK,SERPINC1,TIMP1	6
Cellular Movement, Hematological System Development and Function, Immune Cell Trafficking	cell movement of mononuclear leukocytes	0.000085	Decreased	-2.199	ACTB,ANXA2,APOE,BGN,ITGB1,LGALS1,MIF,MYLK,PF4,TIMP1	10
Organismal Injury and Abnormalities	Organ Degeneration	1.46E-05	Decreased	-2.212	APOE,ASPM,ATP1B1,CAV1,CTSB,CTSD,GAPDH,PTGS1,SERPINC1,SOD1,TXN,VIM	12
Cellular Function and Maintenance	ion homeostasis of cells	0.000143	Decreased	-2.219	ALB,ANXA2,APOE,ATP1A1,ATP1B1,CAV1,FTL,ITGB1,PF4,PYGM,SOD1	11
Cellular Movement, Hematological System Development and Function, Immune Cell Trafficking, Inflammatory Response	cell movement of macrophages	0.000256	Decreased	-2.278	APOE,CAV1,ITGB1,MIF,MYLK,PF4,SFTPA1	7
Cellular Movement, Hematological System Development and Function, Immune Cell Trafficking, Inflammatory Response	cell movement of phagocytes	9.27E-08	Decreased	-2.311	ALB,ANXA2,APOE,CAST,CAV1,CTSB,ITGB1,LGALS1,MIF,MYLK,PF4,SERPINC1,SFTPA1,TIMP1,TXN	15
Cardiovascular System Development and Function, Hematological System Development and Function	blood pressure	1.46E-07	Decreased	-2.386	APOE,ATP1A1,BGN,CAV1,CRYAB,HSD11B1,ITGB1,POMC,PTGS1,SOD1,TIMP1	11

Cellular Development	differentiation of cells	2.94E-06	Decreased	-3.163	ACACA,ACLY,ALB,ANP32B,ANXA2,APOE,ASPM,BGN,CAST,CAV1,CFL1,CTSB,DCN,GAPDH,H2AFZ,HSD11B1,ITGB1,LGALS1,MIF,PF4,PRKACA,PTGS1,SFN,SFXN1,SOD1,TIMP1,VIM,YWHAG,YWHAZ	29
Neurological Disease, Organismal Injury and Abnormalities, Psychological Disorders	Dementia	3.47E-16			ACLY,ACTB,ALB,APOE,ATP1A1,ATP1B1,BGN,CAV1,CNN1,CTSB,CTSD,DCN,GAPDH,HSD11B1,LGALS1,MT-CO2,MT-ND5,PRKACA,PTGS1,SERPINC1,SOD1,TIMP1,TXN,VIM,YWHAZ	25
Metabolic Disease, Neurological Disease, Organismal Injury and Abnormalities, Psychological Disorders	Alzheimer disease	1.25E-15			ACLY,ACTB,ALB,APOE,ATP1A1,ATP1B1,BGN,CAV1,CNN1,CTSB,CTSD,DCN,GAPDH,HSD11B1,LGALS1,MT-CO2,PRKACA,PTGS1,SERPINC1,SOD1,TIMP1,TXN,VIM,YWHAZ	24
Dermatological Diseases and Conditions, Organismal Injury and Abnormalities	psoriasis	2.89E-10			ANXA2,APOE,ATP1B1,CAV1,CFL1,CNN1,CTSB,CYCS,GAPDH,H2AFZ,LGALS1,MIF,PGD,POMC,PTGS1,SFN,YWHAB,YWHAE	18
Cancer, Organismal Injury and Abnormalities, Reproductive System Disease	breast or ovarian cancer	1.4E-09			ALDH1A1,APOE,ASPM,BGN,CALM1 (includes others),CAST,CAV1,CNN1,CRYAB,CTSB,CTSD,CYCS,DCN,EEF1D,FTH1,GAPDH,H2AFZ,HSD11B1,IDH1,IGFBP4,ITGB1,ITGB6,LGALS1,MIF,MT-ND5,MYLK,PF4,POMC,PTGS1,PYGM,SERPINC1,SOD1,STX1B,TES,TIMP1,TSPAN9,VIM,YWHAZ	38
Hereditary Disorder, Organismal Injury and Abnormalities	autosomal dominant disease	4.88E-09			ACLY,ACTB,ALB,APOE,BGN,CALM1 (includes others),CAV1,CFL1,CRYAB,CYCS,FTH1,FTL,MYLK,RPS25,RPS26,RPSA,SERPINC1,SOD1,STX1B,VIM	20
Endocrine System Disorders, Organismal Injury and Abnormalities	thyroid nodule	9.83E-09			AHSG,ALDH1A1,CTSB,EEF1D,FTL,MT-ND5	6
Neurological Disease, Organismal Injury and Abnormalities, Psychological Disorders	disorder of basal ganglia	1.27E-08			ACTB,ALB,ANXA2,APOE,ATP1B1,CAV1,COX7A2,CRYAB,CYCS,FTH1,FTL,GAPDH,MT-ATP6,MT-ND5,RPSA,SOD1,TXN,VIM,YWHAZ	19
Neurological Disease, Skeletal and Muscular Disorders	neuromuscular disease	2.46E-08			ACTB,ALB,ANXA2,APOE,ATP1B1,COX7A2,CRYAB,CSN3,CYCS,FTH1,FTL,GAPDH,MIF,MT-ND5,PTGS1,RPSA,SOD1,TXN,VIM,YWHAZ	20
Cancer, Hematological Disease, Organismal Injury and Abnormalities	lymphohematopoietic neoplasia	5.48E-08			ACTB,AHSG,ALDH1A1,ANXA2,APOE,ATP1B1,CAV1,CFL1,CRYAB,CYCS,DCN,EEF1D,IDH1,IGFBP4,ITGB1,LGALS1,MIF,MT-ATP6,MT-CO2,MT-ND5,PF4,PTGS1,PYGL,PYGM,RPL10,RPS25,RPSA,SERPINC1,SFXN1,SOD1,TIMP1,VIM,YWHAE,YWHAZ	34
Neurological Disease	progressive motor neuropathy	7.14E-08			ACTB,ALB,ANXA2,APOE,CALM1 (includes others),CRYAB,CSN3,FTH1,FTL,MIF,MT-ND5,PTGS1,SOD1,TIMP1,VIM	15
Cancer, Organismal Injury and Abnormalities	benign neoplasia	7.67E-08			ALB,ALDH1A1,ANXA2,APOE,ATP1A1,CRYAB,CTSB,DCN,FTH1,HSD11B1,IDH1,IGFBP4,ITGB1,LGALS1,MT-CO2,POMC,PRKACA,PTGS1,RPS25,TIMP1	20
Cancer, Hematological Disease, Organismal Injury and Abnormalities	lymphohematopoietic cancer	1.01E-07			ACTB,AHSG,ALDH1A1,ANXA2,APOE,ATP1B1,CAV1,CFL1,CRYAB,CYCS,DCN,EEF1D,IDH1,IGFBP4,ITGB1,LGALS1,MIF,MT-ATP6,MT-CO2,MT-ND5,PF4,PTGS1,PYGL,PYGM,RPL10,RPS25,RPSA,SERPINC1,SFXN1,TIMP1,VIM,YWHAE,YWHAZ	33
Cardiovascular Disease, Organismal Injury and Abnormalities	bleeding of blood vessel	1.2E-07			APOE,BGN,CNN1,POMC	4
Cancer, Organismal Injury and Abnormalities, Reproductive System Disease	breast cancer	1.29E-07			ALDH1A1,APOE,BGN,CALM1 (includes others),CAV1,CNN1,CRYAB,CTSB,CTSD,CYCS,DCN,FTH1,H2AFZ,IDH1,ITGB1,ITGB6,LGALS1,MIF,MT-	26

			ND5,MYLK,PTGS1,SERPINC1,SOD1,TES,TIMP1,YWHAZ	
Inflammatory Disease	chronic inflammatory disorder	1.5E-07	ACLY,AHSG,ALB,APOE,ATP1B1,BGN,CTSB,CTSD,FTH1,HSD11B1,IGFBP4,ITGB6,LGALS1,MIF,POMC,PTGS1,RPSA,SERPINC1,TIMP1,TXN,VIM	21
Connective Tissue Disorders, Immunological Disease, Inflammatory Disease, Inflammatory Response, Organismal Injury and Abnormalities, Skeletal and Muscular Disorders	juvenile rheumatoid arthritis	3.08E-07	ACLY,ALB,APOE,ATP1B1,LGALS1,MIF,PTGS1,RPSA,TXN	9
Connective Tissue Disorders, Immunological Disease, Inflammatory Disease, Inflammatory Response, Organismal Injury and Abnormalities, Skeletal and Muscular Disorders	rheumatoid arthritis	3.12E-07	ACLY,AHSG,ALB,APOE,ATP1B1,BGN,CTSB,FTH1,IGFBP4,LGALS1,MIF,PTGS1,RPSA,SERPINC1,TIMP1,TXN,VIM	17
Endocrine System Disorders, Organismal Injury and Abnormalities	benign thyroid nodule	3.14E-07	AHSG,ALDH1A1,CTSB,EEF1D,FTL	5
Cellular Function and Maintenance, Small Molecule Biochemistry	homeostasis of metal ion	3.9E-07	APOE,ATP1A1,ATP1B1,CAV1,FTL,ITGB1,PF4,PYGM,SOD1	9
Infectious Diseases	attachment of virus	3.95E-07	ANXA2,APOE,FTL,LGALS1	4
Cancer, Hematological Disease, Organismal Injury and Abnormalities	hematological neoplasia	6.04E-07	ACTB,ALDH1A1,ANXA2,ATP1B1,CAV1,CFL1,CRYAB,CYCS,DCN,EEF1D,IDH1,IGFBP4,ITGB1,LGALS1,MIF,MT-ATP6,MT-CO2,MT-ND5,PF4,PTGS1,PYGL,PYGM,RPL10,RPS25,RPSA,SERPINC1,SFXN1,SOD1,TIMP1,VIM,YWHAE,YWHAZ	32
Cancer, Organismal Injury and Abnormalities	adenoma	9.6E-07	ANXA2,APOE,ATP1A1,CRYAB,CTSB,DCN,HSD11B1,IGFBP4,ITGB1,LGALS1,POMC,PRKACA,PTGS1,TIMP1	14
Cardiovascular System Development and Function, Organ Morphology	contraction of heart	9.67E-07	ATP1A1,ATP1B1,CALM1 (includes others),CRYAB,ITGB1,MYLK,PRKACA,SOD1	8
Organismal Injury and Abnormalities, Respiratory Disease	acute lung injury	9.94E-07	AHSG,ALB,CAV1,GAPDH,MIF,PTGS1,SFTPA1	7
Cancer, Hematological Disease, Organismal Injury and Abnormalities	hematologic cancer	1.05E-06	ACTB,ALDH1A1,ANXA2,ATP1B1,CAV1,CFL1,CRYAB,CYCS,DCN,EEF1D,IDH1,IGFBP4,ITGB1,LGALS1,MIF,MT-ATP6,MT-CO2,MT-ND5,PF4,PTGS1,PYGL,PYGM,RPL10,RPS25,RPSA,SERPINC1,SFXN1,TIMP1,VIM,YWHAE,YWHAZ	31
Cellular Function and Maintenance, Small Molecule Biochemistry	homeostasis of divalent cations	1.16E-06	APOE,ATP1B1,CAV1,FTL,ITGB1,PF4,PYGM,SOD1	8
Hematological Disease	blood protein disorder	1.27E-06	ALB,ANXA2,ATP1B1,CAV1,CRYAB,PF4,PTGS1,SERPINC1,TIMP1,VIM,YWHAE,YWHAZ	12
Cellular Assembly and Organization, Cellular Compromise	formation of cellular inclusion bodies	1.39E-06	APOE,CAST,CRYAB,CTSB,FTL,SOD1	6
Carbohydrate Metabolism	synthesis of monosaccharide	1.48E-06	ALDH1A1,APOE,GAPDH,MIF,PGD,POMC	6
Lipid Metabolism, Small Molecule Biochemistry	regulation of cholesterol	1.68E-06	APOE,CAV1,POMC	3
Neurological Disease, Organismal Injury and Abnormalities	syndromic encephalopathy	1.7E-06	ATP1B1,IDH1,MT-ATP6,MT-ND5,POMC,SERPINC1,TXN,YWHAB,YWHAE	9

Cancer, Organismal Injury and Abnormalities	Lymphoid Cancer and Tumors	1.81E-06	ACTB,AHSG,ALDH1A1,APOE,ATP1B1,CFL1,CYCS,DCN,EEF1D,IDH1,IGFBP4,ITGB1,LGALS1,MIF,MT-ATP6,MT-CO2,MT-ND5,PTGS1,PYGL,PYGM,RPL10,RPS25,RPSA,SERPINC1,SFXN1,SOD1,TIMP1,VIM,YWHAE,YWHAZ	30
Cancer, Hematological Disease, Immunological Disease, Organismal Injury and Abnormalities	plasma cell dyscrasia	1.98E-06	ANXA2,ATP1B1,CAV1,CRYAB,PF4,PTGS1,SERPINC1,TIMP1,VIM,YWHAE,YWHAZ	11
Cell Morphology	morphology of cells	2.21E-06	ANXA2,APOE,ASPM,BGN,CAST,CAV1,CFL1,CRYAB,CTSB,CTSD,DCN,GAPDH,H2AFZ,HSD11B1,IGFBP4,ITGB1,ITGB6,LGALS1,MIF,MYLK,POMC,RPSA,SFTPA1,SOD1,STX1B,VIM,YWHAG,YWHAZ	28
Cell Signaling, Cellular Function and Maintenance, Small Molecule Biochemistry, Vitamin and Mineral Metabolism	homeostasis of Ca2+	2.49E-06	APOE,ATP1B1,CAV1,ITGB1,PF4,PYGM,SOD1	7
Metabolic Disease, Neurological Disease	beta amyloidosis	2.68E-06	APOE,CAST,VIM	3
Connective Tissue Development and Function, Skeletal and Muscular System Development and Function, Tissue Morphology	quantity of osteoprogenitor cells	2.68E-06	BGN,DCN,SOD1	3
Neurological Disease, Organismal Injury and Abnormalities, Psychological Disorders, Skeletal and Muscular Disorders	Parkinson's disease	3.78E-06	ALB,ANXA2,APOE,CRYAB,FTH1,FTL,MT-ND5,SOD1,VIM	9
Developmental Disorder, Hereditary Disorder, Ophthalmic Disease, Organismal Injury and Abnormalities	familial congenital cataract	3.81E-06	CAV1,CRYAB,FTL,VIM	4
Carbohydrate Metabolism	catabolism of polysaccharide	4.19E-06	APOE,CTSB,PYGB,PYGL,PYGM	5
Immunological Disease	systemic autoimmune syndrome	5.33E-06	ACLY,AHSG,ALB,APOE,ATP1B1,BGN,CSN3,CTSB,FTH1,HSD11B1,IGFBP4,LGALS1,MIF,PTGS1,RPSA,SERPINC1,TIMP1,TXN,VIM	19
Cancer, Gastrointestinal Disease, Hepatic System Disease, Organismal Injury and Abnormalities	hepatocellular carcinoma	5.65E-06	ALB,ASPM,ATP1A1,ATP1B1,CTSD,DCN,FTL,IDH1,ITGB1,PTGS1,SERPINC1,SOD1,TXN,YWHAG	14
Skeletal and Muscular System Development and Function	morphology of muscle	7.22E-06	APOE,BGN,CAST,CAV1,DCN,HSD11B1,IGFBP4,ITGB1,SERPINC1,SOD1,YWHAE	11
Cellular Function and Maintenance	uptake of bacteria	7.33E-06	CAV1,ITGB1,RPSA,SFTPA1	4
Developmental Disorder, Hereditary Disorder, Metabolic Disease, Neurological Disease, Ophthalmic Disease, Organismal Injury and Abnormalities, Skeletal and Muscular Disorders	Leber optic atrophy	7.82E-06	MT-ATP6,MT-ND3,MT-ND5	3
Cancer, Organismal Injury and Abnormalities, Reproductive System Disease	tumorigenesis of reproductive tract	8.14E-06	ALB,ALDH1A1,ALDOB,ANP32B,ANXA2,APOE,ASPM,CALM1 (includes others),CAST,CAV1,CNN1,COX7A1,CSN2,CTSB,DCN,EEF1D,FTH1,GAPDH,HSD11B1,IDH1,IGFBP4,MIF,MT-CO2,MT-ND5,MYLK,PDXK,PF4,PLP2,POMC,PTGS1,PYGM,RPS25,SERPINC1,STX1B,TES,TIMP1,TSPAN9,UROD,VIM,YWHAE	40
Cardiovascular Disease	peripheral vascular disease	8.24E-06	AHSG,ALB,APOE,ATP1A1,CTSB,FTH1,PLP2,PTGS1,PYGL,SERPINC1,VIM	11

Cancer, Organismal Injury and Abnormalities, Reproductive System Disease	female genital neoplasm	8.32E-06	ALB,ALDH1A1,ALDOB,ANP32B,ANXA2,APOE,ASPM,CALM1 (includes others),CAST,CAV1,CNN1,COX7A1,CSN2,CTSB,DCN,EEF1D,FTH1,GAPDH,HSD11B1,IDH1,IGFBP4,MIF,MT-CO2,MT-ND5,MYLK,PDXK,PF4,PLP2,POMC,PTGS1,PYGM,RPS25,SERPINC1,STX1B,TES,TIMP1,TSPAN9,UROD,VIM,YWHAE	40
Cancer, Organismal Injury and Abnormalities	urogenital cancer	8.78E-06	ACTB,ALB,ALDH1A1,ALDOB,ANP32B,ANXA2,APOE,ASPM,ATP1B1,BGN,CALM1 (includes others),CAST,CAV1,CNN1,COX7A1,CSN2,CTSB,DCN,EEF1D,GAPDH,HSD11B1,IDH1,IGFBP4,ITGB1,LGALS1,MIF,MT-ND5,MYLK,PDXK,PF4,PLP2,POMC,PTGS1,PYGB,PYGL,PYGM,SERPINC1,SFN,STX1B,TES,TIMP1,TSPAN9,TXN,UROD,VIM,YWHAE	46
Organ Morphology	abnormal morphology of gland	1.03E-05	ALDH1A1,APOE,CAV1,CTSB,HSD11B1,IGFBP4,POMC,RPSA,SOD1	9
Cardiovascular Disease, Neurological Disease	ischemia of central nervous system	1.03E-05	ALB,CAV1,PLP2,PTGS1,PYGL,SERPINC1	6
Lipid Metabolism, Small Molecule Biochemistry	regulation of lipid	1.04E-05	APOE,CAV1,POMC,PTGS1	4
Ophthalmic Disease, Organismal Injury and Abnormalities	damage of retina	1.04E-05	CRYAB,SOD1,TXN	3
Molecular Transport, Protein Trafficking	excretion of protein	1.04E-05	CNN1,MIF,PRKACA	3
Energy Production, Lipid Metabolism, Small Molecule Biochemistry	oxidation of polyunsaturated fatty acids	1.04E-05	APOE,CYCS,PTGS1	3
Organ Morphology	morphology of gland	1.07E-05	ALDH1A1,APOE,CAV1,CTSB,HSD11B1,IGFBP4,ITGB1,POMC,RPSA,SOD1	10
Cancer, Hematological Disease, Organismal Injury and Abnormalities	lymphoid cancer	1.21E-05	ACTB,AHSG,ALDH1A1,APOE,ATP1B1,CFL1,CYCS,DCN,EEF1D,IDH1,IGFBP4,ITGB1,LGALS1,MIF,MT-ATP6,MT-CO2,MT-ND5,PTGS1,PYGL,PYGM,RPL10,RPS25,RPSA,SERPINC1,SFXN1,TIMP1,YWHAE,YWHAZ	28
Cell Cycle	neurite outgrowth stage of dorsal root ganglion cells	1.35E-05	ITGB1,VIM	2
Cellular Development, Cellular Growth and Proliferation	re-entry into growth of leukemia cell lines	1.35E-05	FTH1,FTL	2
Cardiovascular System Development and Function, Organismal Development, Tissue Morphology	area of blood vessel	1.35E-05	APOE,PF4,VIM	3
Free Radical Scavenging	modification of hydrogen peroxide	1.35E-05	PTGS1,SOD1,TXN	3
Cancer, Organismal Injury and Abnormalities, Reproductive System Disease	tumorigenesis of genital organ	1.38E-05	ALB,ALDH1A1,ALDOB,ANP32B,ANXA2,APOE,ASPM,CALM1 (includes others),CAST,CAV1,CNN1,COX7A1,CSN2,CTSB,DCN,EEF1D,FTH1,GAPDH,HSD11B1,IDH1,IGFBP4,LGALS1,MIF,MT-CO2,MT-ND5,MYLK,PDXK,PF4,PLP2,POMC,PTGS1,PYGM,RPS25,SERPINC1,SFN,STX1B,TES,TIMP1,TSPAN9,TXN,UROD,VIM,YWHAE	43
Cancer, Organismal Injury and Abnormalities, Reproductive System Disease	genital tumor	0.000014	ALB,ALDH1A1,ALDOB,ANP32B,ANXA2,APOE,ASPM,CALM1 (includes others),CAST,CAV1,CNN1,COX7A1,CSN2,CTSB,DCN,EEF1D,FTH1,GAPDH,HSD11B1,IDH1,IGFBP4,LGALS1,MIF,MT-CO2,MT-ND5,MYLK,PDXK,PF4,PLP2,POMC,PTGS1,PYGM,RPS25,SERPINC1,SFN,STX1B,TES,TIMP1,TSPAN9,TXN,UROD,VIM,YWHAE	43
Nervous System Development and Function	morphology of nervous system	1.51E-05	APOE,ASPM,CAST,CAV1,CFL1,CTSB,CTSD,HSD11B1,ITGB1,LGALS1,MIF,PRKACA,SOD1,STX1B,VIM,YWHAE	16

Cancer, Organismal Injury and Abnormalities, Respiratory Disease	carcinoma in lung	0.000016	AHSG,ANXA2,ATP1A1,ATP1B1,CAV1,CTSD,DCN,FTL,IDH1,ITGB1,PTGS1,SERPINC1,TIMP1,VIM,YWHAE,YWHAZ	16
Skeletal and Muscular System Development and Function	relaxation of muscle	1.66E-05	APOE,ATP1A1,ATP1B1,MYLK,SOD1	5
Cardiovascular System Development and Function	contractility of artery	1.71E-05	CAV1,IGFBP4,SOD1	3
Hereditary Disorder, Neurological Disease, Organismal Injury and Abnormalities, Psychological Disorders	familial dementia	1.73E-05	APOE,BGN,CTSD,SOD1	4
Lipid Metabolism, Molecular Transport, Nucleic Acid Metabolism, Small Molecule Biochemistry	concentration of malonyl-coenzyme A	2.13E-05	ACACA,ACLY,IDH1	3
Psychological Disorders	schizophrenia spectrum disorder	2.14E-05	ATP1A1,CAV1,CTSB,HPCAL1,LGALS1,MT-ATP6,MT-CO2,POMC,PTGS1,RPL10,YWHAE	11
Dermatological Diseases and Conditions, Organismal Injury and Abnormalities	chronic psoriasis	2.44E-05	APOE,ATP1B1,CNN1,CTSB,H2AFZ,PGD	6
Cellular Movement	invasion of pancreatic cancer cell lines	2.49E-05	CAV1,CTSD,SFN,TIMP1	4
Developmental Disorder, Organismal Injury and Abnormalities	dystrophy	2.65E-05	ACLY,APOE,BGN,CAST,CFL1,CYCS,ITGB1,VIM	8
Inflammatory Disease, Organismal Injury and Abnormalities, Respiratory Disease	acute respiratory distress syndrome	2.69E-05	ALB,GAPDH,MIF,PTGS1,SFTPA1	5
Organismal Injury and Abnormalities, Tissue Morphology	size of lesion	2.85E-05	APOE,CAV1,CRYAB,CTSB,MIF,PF4,SOD1,TIMP1,TXN	9
Cardiovascular Disease, Neurological Disease, Organismal Injury and Abnormalities	cerebrovascular dysfunction	3.02E-05	ALB,APOE,ATP1A1,PLP2,PTGS1,PYGL,SERPINC1,VIM	8
Cancer, Organismal Injury and Abnormalities	papillary carcinoma	3.08E-05	ATP1B1,HSD11B1,IDH1,IGFBP4,MT-ND3,MT-ND5,TIMP1,VIM	8
Cardiovascular Disease, Hematological Disease, Organismal Injury and Abnormalities	venous thromboembolism	3.17E-05	ALB,PTGS1,SERPINC1	3
Hereditary Disorder, Neurological Disease, Organismal Injury and Abnormalities	hereditary neuropathy	0.000034	APOE,BGN,CAV1,MT-ATP6,MT-ND3,MT-ND5,SOD1	7
Cell-To-Cell Signaling and Interaction, Nervous System Development and Function	activation of astrocytes	3.48E-05	ALB,MIF,SOD1,VIM	4
Organismal Development	morphology of body cavity	3.65E-05	ALB,APOE,CAV1,CNN1,COX7A1,CTSD,DCN,HSD11B1,IGFBP4,ITGB1,ITGB6,MIF,PTGS1,RPSA,SERPINC1,SFN,SFTPA1,SOD1,TIMP1,YWHAE	20
Connective Tissue Disorders, Immunological Disease, Inflammatory Disease, Inflammatory Response, Organismal Injury and Abnormalities, Skeletal and Muscular Disorders	polyarticular juvenile rheumatoid arthritis	3.98E-05	APOE,LGALS1,PTGS1,RPSA,TXN	5
Cell Death and Survival	apoptosis of bone marrow stromal cells	4.03E-05	BGN,DCN	2
Cell-To-Cell Signaling and Interaction, Connective Tissue Development and Function	binding of bone marrow stromal cells	4.03E-05	BGN,DCN	2

Neurological Disease, Organismal Injury and Abnormalities	leukoencephalopathy	4.36E-05	APOE,CAV1,MT-ATP6,MT-ND3,MT-ND5	5
Lipid Metabolism, Small Molecule Biochemistry	stimulation of prostaglandin	0.000045	ANXA2,MIF,PTGS1	3
Organ Morphology	morphology of endocrine gland	0.000046	APOE,CAV1,CTSB,HSD11B1,IGFBP4,POMC,RPSA	7
Hereditary Disorder, Organismal Injury and Abnormalities, Skeletal and Muscular Disorders	hereditary myopathy	5.07E-05	ACLY,BGN,CAST,CFL1,CRYAB,CYCS,ITGB1,MT-ATP6,MT-ND3,MT-ND5	10
Metabolic Disease	abnormal metabolism	5.27E-05	APOE,HSD11B1,IGFBP4,ITGB6,POMC,PTGS1	6
Molecular Transport	import of metal ion	5.28E-05	ATP1A1,ATP1B1,CFL1	3
Nervous System Development and Function, Organ Morphology, Organismal Development	morphology of cerebral cortex	5.32E-05	APOE,ASPM,CAV1,CTSB,HSD11B1,VIM,YWHAE	7
Cardiovascular System Development and Function, Organ Morphology, Skeletal and Muscular System Development and Function	contraction of cardiac muscle	5.45E-05	ATP1A1,ATP1B1,CALM1 (includes others),MYLK,PRKACA	5
Skeletal and Muscular System Development and Function	mass of muscle	5.45E-05	CAST,HSD11B1,IGFBP4,ITGB1,SOD1	5
Respiratory System Development and Function	morphology of respiratory tract	5.45E-05	ALDH1A1,APOE,CAV1,HSD11B1,ITGB6,LGALS1,SFTPA1	7
Cancer, Gastrointestinal Disease, Hepatic System Disease, Organismal Injury and Abnormalities	bile duct adenocarcinoma	5.94E-05	ALB,ANXA2,IDH1,SERPINC1,VIM	5
Cancer, Organismal Injury and Abnormalities, Reproductive System Disease	female genital tract cancer	6.08E-05	ALB,ALDH1A1,ALDOB,ANP32B,ANXA2,APOE,ASPM,CALM1 (includes others),CAST,CAV1,CNN1,COX7A1,CSN2,CTSB,DCN,EEF1D,GAPDH,HSD11B1,IDH1,IGFBP4,MIF,MT-ND5,MYLK,PDXK,PF4,PLP2,POMC,PTGS1,PYGM,SERPINC1,STX1B,TES,TIMP1,TSPAN9,UROD,VIM,YWHAE	37
Endocrine System Development and Function, Lipid Metabolism, Molecular Transport, Small Molecule Biochemistry	secretion of corticosterone	6.14E-05	APOE,HSD11B1,POMC	3
Drug Metabolism, Lipid Metabolism, Small Molecule Biochemistry	synthesis of epoprostenol	6.14E-05	PTGS1,SERPINC1,SOD1	3
Cardiovascular Disease, Organismal Injury and Abnormalities	arrhythmia	6.43E-05	ATP1A1,ATP1B1,CALM1 (includes others),PTGS1,SERPINC1,TIMP1,TXN	7
Respiratory System Development and Function	compliance of lung	7.09E-05	APOE,CAV1,SFTPA1	3
Lipid Metabolism, Small Molecule Biochemistry	induction of lipid	7.09E-05	LGALS1,MIF,PTGS1	3
Neurological Disease, Psychological Disorders	Schizophrenia	7.42E-05	ATP1A1,CAV1,CTSB,HPCAL1,LGALS1,MT-ATP6,MT-CO2,POMC,PTGS1,YWHAE	10
Connective Tissue Disorders, Organismal Injury and Abnormalities, Tissue Morphology	abnormal morphology of fat pad	7.65E-05	APOE,CAV1,HSD11B1,IGFBP4	4

Cancer, Organismal Injury and Abnormalities	pelvic cancer	7.83E-05	ACTB,ALB,ALDH1A1,ALDOB,ANP32B,ANXA2,APOE,ASPM,CALM1 (includes others),CAST,CAV1,CNN1,COX7A1,CSN2,CTSB,DCN,EEF1D,GAPDH,HSD11B1,IDH1,IGFBP4,LGALS1,MIF,MT-ND5,MYLK,PDXK,PF4,PLP2,POMC,PTGS1,PYGM,SERPINC1,SFN,SFTPA1,STX1B,TES,TIMP1,TSPAN9,TXN,UROD,VIM,YWHAE	42
Cell Morphology, Endocrine System Development and Function, Endocrine System Disorders, Organ Morphology, Organismal Development, Organismal Injury and Abnormalities	abnormal morphology of thyroid follicle cells	8.04E-05	CAV1,CTSB	2
Cardiovascular System Development and Function, Organismal Development, Tissue Morphology	area of carotid artery	8.04E-05	APOE,VIM	2
Drug Metabolism, Endocrine System Development and Function, Lipid Metabolism, Small Molecule Biochemistry	conversion of hydrocortisone	8.04E-05	HSD11B1,POMC	2
Free Radical Scavenging	modification of superoxide	8.04E-05	CYCS,SOD1	2
Energy Production, Lipid Metabolism, Small Molecule Biochemistry	oxidation of arachidonic acid	8.04E-05	APOE,PTGS1	2
Cell Death and Survival, Organismal Injury and Abnormalities, Renal and Urological Disease	apoptosis of mesangial cells	8.13E-05	APOE,BGN,ITGB1	3
Developmental Disorder, Hereditary Disorder, Metabolic Disease, Neurological Disease, Organismal Injury and Abnormalities, Psychological Disorders	familial Alzheimer disease	8.13E-05	APOE,BGN,CTSD	3
Lipid Metabolism, Small Molecule Biochemistry	redistribution of lipid	8.13E-05	APOE,ATP1A1,LGALS1	3
Cancer, Organismal Injury and Abnormalities	breast or ovarian carcinoma	8.61E-05	APOE,ASPM,BGN,CALM1 (includes others),CAST,CAV1,CNN1,CTSD,EEF1D,H2AFZ,HSD11B1,IDH1,IGFBP4,ITGB1,LGALS1,MT-ND5,MYLK,PF4,PTGS1,PYGM,SOD1,STX1B,TES,TSPAN9	24
Nervous System Development and Function, Neurological Disease, Organ Morphology, Organismal Development, Organismal Injury and Abnormalities	abnormal morphology of hippocampus	8.92E-05	APOE,CAV1,CTSB,HSD11B1,YWHAE	5
Ophthalmic Disease, Organismal Injury and Abnormalities	cataract disease	8.92E-05	ALDH1A1,CAV1,CRYAB,FTL,VIM	5
Organismal Injury and Abnormalities, Tissue Morphology	volume of lesion	8.92E-05	CAV1,CRYAB,MIF,SOD1,TIMP1	5
Cell Cycle	interphase of blood cells	9.23E-05	DCN,ITGB1,LGALS1,TIMP1	4
Carbohydrate Metabolism	catabolism of glycogen	9.27E-05	PYGB,PYGL,PYGM	3
Free Radical Scavenging, Small Molecule Biochemistry	degradation of hydrogen peroxide	9.27E-05	PTGS1,SOD1,TXN	3
Endocrine System Development and Function, Lipid Metabolism, Small Molecule Biochemistry, Vitamin and Mineral Metabolism	synthesis of glucocorticoid	9.27E-05	ATP1A1,HSD11B1,POMC	3
Cardiovascular Disease	aneurysm	9.27E-05	APOE,FTL,MYLK,PTGS1,TIMP1	5

Cell Morphology, Cell-To-Cell Signaling and Interaction	morphology of intercellular junctions	9.27E-05	APOE,CAV1,LGALS1,STX1B,YWHAG	5
Cancer, Immunological Disease, Organismal Injury and Abnormalities	neoplasia of lymphoid organ	9.74E-05	AHSG,APOE,DCN,ITGB1,PTGS1,VIM	6
Cancer, Organismal Injury and Abnormalities, Reproductive System Disease	genital tract cancer	0.000104	ALB,ALDH1A1,ALDOB,ANP32B,ANXA2,APOE,ASPM,CALM1 (includes others),CAST,CAV1,CNN1,COX7A1,CSN2,CTSB,DCN,EEF1D,GAPDH,HSD11B1,IDH1,IGFBP4,LGALS1,MIF,MT-ND5,MYLK,PDXK,PF4,PLP2,POMC,PTGS1,PYGM,SERPINC1,SFN,STX1B,TES,TIMP1,TSPAN9,TXN,UROD,VIM,YWHAE	40
Nervous System Development and Function, Neurological Disease	abnormal morphology of nervous system	0.000104	APOE,ASPM,CAST,CAV1,CTSB,CTSD,HSD11B1,LGALS1,MIF,PRKACA,SOD1,STX1B,YWHAE	13
Organ Morphology	morphology of skin	0.000106	APOE,BGN,CAST,CTSB,DCN,ITGB1,ITGB6,POMC	8
Embryonic Development, Organ Development, Organ Morphology, Organismal Development, Organismal Injury and Abnormalities, Respiratory Disease, Respiratory System Development and Function, Tissue Development	abnormal morphology of pulmonary alveolus	0.000108	APOE,CAV1,HSD11B1,ITGB6,SFTPA1	5
Inflammatory Response, Neurological Disease	neuroinflammation	0.000118	MIF,SOD1,VIM	3
Cancer, Hematological Disease, Immunological Disease, Organismal Injury and Abnormalities	multiple myeloma	0.000119	CRYAB,PF4,PTGS1,SERPINC1,TIMP1,VIM,YWHAZ	7
Developmental Disorder, Hereditary Disorder, Organismal Injury and Abnormalities, Skeletal and Muscular Disorders	Duchenne muscular dystrophy	0.00012	ACLY,BGN,CAST,CFL1,CYCS	5
Neurological Disease	neurological signs	0.000124	ACTB,APOE,ATP1B1,CAV1,COX7A2,CRYAB,CYCS,GAPDH,RPSA,SOD1,TXN,YWHAZ	12
Cardiovascular Disease, Neurological Disease, Organismal Injury and Abnormalities	ischemia of brain	0.000125	ALB,PLP2,PTGS1,PYGL,SERPINC1	5
Cancer, Organismal Injury and Abnormalities, Respiratory Disease	non-small cell lung cancer	0.000128	ANXA2,ATP1A1,ATP1B1,CAV1,CTSD,DCN,FTL,IDH1,ITGB1,PTGS1,SERPINC1,TIMP1,VIM,YWHAZ	14
Cell-To-Cell Signaling and Interaction, Embryonic Development	binding of embryonic cell lines	0.000133	ANXA2,CAV1,ITGB1	3
Cellular Function and Maintenance	engulfment of mononuclear leukocytes	0.000133	APOE,PF4,SFTPA1	3
Lipid Metabolism, Small Molecule Biochemistry	mobilization of lipid	0.000133	CAV1,LGALS1,POMC	3
Hematological System Development and Function, Immune Cell Trafficking, Inflammatory Response, Tissue Development	accumulation of monocyte-derived macrophages	0.000134	APOE,SOD1	2
Cardiovascular Disease, Hematological Disease, Organismal Injury and Abnormalities	atherothrombosis	0.000134	APOE,PTGS1	2
Cell-To-Cell Signaling and Interaction	attachment of melanoma cell lines	0.000134	ITGB1,RPSA	2
Lipid Metabolism, Molecular Transport, Nucleic Acid Metabolism, Small Molecule Biochemistry	concentration of acetyl-coenzyme A	0.000134	ACLY,IDH1	2

Lipid Metabolism, Nucleic Acid Metabolism, Small Molecule Biochemistry	conversion of acetyl-coenzyme A	0.000134	ACACA,ACLY	2
Cellular Compromise	degradation of autophagosomes	0.000134	CTSB,CTSD	2
Tissue Development	development of stroma	0.000134	ALDH1A1,CAV1	2
Lipid Metabolism, Small Molecule Biochemistry	incorporation of arachidonic acid	0.000134	ACLY,CAV1	2
Cell-To-Cell Signaling and Interaction, Cellular Function and Maintenance, Hematological System Development and Function, Inflammatory Response	phagocytosis of monocytes	0.000134	PF4,SFTPA1	2
Lipid Metabolism, Small Molecule Biochemistry	stimulation of phospholipid	0.000134	LGALS1,POMC	2
Neurological Disease, Skeletal and Muscular Disorders	tremor of limb	0.000134	SOD1,TIMP1	2
Cancer, Endocrine System Disorders, Organismal Injury and Abnormalities, Reproductive System Disease	Ovarian Cancer and Tumors	0.000136	ALB,ALDH1A1,APOE,ASPM,CAST,EEF1D,GAPDH,HSD11B1,IGFBP4,MIF,PF4,POMC,PTGS1,PYGM,SERPINC1,STX1B,TES,TIMP1,TSPAN9,VIM	20
Neurological Disease	abnormality of peripheral ganglia	0.000144	APOE,LGALS1,MIF,PRKACA,SOD1	5
Lipid Metabolism, Small Molecule Biochemistry, Vitamin and Mineral Metabolism	synthesis of steroid hormone	0.000146	ATP1A1,HSD11B1,POMC,VIM	4
Cancer, Organismal Injury and Abnormalities, Reproductive System Disease	female genital tract serous carcinoma	0.000146	ALDH1A1,ANXA2,APOE,CNN1,HSD11B1,IGFBP4,MYLK,PDXK,PTGS1	9
Hematological System Development and Function, Organismal Functions	coagulation of blood	0.000148	ANXA2,APOE,CAV1,PF4,PTGS1,SERPINC1	6
Immunological Disease	allergy	0.000153	ACTB,ALB,BGN,CFL1,GAPDH,LGALS1,POMC,PTGS1,TIMP1	9
Nervous System Development and Function, Neurological Disease, Organ Morphology, Organismal Development, Organismal Injury and Abnormalities	abnormal morphology of cerebral cortex	0.00016	APOE,ASPM,CAV1,CTSB,HSD11B1,YWHAE	6
Cancer, Endocrine System Disorders, Organismal Injury and Abnormalities	benign neoplasm of endocrine gland	0.00016	ANXA2,ATP1A1,CTSB,DCN,POMC,PRKACA	6
Cancer, Organismal Injury and Abnormalities	papillary adenocarcinoma	0.000161	ATP1B1,HSD11B1,IGFBP4,MT-ND3,MT-ND5,TIMP1,VIM	7
Embryonic Development, Organ Development, Organismal Development, Reproductive System Development and Function, Tissue Development	lactation	0.000163	CAV1,CSN2,CSN3,ITGB1	4
Hematological Disease, Organismal Injury and Abnormalities	thrombocytosis	0.000163	ATP1B1,IDH1,PF4,PTGS1	4
Cell-To-Cell Signaling and Interaction, Hair and Skin Development and Function	binding of epithelial cell lines	0.000165	ANXA2,CAV1,ITGB1	3
Cancer, Gastrointestinal Disease, Organismal Injury and Abnormalities	oral cancer	0.000195	BGN,CNN1,CRYAB,DCN,LGALS1,RPL10,TIMP1	7

Cellular Movement	scattering of cells	0.000199	ANXA2,CFL1,ITGB1,TIMP1	4
Cardiovascular Disease, Connective Tissue Disorders, Hematological Disease, Organismal Injury and Abnormalities	heparin-induced thrombocytopenia	0.0002	PTGS1,SERPINC1	2
Cell Morphology, Nervous System Development and Function, Neurological Disease, Tissue Morphology	loss of motor axons	0.0002	CAST,SOD1	2
Organismal Injury and Abnormalities, Reproductive System Disease	placental insufficiency	0.0002	PTGS1,SERPINC1	2
Molecular Transport, Small Molecule Biochemistry	quantity of melanin	0.0002	MIF,POMC	2
Drug Metabolism, Lipid Metabolism, Molecular Transport, Small Molecule Biochemistry	release of epoprostenol	0.0002	PTGS1,SERPINC1	2
Cancer, Organismal Injury and Abnormalities, Tissue Morphology, Tumor Morphology	size of tumor	0.000201	CAV1,CTSB,MIF,PF4,TIMP1	5
Embryonic Development, Organ Development, Organ Morphology, Organismal Development, Reproductive System Development and Function, Tissue Development	morphogenesis of mammary gland	0.000202	CAV1,ITGB1,TIMP1	3
Cardiovascular Disease, Organismal Injury and Abnormalities	aortic aneurysm	0.000209	APOE,FTL,MYLK,TIMP1	4
Organismal Injury and Abnormalities	calcinosis	0.000209	AHSG,APOE,PTGS1,TIMP1	4
Nervous System Development and Function	thermal nociception	0.000209	APOE,LGALS1,POMC,PTGS1	4
Cardiovascular Disease, Organismal Injury and Abnormalities, Skeletal and Muscular Disorders	atrial fibrillation	0.000214	ATP1A1,ATP1B1,PTGS1,SERPINC1,TIMP1	5
Cancer, Organismal Injury and Abnormalities	malignant neoplasm of aerodigestive tract	0.000214	ALDOB,BGN,CAV1,CNN1,CRYAB,DCN,FTH1, LGALS1,PTGS1,RPL10,SFN,TIMP1,YWHAB	13
Dermatological Diseases and Conditions, Inflammatory Disease, Inflammatory Response, Organismal Injury and Abnormalities	Dermatitis	0.00022	APOE,ATP1A1,BGN,CFL1,LGALS1,POMC,PTGS1,SFN,TIMP1	9
Hereditary Disorder, Metabolic Disease, Neurological Disease, Organismal Injury and Abnormalities, Skeletal and Muscular Disorders	Leigh syndrome	0.000222	MT-ATP6,MT-ND3,MT-ND5	3
Cellular Movement	cell movement of pericytes	0.000222	ITGB1,LGALS1,MIF	3
Inflammatory Response, Skeletal and Muscular Disorders	inflammation of limb	0.000222	APOE,LGALS1,MIF	3
Developmental Disorder, Ophthalmic Disease, Organismal Injury and Abnormalities	congenital anomaly of eye	0.000224	ACTB,APOE,CAV1,CRYAB,FTL,VIM	6
Hematological System Development and Function, Immune Cell Trafficking, Inflammatory Response, Tissue Development	accumulation of macrophages	0.000231	APOE,MIF,SOD1,TIMP1	4
Hematological Disease, Metabolic Disease	dyslipidemia	0.000257	APOE,HSD11B1,IDH1,PTGS1,SOD1	5

Cellular Assembly and Organization, Neurological Disease, Organismal Development, Tissue Development	formation of amyloid fibrils	0.000267	APOE,CRYAB,SOD1	3
Neurological Disease	dyskinesia	0.000267	ACTB,APOE,ATP1B1,CAV1,COX7A2,CRYAB,CYCS,GAPDH,RPSA,TXN,YWHAZ	11
Nervous System Development and Function	morphology of nerves	0.000273	APOE,ITGB1,LGALS1,MIF,SOD1	5
Metabolic Disease	disorder of lipid metabolism	0.000274	APOE,CAV1,HSD11B1,IDH1,PTGS1,SOD1	6
Cancer, Endocrine System Disorders, Organismal Injury and Abnormalities, Reproductive System Disease	ovarian cancer	0.000274	ALDH1A1,APOE,ASPM,CAST,EEF1D,GAPDH,HSD11B1,IGFBP4,MIF,PF4,POMC,PTGS1,PYGM,SERPINC1,STX1B,TES,TIMP1,TSPAN9,VIM	19
Vitamin and Mineral Metabolism	quantity of vitamin	0.000278	ALDH1A1,APOE,FTH1,SOD1	4
Connective Tissue Disorders, Organismal Injury and Abnormalities, Skeletal and Muscular Disorders, Tissue Morphology	abnormal morphology of superficial fascia	0.000279	BGN,DCN	2
Metabolic Disease, Neurological Disease, Organismal Injury and Abnormalities	amyloid load of hippocampus	0.000279	APOE,VIM	2
Cell Cycle	interphase of antigen presenting cells	0.000279	DCN,ITGB1	2
Cancer, Developmental Disorder, Embryonic Development, Organismal Injury and Abnormalities	invasion of mesenchyme	0.000279	ALDH1A1,MIF	2
Neurological Disease, Organismal Injury and Abnormalities	reactive astrogliosis	0.000279	CTSB,SOD1	2
Infectious Diseases, Organismal Injury and Abnormalities	septic shock	0.00028	ALB,ATP1B1,CAV1,MIF,PTGS1,SERPINC1	6
Cancer, Organismal Injury and Abnormalities, Respiratory Disease	advanced lung cancer	0.000293	CTSB,FTL,ITGB1,LGALS1,PTGS1,YWHAE	6
Nucleic Acid Metabolism, Small Molecule Biochemistry	metabolism of nucleoside triphosphate	0.000307	ATP1B1,CAV1,CYCS,MT-ATP6,SOD1	5
Cellular Movement, Hematological Disease, Immunological Disease, Inflammatory Disease, Inflammatory Response, Organismal Injury and Abnormalities, Respiratory Disease	allergic pulmonary eosinophilia	0.000317	ACTB,ALB,GAPDH	3
Cancer, Cell Death and Survival, Organismal Injury and Abnormalities, Tumor Morphology	apoptosis of chronic lymphocytic leukemia cells	0.000317	ALB,MIF,TXN	3
Cell-To-Cell Signaling and Interaction, Cellular Assembly and Organization, Cellular Compromise	disruption of cell-cell contacts	0.000317	ITGB1,MYLK,SOD1	3
Cellular Assembly and Organization, Cellular Compromise	disruption of cytoskeleton	0.000317	CAST,CAV1,ITGB1	3
Psychological Disorders	depressive disorder	0.000322	ALB,APOE,ATP1A1,CRYAB,PF4,POMC,VIM	7
Drug Metabolism, Molecular Transport, Small Molecule Biochemistry	concentration of glutathione	0.000331	ALDH1A1,FTH1,SOD1,TXN	4
Skeletal and Muscular System Development and Function	contraction of smooth muscle	0.000331	CAV1,CNN1,MYLK,PTGS1	4

Cell Death and Survival	cell death of ganglion cells	0.00034 4	CYCS,PRKACA,SOD1	3
Cell Morphology	abnormal morphology of plasma membrane	0.00034 5	APOE,CAV1,LGALS1,STX1B	4
Neurological Disease, Organismal Injury and Abnormalities	astrocytosis	0.00036	APOE,CAV1,CTSB,SOD1	4
Drug Metabolism, Endocrine System Development and Function, Lipid Metabolism, Small Molecule Biochemistry, Vitamin and Mineral Metabolism	synthesis of progesterone	0.00036	IGFBP4,POMC,VIM,YWHAG	4
Hematological Disease	hypercoagulation	0.00037 1	PTGS1,SERPINC1	2
Cell Cycle	interphase of phagocytes	0.00037 1	DCN,ITGB1	2
Lipid Metabolism, Molecular Transport, Small Molecule Biochemistry	quantity of ganglioside GM2	0.00037 1	APOE,CTSD	2
Cell Death and Survival	cell death of astrocytes	0.00037 2	ALB,CRYAB,SOD1	3
Cardiovascular Disease	damage of blood vessel	0.00037 2	APOE,BGN,POMC	3
Cellular Development, Connective Tissue Development and Function, Tissue Development	differentiation of stromal cells	0.00037 2	HSD11B1,ITGB1,SOD1	3
Lipid Metabolism, Small Molecule Biochemistry	esterification of cholesterol	0.00037 2	APOE,CAV1,HSD11B1	3
Cardiovascular Disease, Neurological Disease, Organismal Injury and Abnormalities	cerebral ischemia	0.00039 1	ALB,PTGS1,PYGL,SERPINC1	4
Cell Death and Survival, Organismal Injury and Abnormalities, Renal and Urological Disease	apoptosis of tubular cells	0.00040 2	ALB,ATP1A1,DCN	3
Cancer, Cellular Development, Cellular Growth and Proliferation, Organismal Injury and Abnormalities, Tumor Morphology	colony formation of cancer cells	0.00040 2	CAV1,CTSB,DCN	3
Inflammatory Response, Organismal Functions	fever	0.00040 2	MIF,POMC,PTGS1	3
Organ Development, Renal and Urological System Development and Function	function of kidney	0.00040 8	ITGB1,MIF,PTGS1,SERPINC1	4
Organismal Development	abnormal morphology of body cavity	0.00041	APOE,CAV1,CTSD,DCN,HSD11B1,IGFBP4,ITGB1,ITGB6,MIF,PTGS1,RPSA,SERPINC1,SFN,SFTPA1,SOD1,YWHAE	16
Reproductive System Development and Function	morphology of reproductive system	0.00042 3	ALB,APOE,ASPM,CAV1,CNN1,HSD11B1,ITGB1,POMC,PTGS1,SOD1,TIMP1	11
Skeletal and Muscular System Development and Function	function of smooth muscle	0.00042 4	APOE,CAV1,ITGB1,SOD1	4

APPENDIX B

Matlab Code to quantify sprouting length and average branch number:

```
close all
clear
clc


%User must update folder location and make sure all images are numbered
PicLoc ='C:\Users\Alberto\OneDrive\Documents\Lab Stuff\Hydrogel and OCT
Conf 020819\5x Carb Live Dead Dapi edU\Live\num\';
PicName='1';
PicType= '.tif';

NumIm=3; %User input for specific # of images in the folder
for v=1:NumIm
PicName=num2str(v);
I = imread(strcat(PicLoc,PicName,PicType));
% I=imadjust(I);
% imshow(I)
figure
imagesc(I)



[x,y]=ginput(1); %User selects center of vessel (gives decimals)
xO(v)=round(x,0);
yO(v)=round(y,0);
end
close all
%-------------------------------------

for v=1:NumIm
PicName=num2str(v);
I = imread(strcat(PicLoc,PicName,PicType));

pix2mm=491.5;

inc=7;
aO = inc; %tracing for background sample and vessel core sizes
a = inc; %First tracing (52pixels is about 0.25mm)

[Isizex,Isizey]=size(I);
Squarelimit=min(Isizex,Isizey);

maxdist=round((Squarelimit/2)/inc);
th=9; %thickness of square to average pixel values across
```

```
I4 = imread(strcat(PicLoc,PicName,PicType));
I5=imadjust(I4);
% figure
% imshow(I5)

level = graythresh(I5);
level=(level-0.25*level); %Usuallt 0.15
bw = im2bw(I5,level);
% bw = im2bw(I5);
bw = bwareaopen(bw,10);
% figure
% imshow(bw)


filled = imfill(bw, 'holes');
% filled = imfill(bw);

% figure
% imshow(filled)

holes = filled & ~bw;
bigholes = bwareaopen(holes, 40); %Usualy 50
smallholes = holes & ~bigholes;
bw = bw | smallholes;

sb2=5*(inc+1);
for i=1:sb2
    c1=xO(v)+(-(sb2/2)+i);
    for j=1:(sb2)
        r1=yO(v)+(-(sb2/2)+j);

        bw(r1,c1)=1;

    end
end

figure
imshow(bw)


[m,n]=size(bw);
% Squares=zeros(m,n);
Intersection=zeros(maxdist*4,th);
for i=1:maxdist

    for k=1:th
        b=a+(-(round(th/2))+k);

    l=length((xO(v)-b):(xO(v)+b));
    cxO1=repmat((xO(v)-b),l,1); %define x position of left line
    cxO2=repmat((xO(v)+b),l,1); %define x position of right line
    ryO1=repmat((yO(v)-b),l,1); %define y position of top line
    ryO2=repmat((yO(v)+b),l,1); %define y position of bottom line
```

```
    c=[(xO(v)-b):(xO(v)+b) cxO1' (xO(v)-b):(xO(v)+b) cxO2']; %all x
positions of square
    r=[ryO1' (yO(v)-b):(yO(v)+b) ryO2' (yO(v)-b):(yO(v)+b)]; %all y
positions of square

%         for j=1:length(c)
%              Squares(c(j),r(j))=1;
%         end

    pixels = impixel(bw,c,r); %pixel values of all pixels along the
square
    S=sum(pixels);
    branchdensity(k,i)=(S(1)/(l*4));

    for g=1:length(pixels(:,1))-1
        Intersection(g,k)= abs(pixels((g+1),1) - pixels((g),1));
%Determine if there is an intersection by seeing if pixel changes from
a 0 to 1 or 1 to 0
    end

    %Eliminating noise (Branch must be 2 pixels in width)
    for g=1:length(pixels(:,1))-2
        CurrentBranchLength(g)=0;
        if Intersection(g,k)+Intersection(g+1,k)>1
            Intersection(g,k)=0;
        elseif Intersection(g,k)+Intersection(g+1,k)==1
            CurrentBranchLength(g)=sqrt((abs(xO(v)-c(g)))^2+(abs(yO(v)-
r(g)))^2);
        end
    end

    MaxBranchLength(i)=max(CurrentBranchLength)/pix2mm;



    Intersection((length(pixels(:,1))+1),k) = sum(Intersection(:,k));
    MaxInt(i,k)= max(Intersection(:,k));
    end

    branchdensity((th+1),i) = mean(branchdensity(:,i));
    NumInter(i)=mean(MaxInt(i,:))/2;
    a=a+inc;

end

branchdensity(isnan(branchdensity))=0;
BranchLengthindex = find(branchdensity((th+1),:)<0.015,1);
BranchLengthindex2 = find(branchdensity((th+1),:)<(5/l),1);

TF = isempty(BranchLengthindex);

if TF==1
    BranchLengthindex = maxdist;
end
```

```
clear branchdensity
clear BranchLengthindex
clear NumInter
clear Intersection
clear pixels
clear Density2
clear NumInter
clear MaxBranchLength
clear CurrentBranchLength
clear background
clear c r a
end

BranchLength
BranchLength2
AvgBranchNum
BranchArea

VarMatrix(1,:)=BranchLength;
VarMatrix(2,:)=AvgBranchNum;
VarMatrix(3,:)=BranchArea;
VarMatrix(4,:)=BranchLength2;
```

REFERENCES

1. Swartz, M. A. The physiology of the lymphatic system. *Adv. Drug Deliv. Rev.* **50**, 3–20 (2001).

2. Baluk, P. *et al.* Functionally specialized junctions between endothelial cells of lymphatic vessels. *J. Exp. Med.* **204**, 2349–62 (2007).

3. Aukland, K. & Reed, R. K. Interstitial-lymphatic mechanisms in the control of extracellular fluid volume. *Physiol. Rev.* **73**, 1 LP – 78 (1993).

4. Leak, L. Electron microscopic observations on lymphatic capillaries and the structural components of the connective tissue-lymph interface. *Microvasc Res* **2**, 361–391 (1970).

5. Schmid-Schonbein, G. W. Mechanisms causing initial lymphatics to expand and compress to promote lymph flow. *Arch. Histol. Cytol.* **53 Suppl**, 107–114 (1990).

6. Casley-Smith, J. R. Are the initial lymphatics normally pulled open by the anchoring filaments? *Lymphology* **13**, 120–129 (1980).

7. Negrini, D. & Moriondo, A. Lymphatic anatomy and biomechanics. *J Physiol* **589**, 2927–2934 (2011).

8. Gashev, A. A. Physiological aspects of lymphatic contractile function. *Ann. N. Y. Acad. Sci.* (2002).

9. Scavelli, C. *et al.* Lymphatics at the crossroads of angiogenesis and lymphangiogenesis. *J. Anat.* **204**, 433–449 (2004).

10. Albertine, K. H., Fox, L. M. & O'Morchoe, C. C. C. The morphology of canine lymphatic valves. *Anat. Rec.* **202**, 453–461 (1982).

11. Pan, W.-R., le Roux, C. M., Levy, S. M. & Briggs, C. A. The morphology of the human lymphatic vessels in the head and neck. *Clin. Anat.* **23**, 654–661 (2010).

12. Bazigou, E., Wilson, J. T. & Moore, J. E. Primary and secondary lymphatic valve development: Molecular, functional and mechanical insights. *Microvasc. Res.* **96**, 38–45 (2014).

13. Davis, M. J., Rahbar, E., Gashev, A. a, Zawieja, D. C. & Moore, J. E. Determinants of valve gating in collecting lymphatic vessels from rat mesentery. *Am. J. Physiol. Heart Circ. Physiol.* **301**, 48–60 (2011).

14. McHale, N. G. & Roddie, I. C. The effect of transmural pressure on pumping activity in isolated bovine lymphatic vessels. *J. Physiol.* **261**, 255–269 (1976).

15. Muthuchamy, M., Gashev, A. & Boswell, N. Molecular and functional analyses of the contractile apparatus in lymphatic muscle. *FASEB J.* (2003).

16. Moriondo, A., Solari, E., Marcozzi, C. & Negrini, D. Diaphragmatic lymphatic vessel behavior during local skeletal muscle contraction. *Am. J. Physiol. Hear. Circ. Physiol.* **308**, pH193-H205 (2015).

17. Adair, T. H. & Guyton, A. C. Modification of lymph by lymph nodes. III. Effect of increased lymph hydrostatic pressure. *Am. J. Physiol. - Hear. Circ. Physiol.* **249**, H777 LP-H782 (1985).

18. Yu, D. Y. *et al.* The critical role of the conjunctiva in glaucoma filtration surgery. *Prog. Retin. Eye Res.* **28**, 303–328 (2009).

19. Stacker, S. a *et al.* Lymphangiogenesis and lymphatic vessel remodelling in cancer. *Nat. Rev. Cancer* **14**, 159–172 (2014).

20. Gnepp, D. R. & Green, F. H. Y. Scanning Electron Microscopic Study of Canine Lymphatic Vessels and Their Valves Douglas. *Lymphology* **13**, 91–99 (1980).

21. Lee, S., Roizes, S. & von der Weid, P.-Y. Distinct roles of L- and T-type voltage-dependent Ca2+ channels in regulation of lymphatic vessel contractile activity. *J. Physiol.* **592**, 5409–5427 (2014).

22. Beckett, E. a H., Hollywood, M. a, Thornbury, K. D. & McHale, N. G. Spontaneous electrical activity in sheep mesenteric lymphatics. *Lymphat. Res. Biol.* **5**, 29–43 (2007).

23. von der Weid, P.-Y., Lee, S., Imtiaz, M. S., Zawieja, D. C. & Davis, M. J. Electrophysiological properties of rat mesenteric lymphatic vessels and their regulation by stretch. *Lymphat. Res. Biol.* **12**, 66–75 (2014).

24. Nepiyushchikh, Z. V *et al.* Differential effects of myosin light chain kinase inhibition on contractility, force development and myosin light chain 20 phosphorylation of rat cervical and thoracic duct lymphatics. *J. Physiol.* **589**, 5415–29 (2011).

25. Nepiyushchikh, Z. V *et al.* Expression and functional role of Caldesmon in modulating Lymphatic Muscle Contraction. Running Title: Role of Caldesmon in Lymphatic Muscle Contraction.

26. Muthuchamy, M. & Zawieja, D. Molecular regulation of lymphatic contractility. *Ann. N. Y. Acad. Sci.* **1131**, 89–99 (2008).

27. Eisenhoffer, J., Kagal, a, Klein, T. & Johnston, M. G. Importance of valves and lymphangion contractions in determining pressure gradients in isolated lymphatics exposed to elevations in outflow pressure. *Microvascular research* **49**, 97–110 (1995).

28. Davis, M. J. *et al.* Maximum shortening velocity of lymphatic muscle approaches that of striated muscle. *Am. J. Physiol. Circ. Physiol.* **305**, H1494–H1507 (2013).

29. Unno, N. *et al.* A novel method of measuring human lymphatic pumping using indocyanine green fluorescence lymphography. *J. Vasc. Surg.* **52**, 946–952 (2010).

30. Cintolesi, V. *et al.* Constitutively Enhanced Lymphatic Pumping in the Upper Limbs of Women Who Later Develop Breast Cancer-Related Lymphedema. **14**, 50–61 (2016).

31. Nelson, T. S. *et al.* Minimally invasive method for determining the effective lymphatic pumping pressure in rats using near-infrared imaging. *Am. J. Physiol. Regul. Integr. Comp. Physiol.* **306**, R281-90 (2014).

32. Rzucidlo, E. M., Martin, K. a. & Powell, R. J. Regulation of vascular smooth muscle cell differentiation. *J. Vasc. Surg.* **45**, 25–32 (2007).

33. Louis, S. F. & Zahradka, P. Vascular smooth muscle cell motility: From migration to invasion. *Exp. Clin. Cardiol.* **15**, 75–85 (2010).

34. Mack, C. Signaling mechanisms that regulate smooth muscle cell differentiation. *Arterioscler. Thromb. Vasc. Biol.* **31**, 1495–1505 (2011).

35. MUTHUCHAMY, M., GASHEV, A., BOSWELL, N., DAWSON, N. & ZAWIEJA, D. Molecular and functional analyses of the contractile apparatus in lymphatic muscle. *FASEB J.* **17**, 920–922 (2003).

36. Trayes, K. P., Studdiford, J. S., Pickle, S. & Tully, A. S. Edema: diagnosis and management. *Am. Fam. Physician* **88**, 102–10 (2013).

37. Tobbia, D. *et al.* Lymphedema development and lymphatic function following lymph node excision in sheep. *J. Vasc. Res.* **46**, 426–34 (2009).

38. Rockson, S. G. Causes and consequences of lymphatic disease. *Ann. N. Y. Acad. Sci.* **1207 Suppl**, E2-6 (2010).

39. Mortimer, P. S. *et al.* The prevalence of arm oedema following treatment for breast cancer. *Qjm* **89**, 377–380 (2012).

40. Rockson, S. G. Precipitating factors in lymphedema: myths and realities. *Cancer* **83**, 2814–6 (1998).

41. Cintolesi, V. *et al.* Constitutively Enhanced Lymphatic Pumping in the Upper Limbs of Women Who Later Develop Breast Cancer-Related Lymphedema. *Lymphat. Res. Biol.* **14**, 50–61 (2016).

42. Bains, S. K. *et al.* A constitutional predisposition to breast cancer-related lymphoedema and effect of axillary lymph node surgery on forearm muscle lymph flow. *Breast* **24**, 68–74 (2015).

43. Gretener, S. B., Läuchli, S., Leu, A. J., Koppensteiner, R. & Franzeck, U. K. Effect of Venous and Lymphatic Congestion on Lymph Capillary Pressure of the Skin in Healthy Volunteers and Patients with Lymph Edema. 61–67 (2000).

44. Mihara, M. *et al.* Pathological steps of cancer-related lymphedema: histological changes in the collecting lymphatic vessels after lymphadenectomy. *PLoS One* **7**, 1–10 (2012).

45. Ogata, F., Fujiu, K., Koshima, I., Nagai, R. & Manabe, I. Phenotypic modulation of smooth muscle cells in lymphoedema. *Br. J. Dermatol.* **172**, 1286–1293 (2015).

46. Wilson, J. L., Yu, J., Taylor, L. & Polgar, P. Hyperplastic growth of pulmonary artery smooth muscle cells from subjects with pulmonary arterial hypertension is activated through JNK and p38 MAPK. *PLoS One* (2015). doi:10.1371/journal.pone.0123662

47. Weiler, M. Development and Optimization of Near-Infrared Functional Lymphatic Imaging in Health and Lymphedema. *Georg. Insitute Technol.* (2015).

48. Ogata, F. *et al.* Excess Lymphangiogenesis Cooperatively Induced by Macrophages and CD4+ T Cells Drives the Pathogenesis of Lymphedema. *J. Invest. Dermatol.* **136**, 706–714 (2016).

49. Avraham, T. *et al.* Fibrosis is a key inhibitor of lymphatic regeneration. *Plast. Reconstr. Surg.* **124**, 438–450 (2009).

50. Lynch, L. L. *et al.* Fibrosis worsens chronic lymphedema in rodent tissues. *Am. J. Physiol. - Hear. Circ. Physiol.* **308**, H1229–H1236 (2015).

51. Gousopoulos, E. *et al.* An Important Role of VEGF-C in Promoting Lymphedema Development. *J. Invest. Dermatol.* **137**, 1995–2004 (2017).

52. Jin, D. P., An, A., Liu, J., Nakamura, K. & Rockson, S. G. Therapeutic Responses to Exogenous VEGF-C Administration in Experimental Lymphedema: Immunohistochemical and Molecular Characterization. *Lymphat. Res. Biol.* **7**, 47–57 (2009).

53. Hadrian, R. & Palmes, D. Animal Models of Secondary Lymphedema: New Approaches in the

Search for Therapeutic Options. *Lymphat. Res. Biol.* **15**, (2017).

54. Pabst, R., Breves, G., Buettner, M., Schindewolffs, L. & Hadamitzky, C. VEGF-C improves regeneration and lymphatic reconnection of transplanted autologous lymph node fragments: An animal model for secondary lymphedema treatment. *Immunity, Inflamm. Dis.* **2**, 152–161 (2014).

55. Kim, H., Kataru, R. P. & Koh, G. Y. Review series In fl ammation-associated lymphangiogenesis : a double-edged sword ? *J. Clin. Invest.* **124**, 1–8 (2014).

56. Tian, W. *et al.* Leukotriene B 4 antagonism ameliorates experimental lymphedema. *Sci. Transl. Med.* **9**, eaal3920 (2017).

57. Bruyère, F. *et al.* Modeling lymphangiogenesis in a three-dimensional culture system. *Nat. Methods* **5**, 431–437 (2008).

58. Sweat, R. S., Sloas, D. C. & Murfee, W. L. VEGF-C Induces Lymphangiogenesis and Angiogenesis in the Rat Mesentery Culture Model. *Microcirculation* **21**, 532–540 (2014).

59. Tammela, T. & Alitalo, K. Lymphangiogenesis: Molecular mechanisms and future promise. *Cell* **140**, 460–76 (2010).

60. Tammela, T. *et al.* Therapeutic differentiation and maturation of lymphatic vessels after lymph node dissection and transplantation. *Nat. Med.* **13**, 1458–1466 (2007).

61. Breslin, J. W., Yuan, S. Y. & Wu, M. H. VEGF-C Alters Barrier Function of Cultured Lymphatic Endothelial Cells Through a VEGFR-3-Dependent Mechanism. *Lymphat. Res. Biol.* **5**, 105–114 (2007).

62. Tacconi, C. *et al.* Vascular endothelial growth factor C disrupts the endothelial lymphatic barrier to promote colorectal cancer invasion. *Gastroenterology* **148**, 1438-1451.e8 (2015).

63. Xu, Y. *et al.* Neuropilin-2 mediates VEGF-C-induced lymphatic sprouting together with VEGFR3. *J. Cell Biol.* **188**, 115–130 (2010).

64. Dixelius, J. *et al.* Ligand-induced Vascular Endothelial Growth Factor Receptor-3 (VEGFR-3) Heterodimerization with VEGFR-2 in Primary Lymphatic Endothelial Cells Regulates Tyrosine Phosphorylation Sites. *J. Biol. Chem.* **278**, 40973–40979 (2003).

65. Nilsson, I. *et al.* VEGF receptor 2/-3 heterodimers detected in situ by proximity ligation on angiogenic sprouts. *EMBO J.* **29**, 1377–1388 (2010).

66. Weitman, E., Cuzzone, D. & Mehrara, B. J. Tissue engineering and regeneration of lymphatic

structures. *Futur. Oncol.* **9**, 1365–1374 (2013).

67. Athanasiou, D. *et al.* The passive biomechanics of human pelvic collecting lymphatic vessels. *PLoS One* **12**, 1–12 (2017).

68. Rahbar, E. *et al.* Passive Pressure–Diameter Relationship and Structural Composition of Rat Mesenteric Lymphangions. *Lymphat. Res. Biol.* **10**, 152–163 (2012).

69. Wiig, H., Keskin, D. & Kalluri, R. Interaction between the extracellular matrix and lymphatics: Consequences for lymphangiogenesis and lymphatic function. *Matrix Biol.* **29**, 645–656 (2010).

70. Ito, K. *et al.* Integrin α9 on lymphatic endothelial cells regulates lymphocyte egress. *Proc. Natl. Acad. Sci.* **111**, 3080–3085 (2014).

71. Sorokin, L. *et al.* Integrin-α9 Is Required for Fibronectin Matrix Assembly during Lymphatic Valve Morphogenesis. *Dev. Cell* **17**, 175–186 (2009).

72. Foubert, P. & Varner, J. A. Integrins in Angiogenesis and Lymphangiogenesis. in *Methods in Molecular Biology* **757**, 471–486 (2011).

73. Blindt, R. *et al.* Expression patterns of integrins on quiescent and invasive smooth muscle cells and impact on cell locomotion. *J. Mol. Cell. Cardiol.* **34**, 1633–1644 (2002).

74. Rocnik, E. F. *et al.* α5β1 Integrin Expression and Luminal Edge Fibronectin Matrix Assembly by Smooth Muscle Cells after Arterial Injury. *Am. J. Pathol.* **156**, 453–465 (2011).

75. Okazaki, T. *et al.* α5β1 Integrin Blockade Inhibits Lymphangiogenesis in Airway Inflammation. *Am. J. Pathol.* **174**, 2378–2387 (2009).

76. Kim, S. H., Turnbull, J. & Guimond, S. Extracellular matrix and cell signalling: The dynamic cooperation of integrin, proteoglycan and growth factor receptor. *J. Endocrinol.* **209**, 139–151 (2011).

77. Engler, A. J., Sen, S., Sweeney, H. L. & Discher, D. E. Matrix elasticity directs stem cell lineage specification. *Cell* **126**, 677–89 (2006).

78. Enemchukwu, N. O. *et al.* Synthetic matrices reveal contributions of ECM biophysical and biochemical properties to epithelial morphogenesis. **212**, (2015).

79. Mäkinen, T. *et al.* Matrix stiffness controls lymphatic vessel formation through regulation of a GATA2-dependent transcriptional program. *Nat. Commun.* **9**, 1–16 (2018).

80. Brown, X. Q. *et al.* Effect of substrate stiffness and PDGF on the behavior of vascular smooth muscle cells: Implications for atherosclerosis. *J. Cell. Physiol.* **225**, 115–122 (2010).

81. Griffin, M. A. *et al.* Myotubes differentiate optimally on substrates with tissue-like stiffness. *J. Cell Biol.* **166**, 877–887 (2004).

82. Peyton, S. R., Kim, P. D., Ghajar, C. M., Seliktar, D. & Putnam, A. J. The effects of matrix stiffness and RhoA on the phenotypic plasticity of smooth muscle cells in a 3-D biosynthetic hydrogel system. *Biomaterials* **29**, 2597–2607 (2008).

83. Caulk, A. W., Dixon, J. B. & Gleason, R. L. A lumped parameter model of mechanically mediated acute and long-term adaptations of contractility and geometry in lymphatics for characterization of lymphedema. *Biomech. Model. Mechanobiol.* (2016). doi:10.1007/s10237-016-0785-2

84. Gashev, A. a, Davis, M. J., Delp, M. D. & Zawieja, D. C. Regional variations of contractile activity in isolated rat lymphatics. *Microcirculation* **11**, 477–92 (2004).

85. McHale, N. G. & Roddie, I. C. Pumping activity in isolated segments of bovine mesenteric lymphatics. *J. Physiol.* **261**, 70–72 (1975).

86. Jamalian, S., Davis, M. J., Zawieja, D. C. & Moore, J. E. Network Scale Modeling of Lymph Transport and Its Effective Pumping Parameters. *PLoS One* **11**, 1–18 (2016).

87. Dixon, J. B. *et al.* Lymph flow, shear stress, and lymphocyte velocity in rat mesenteric prenodal lymphatics. *Microcirculation* **13**, 597–610 (2006).

88. Ng, C. P. Interstitial fluid flow induces myofibroblast differentiation and collagen alignment in vitro. *J. Cell Sci.* **118**, 4731–4739 (2005).

89. Marinković, A., Liu, F. & Tschumperlin, D. J. Matrices of physiologic stiffness potently inactivate idiopathic pulmonary fibrosis fibroblasts. *Am. J. Respir. Cell Mol. Biol.* **48**, 422–30 (2013).

90. Mantella, L., Quan, A. & Verma, S. Variability in vascular smooth muscle cell stretch-induced responses in 2D culture. *Vasc. Cell* 1–9 (2015). doi:10.1186/s13221-015-0032-0

91. Rensen, S. S. M., Doevendans, P. A. F. M. & van Eys, G. J. J. M. Regulation and characteristics of vascular smooth muscle cell phenotypic diversity. *Neth. Heart J.* **15**, 100–8 (2007).

92. Chen, Q., Li, W., Quan, Z. & Sumpio, B. E. Modulation of vascular smooth muscle cell alignment by cyclic strain is dependent on reactive oxygen species and P38 mitogen-activated protein kinase. *J. Vasc. Surg.* **37**, 660–668 (2003).

93. Lynch, L. L. *et al.* Fibrosis worsens chronic lymphedema in rodent tissues. *Am. J. Physiol. Heart Circ. Physiol.* **308**, H1229-36 (2015).

94. Ozturk, C. N. *et al.* Free vascularized lymph node transfer for treatment of lymphedema: A systematic evidence based review. *J. Plast. Reconstr. Aesthetic Surg.* **69**, 1234–1247 (2016).

95. Schaverien, M. V., Badash, I., Patel, K. M., Selber, J. C. & Cheng, M. H. Vascularized Lymph Node Transfer for Lymphedema. *Semin. Plast. Surg.* **32**, 28–35 (2018).

96. Scallan, J. P., Davis, M. J. & Huxley, V. H. Permeability and contractile responses of collecting lymphatic vessels elicited by atrial and brain natriuretic peptides. *J. Physiol.* **591**, 5071–81 (2013).

97. Kuan, E. L. *et al.* Collecting Lymphatic Vessel Permeability Facilitates Adipose Tissue Inflammation and Distribution of Antigen to Lymph Node-Homing Adipose Tissue Dendritic Cells. *J. Immunol.* **6389**, 0–3 (2015).

98. Ivanov, S. *et al.* CCR7 and IRF4-dependent dendritic cells regulate lymphatic collecting vessel permeability. *J. Clin. Invest.* **126**, 1581–1591 (2016).

99. Ogata, F., Fujiu, K., Koshima, I., Nagai, R. & Manabe, I. Phenotypic modulation of smooth muscle cells in lymphoedema. *Br. J. Dermatol.* **172**, 1286–1293 (2015).

100. Mihara, M. *et al.* Pathological steps of cancer-related lymphedema: Histological changes in the collecting lymphatic vessels after lymphadenectomy. *PLoS One* (2012). doi:10.1371/journal.pone.0041126

101. Li, S., Sims, S., Jiao, Y., Chow, L. H. & Pickering, J. G. Evidence From a Novel Human Cell Clone That Adult Between Noncontractile and Contractile Phenotypes. *Circ. Res.* **85**, 338–348 (1999).

102. Martin, K. A. *et al.* The mTOR/p70 S6K1 pathway regulates vascular smooth muscle cell differentiation. *Am J Physiol Cell Physiol* **286**, C507–C517 (2004).

103. Abouhamed, M., Reichenberg, S., Robenek, H. & Plenz, G. Tropomyosin 4 expression is enhanced in dedifferentiating smooth muscle cells in vitro and during atherogenesis. *Eur. J. Cell Biol.* **82**, 473–482 (2003).

104. Hultgårdh-Nilsson, A., Lövdahl, C., Blomgren, K., Kallin, B. & Thyberg, J. Expression of phenotype- and proliferation-related genes in rat aortic smooth muscle cells in primary culture. *Cardiovasc. Res.* **34**, 418–30 (1997).

105. Gallagher, P. J., Jin, Y., Killough, G., Blue, E. K. & Lindner, V. Alterations in expression of myosin and myosin light chain kinases in response to vascular injury. *Am J Physiol Cell Physiol* **279**, 1–17 (2010).

106. Martin, K. A. *et al.* Rapamycin Promotes Vascular Smooth Muscle Cell Feedback Signaling *. **282**, 36112–36120 (2007).

107. Fisher, S. A. Vascular smooth muscle phenotypic diversity and function. *Physiol. Genomics* **42A**, 169–187 (2010).

108. Wang, D. G. *et al.* Culture of smooth muscle cells from guinea pig mesenteric lymphatic vessels. *Lymphology* **40**, 14–18 (2007).

109. Moiseeva, E. P. Adhesion receptors of vascular smooth muscle cells and their functions. *Cardiovasc. Res.* **52**, 372–386 (2001).

110. Eberini, I. *et al.* A proteomic portrait of atherosclerosis. *J. Proteomics* **82**, 92–112 (2013).

111. Kottke-marchant, K. & Ph, D. Molecular Regulation of Contractile Smooth Muscle Cell Phenotype : Implications for Vascular. **16**, (2010).

112. Qiu, J. *et al.* Biomechanical regulation of vascular smooth muscle cell functions: from in vitro to in vivo understanding. *J. R. Soc. Interface* **11**, 20130852 (2014).

113. Ogata, F., Fujiu, K., Koshima, I., Nagai, R. & Manabe, I. Phenotypic modulation of smooth muscle cells in lymphoedema. *Br. J. Dermatol.* **172**, 1286–1293 (2015).

114. Munn, L. L. Mechanobiology of lymphatic contractions. *Semin. Cell Dev. Biol.* **38**, 67–74 (2015).

115. Gashev, A. A., Zhang, R. Z., Muthuchamy, M., Zawieja, D. C. & Davis, M. J. Regional heterogeneity of length-tension relationships in rat lymph vessels. *Lymphat Res Biol* **10**, 14–19 (2012).

116. Wiśniewski, J. R., Zougman, A., Nagaraj, N. & Mann, M. Universal sample preparation method for proteome analysis. *Nat. Methods* **6**, 359–362 (2009).

117. Nesvizhskii, A. I., Keller, A., Kolker, E. & Aebersold, R. A statistical model for identifying proteins by tandem mass spectrometry. *Anal. Chem.* **75**, 4646–4658 (2003).

118. Keller, A., Nesvizhskii, A. I., Kolker, E. & Aebersold, R. Empirical statistical model to estimate the accuracy of peptide identifications made by MS/MS and database search. *Anal. Chem.* **74**, 5383–5392 (2002).

119. Mihara, M. *et al.* Pathological steps of cancer-related lymphedema: Histological changes in the collecting lymphatic vessels after lymphadenectomy. *PLoS One* **7**, 1–10 (2012).

120. Lv, S. *et al.* A review of the postoperative lymphatic leakage. *Oncotarget* **8**, 69062–69075 (2017).

121. Hansen, K. C., D'Alessandro, A., Clement, C. C. & Santambrogio, L. Lymph formation, composition and circulation: A proteomics perspective. *Int. Immunol.* **27**, 219–227 (2015).

122. Bornfeldt, K. E. *et al.* Insulin-like growth factor-I and platelet-derived growth factor-BB induce directed migration of human arterial smooth muscle cells via signaling pathways that are distinct from those of proliferation. *J. Clin. Invest.* **93**, 1266–74 (1994).

123. Lee, Y., Fluckey, J. D., Chakraborty, S. & Muthuchamy, M. Hyperglycemia- and hyperinsulinemia-induced insulin resistance causes alterations in cellular bioenergetics and activation of inflammatory signaling in lymphatic muscle. *FASEB J.* **31**, 2744–2759 (2017).

124. Chiong, M. *et al.* Influence of glucose metabolism on vascular smooth muscle cell proliferation. *Vasa* (2013). doi:10.1024/0301-1526/a000243

125. Natarajan, R., Gonzales, N., Xu, L. & Nadler, J. L. Vascular smooth muscle cells exhibit increased growth in response to elevated glucose. *Biochem. Biophys. Res. Commun.* **187**, 552–560 (1992).

126. Morrow, D. *et al.* Cyclic Strain Inhibits Notch Receptor Signaling in Vascular Smooth Muscle Cells In Vitro. (2005). doi:10.1161/01.RES.0000159182.98874.43

127. Iwasaki, H., Eguchi, S., Ueno, H., Marumo, F. & Hirata, Y. Mechanical stretch stimulates growth of vascular smooth muscle cells via epidermal growth factor receptor. 521–529 (2000).

128. Mata-greenwood, E. *et al.* Cyclic stretch increases VEGF expression in pulmonary arterial smooth muscle cells via TGF- □ 1 and reactive oxygen species : a requirement for NAD (P) H oxidase. **59802**, 288–298 (2005).

129. Song, L. *et al.* Downregulation of miR-223 and miR-153 mediates mechanical stretch-stimulated proliferation of venous smooth muscle cells via activation of the insulin-like growth factor-1 receptor. *Arch. Biochem. Biophys.* **528**, 204–211 (2012).

130. Weiler, M., Kassis, T. & Dixon, J. B. Sensitivity analysis of near-infrared functional lymphatic imaging. *J. Biomed. Opt.* **17**, 066019 (2012).

131. Caulk, A. W., Dixon, J. B. & Gleason, R. L. A lumped parameter model of mechanically mediated acute and long-term adaptations of contractility and geometry in lymphatics for characterization of lymphedema. *Biomech. Model. Mechanobiol.* **15**, 1601–1618 (2016).

132. Su, B. Y., Shontz, K. M., Flavahan, N. A. & Nowicki, P. T. The effect of phenotype on mechanical stretch-induced vascular smooth muscle cell apoptosis. *J. Vasc. Res.* **43**, 229–237 (2006).

133. Chiong, M. *et al.* Mitochondrial metabolism and the control of vascular smooth muscle cell proliferation. *Front. Cell Dev. Biol.* **2**, 1–9 (2014).

134. Bennett, M. R., Evan, G. & Schwartz, S. M. Apoptosis of Human Vascular Smooth Muscle Cells Derived from Normal Vessels and Coronary Atherosclerotic Plaques. (1995).

135. Brummelen, P., Jie, K. & Zwieten, P. Alpha-adrenergic receptors in human blood vessels. *Br. J. Clin. Pharmacol.* **21**, 33S-39S (1986).

136. Indolfi, C. *et al.* Activation of cAMP-PKA signaling in vivo inhibits smooth muscle cell proliferation induced by vascular injury. *Nat Med* **3**, 775–779 (1997).

137. Guttentag, S. H. *et al.* Lymphatic function is required prenatally for lung inflation at birth. *J. Exp. Med.* **211**, 815–826 (2014).

138. Maltzman, J. S., Reed, H. O. & Kahn, M. L. HA-ving lymphatics improves lung transplantation. *J. Clin. Invest.* **125**, 3999–4001 (2015).

139. Hos, D. *et al.* Cutting Edge: Lymphatic Vessels, Not Blood Vessels, Primarily Mediate Immune Rejections After Transplantation. *J. Immunol.* **184**, 535–539 (2009).

140. Ranghino, A., Segoloni, G. P., Lasaponara, F. & Biancone, L. Lymphatic disorders after renal transplantation: New insights for an old complication. *Clin. Kidney J.* **8**, 615–622 (2015).

141. Nurmi, H. *et al.* VEGF-C is required for intestinal lymphatic vessel maintenance and lipid absorption. *EMBO Mol. Med.* (2015).

142. Makinen, T. *et al.* Inhibition of lymphangiogenesis with resulting lymphedema in transgenic mice expressing soluble VEGF receptor-3. *Nat Med* **7**, 199–205 (2001).

143. Kim, H., Kataru, R. P. & Koh, G. Y. Inflammation-associated lymphangiogenesis: a double-edged sword? *J. Clin. Invest.* **124**, 936–942 (2014).

144. Liao, S. & von der Weid, P.-Y. Inflammation-induced lymphangiogenesis and lymphatic dysfunction. *Angiogenesis* **17**, 325–334 (2014).

145. Zheng, W. *et al.* Notch restricts lymphatic vessel sprouting induced by vascular endothelial growth factor. *Blood* **118**, 1154–1162 (2011).

146. Harris, A. R., Perez, M. J. & Munson, J. M. Docetaxel facilitates lymphatic-tumor crosstalk to promote lymphangiogenesis and cancer progression. 1–16 (2018).

147. TAN, Y. Basic Fibroblast Growth Factor-Mediated Lymphangiogenesis of Lymphatic Endothelial Cells Isolated from Dog Thoracic Ducts: Effects of Heparin. *Jpn. J. Physiol.* **48**, 133–141 (1998).

148. Gambino, T. J. *et al.* A Three-Dimensional Lymphatic Endothelial Cell Tube Formation Assay to Identify Novel Kinases Involved in Lymphatic Vessel Remodeling. *Assay Drug Dev. Technol.* **15**, 30–43 (2017).

149. Miteva, D. O. *et al.* Transmural flow modulates cell and fluid transport functions of lymphatic endothelium. *Circ. Res.* **106**, 920–31 (2010).

150. Kawai, Y. *et al.* Heterogeneity in Immunohistochemical, Genomic, and Biological Properties of Human Lymphatic Endothelial Cells Between Initial and Collecting Lymph Vessels. *Lymphat. Res. Biol.* **6**, 15–27 (2008).

151. Lee, S., Choi, I. & Hong, Y. K. Heterogeneity and plasticity of lymphatic endothelial cells. *Semin. Thromb. Hemost.* **36**, 352–361 (2010).

152. Wang, Y. *et al.* Smooth muscle cell recruitment to lymphatic vessels requires PDGFB and impacts vessel size but not identity. *Development* dev.147967 (2017). doi:10.1242/dev.147967

153. Lutter, S., Xie, S., Tatin, F. & Makinen, T. Smooth muscle–endothelial cell communication activates Reelin signaling and regulates lymphatic vessel formation. *J. Cell Biol.* **197**, 837–849 (2012).

154. Yu, Z.-Y., Sun, D., Luo, Y. & Liu, N.-F. Abnormal mural cell recruitment in lymphatic capillaries: a common pathological feature in chronic lymphedematous skin? *Microcirculation* 495–502 (2016). doi:10.1111/micc.12299

155. Norrmén, C. *et al.* FOXC2 controls formation and maturation of lymphatic collecting vessels through cooperation with NFATc1. *J. Cell Biol.* **185**, 439–457 (2009).

156. Detry, B. *et al.* Matrix metalloproteinase-2 governs lymphatic vessel formation as an interstitial collagenase Matrix metalloproteinase-2 governs lymphatic vessel formation as an interstitial collagenase. **119**, 5048–5057 (2012).

157. Nicosia, R. F. The aortic ring model of angiogenesis: A quarter century of search and discovery. *J. Cell. Mol. Med.* **13**, 4113–4136 (2009).

158. Ribatti, D. & Crivellato, E. 'Sprouting angiogenesis', a reappraisal. *Dev. Biol.* **372**, 157–165 (2012).

159. Horowitz, A. & Simons, M. Branching morphogenesis. *Circ. Res.* **103**, 784–795 (2008).

160. Gerhardt, H. VEGF and endothelial guidance in angiogenic sprouting. *Organogenesis* **4**, 241–246

(2008).

161. Mori, M. *et al.* CAPILLARY GROWTH FROM REVERSED RAT AORTIC SEGMENTS CULTURED IN COLLAGEN GEL. *Pathol. Int.* **38**, 1503–1512 (1988).

162. Van Hinsbergh, V. W. M. & Koolwijk, P. Endothelial sprouting and angiogenesis: Matrix metalloproteinases in the lead. *Cardiovasc. Res.* **78**, 203–212 (2008).

163. Chien, S. Mechanotransduction and endothelial cell homeostasis: the wisdom of the cell. *Am. J. Physiol. Circ. Physiol.* **292**, H1209–H1224 (2006).

164. Eglinger, J., Karsjens, H. & Lammert, E. Quantitative assessment of angiogenesis and pericyte coverage in human cell-derived vascular sprouts. *Inflamm. Regen.* **37**, 1–9 (2017).

165. Keselowsky, B. G., Collard, D. M. & García, A. J. Integrin binding specificity regulates biomaterial surface chemistry effects on cell differentiation. *Proc. Natl. Acad. Sci. U. S. A.* **102**, 5953–5957 (2005).

166. Worley, D. R., Hansen, R. J., Wittenburg, L. A., Chubb, L. S. & Gustafson, D. L. Docetaxel Accumulates in Lymphatic Circulation Following Subcutaneous Delivery Compared. **5078**, 5071–5078 (2016).

167. Chen, J. *et al.* Chemotherapy targeting regional lymphatic tissues to treat rabbits bearing VX2 tumor in the mammary glands. *Cancer Biol. Ther.* **7**, 721–725 (2008).

168. Thomas, S. N. & Schudel, A. Overcoming transport barriers for interstitial-, lymphatic-, and lymph node-targeted drug delivery. *Curr. Opin. Chem. Eng.* **7**, 65–74 (2015).

169. Thomas, S. N., Rohner, N. A. & Edwards, E. E. Implications of Lymphatic Transport to Lymph Nodes in Immunity and Immunotherapy. *Annu. Rev. Biomed. Eng.* **18**, 207–233 (2016).

170. Kim, J., Manspeaker, M. P. & Thomas, S. N. Augmenting the synergies of chemotherapy and immunotherapy through drug delivery. *Acta Biomater.* **88**, 1–14 (2019).

171. Baluk, P. *et al.* Rapamycin reversal of VEGF-C-driven lymphatic anomalies in the respiratory tract. *JCI insight* **2**, 1–21 (2017).

172. Wiegand, S., Wichmann, G. & Dietz, A. Treatment of Lymphatic Malformations with the mTOR Inhibitor Sirolimus: A Systematic Review. *Lymphat. Res. Biol.* **16**, lrb.2017.0062 (2018).

173. Phelps, E. A. *et al.* Maleimide Cross-Linked Bioactive PEG Hydrogel Exhibits Improved Reaction Kinetics and Cross-Linking for Cell Encapsulation and In Situ Delivery. *Adv. Mater.* **24**, 64–70

(2012).

174. Wells, R. G. Tissue mechanics and fibrosis. *Biochim. Biophys. Acta - Mol. Basis Dis.* **1832**, 884–890 (2013).

175. Marinelli, J. P. *et al.* Quantitative assessment of lung stiffness in patients with interstitial lung disease using MR elastography. *J. Magn. Reson. Imaging* **46**, 365–374 (2017).

176. Jin, T., Li, L., Siow, R. C. M. & Liu, K.-K. Collagen matrix stiffness influences fibroblast contraction force. *Biomed. Phys. Eng. Express* **2**, 47002 (2016).

177. Liu, F. *et al.* Feedback amplification of fibrosis through matrix stiffening and COX-2 suppression. *J. Cell Biol.* **190**, 693–706 (2010).

178. Driesen, R. B. *et al.* Reversible and irreversible differentiation of cardiac fibroblasts. *Cardiovasc. Res.* **101**, 411–22 (2014).

179. Mas-Moruno, C. *et al.* A Comprehensive Evaluation of the Activity and Selectivity Profile of Ligands for RGD-binding Integrins. *Sci. Rep.* **7**, 1–13 (2017).

180. Bax, D. V. *et al.* Cell Adhesion to Fibrillin-1 Molecules and Microfibrils Is Mediated by α5β1 and αvβ3 Integrins. *J. Biol. Chem.* **278**, 34605–34616 (2003).

181. Garanger, E., Boturyn, D., Coll, J. L., Favrot, M. C. & Dumy, P. Multivalent RGD synthetic peptides as potent αvβ 3 integrin ligands. *Org. Biomol. Chem.* **4**, 1958–1965 (2006).

182. Brooks, P. C., Clark, R. A. & Cheresh, D. A. Requirement of vascular integrin alpha v beta 3 for angiogenesis. *Science (80-.).* **264**, 569 LP – 571 (1994).

183. Knight, C. G. *et al.* The Collagen-binding A-domains of Integrins α 1 β 1 and α 2 β 1 Recognize the Same Specific Amino Acid Sequence, GFOGER, in Native (Triple-helical) Collagens. *J. Biol. Chem.* **275**, 35–40 (2000).

184. Zhang, W. M. *et al.* α11β1 integrin recognizes the GFOGER sequence in interstitial collagens. *J. Biol. Chem.* **278**, 7270–7277 (2003).

185. Emsley, J., Knight, C. G., Farndale, R. W. & Barnes, M. J. Structure of the Integrin α2β1-binding Collagen Peptide. *J. Mol. Biol.* **335**, 1019–1028 (2004).

186. Pozzi, A. *et al.* Elevated matrix metalloprotease and angiostatin levels in integrin alpha 1 knockout mice cause reduced tumor vascularization. *Proc. Natl. Acad. Sci. U. S. A.* **97**, 2202–7 (2000).

187. Zhang, Z. *et al.* α2β1 integrin expression in the tumor microenvironment enhances tumor angiogenesis in a tumor cell-specific manner. *Blood* **111**, 1980–1988 (2008).

188. Chen, J. *et al.* Drug concentrations in axillary lymph nodes after lymphatic chemotherapy on patients with breast cancer. *Breast Cancer Res.* **6**, 474–477 (2004).

189. Swaroop, M. N. *et al.* Impact of adjuvant taxane-based chemotherapy on development of breast cancer-related lymphedema: results from a large prospective cohort. *Breast Cancer Res. Treat.* **151**, 393–403 (2015).

190. Serruys, P. W. Rapamycin eluting stent: the onset of a new era in interventional cardiology. *Heart* **87**, 305–307 (2002).

191. DiSipio, T., Rye, S., Newman, B. & Hayes, S. Incidence of unilateral arm lymphoedema after breast cancer: a systematic review and meta-analysis. *Lancet. Oncol.* **14**, 500–15 (2013).

192. Pappalardo, M., Patel, K. & Cheng, M. H. Vascularized lymph node transfer for treatment of extremity lymphedema: An overview of current controversies regarding donor sites, recipient sites and outcomes. *J. Surg. Oncol.* **117**, 1420–1431 (2018).

193. Becker, C., Assouad, J., Riquet, M. & Hidden, G. Postmastectomy Lymphedema. *Ann. Surg.* **243**, 313–315 (2006).

194. Slavin, S. A., Van den Abbeele, A. D., Losken, A., Swartz, M. A. & Jain, R. K. Return of lymphatic function after flap transfer for acute lymphedema. *Ann. Surg.* **229**, 421–7 (1999).

195. Swartz, M. A. *et al.* Mechanics of interstitial-lymphatic fluid transport: theoretical foundation and experimental validation. *J. Biomech.* **32**, 1297–1307 (1999).

196. Sarri, A. J. *et al.* Arm lymphoscintigraphy after axillary lymph node dissection or sentinel lymph node biopsy in breast cancer. *Onco. Targets. Ther.* **10**, 1451–1457 (2017).

197. Goldman, J. *et al.* Regulation of lymphatic capillary regeneration by interstitial flow in skin. *Am. J. Physiol. Heart Circ. Physiol.* **292**, H2176–H2183 (2007).

198. Kawai, Y. *et al.* Cell transplantation therapy for a rat model of secondary lymphedema. *J. Surg. Res.* **189**, 184–91 (2014).

199. Avraham, T. *et al.* Th2 differentiation is necessary for soft tissue fibrosis and lymphatic dysfunction resulting from lymphedema. *FASEB J.* **27**, 1114–1126 (2013).

200. Clavin, N. W. *et al.* TGF-β 1 is a negative regulator of lymphatic regeneration during wound repair

. *Am. J. Physiol. Circ. Physiol.* **295**, H2113–H2127 (2008).

201. Boardman, K. C. & Swartz, M. A. Interstitial flow as a guide for lymphangiogenesis. *Circ. Res.* **92**, 801–808 (2003).

202. Mendez, U., Stroup, E. M., Lynch, L. L., Waller, A. B. & Goldman, J. A chronic and latent lymphatic insufficiency follows recovery from acute lymphedema in the rat foreleg. *AJP Hear. Circ. Physiol.* **303**, H1107–H1113 (2012).

203. Braude, A. A. The regeneration of lymph nodes after their partial removal or injury. *Bull. Exp. Biol. Med.* **44**, 869–873 (1957).

204. Hadamitzky, C. *et al.* Aligned nanofibrillar collagen scaffolds – Guiding lymphangiogenesis for treatment of acquired lymphedema. *Biomaterials* **102**, 259–267 (2016).

205. Suematsu, S. & Watanabe, T. Generation of a synthetic lymphoid tissue-like organoid in mice. *Nat. Biotechnol.* **22**, 1539–1545 (2004).

206. Watanabe, T., Okamoto, N., Chihara, R., Shimizu, C. & Nishimoto, S. Artificial Lymph Nodes Induce Potent Secondary Immune Responses in Naive and Immunodeficient Mice. *J. Clin. Invest.* **117**, 997–1007 (2007).

207. Huang, J. J. *et al.* Lymph node transplantation decreases swelling and restores immune responses in a transgenic model of lymphedema. *PLoS One* **11**, 1–17 (2016).

208. García, J. R., Clark, A. Y. & García, A. J. Integrin-specific hydrogels functionalized with VEGF for vascularization and bone regeneration of critical-size bone defects. *J. Biomed. Mater. Res. Part A* **104**, 889–900 (2016).

209. Ruggiero, F. & Koch, M. Making recombinant extracellular matrix proteins. *Methods* **45**, 75–85 (2008).

210. Browne, S., Zeugolis, D. I. & Pandit, A. Collagen: Finding a Solution for the Source. *Tissue Eng. Part A* **19**, 1491–1494 (2012).

211. Lynn, A. K., Yannas, I. V & Bonfield, W. Antigenicity and immunogenicity of collagen. *J. Biomed. Mater. Res. Part B Appl. Biomater.* **71**, 343–354 (2004).